Biomaterials in regenerative medicine.

Matthias Epple

Inorganic Chemistry and Center for Nanointegration Duisburg-Essen (CeNIDE), Universiy of Duisburg-Essen, 45117 Essen, Germany

The need for biomaterials is ever increasing due to an ageing population worldwide. The regeneration of tissue after accidents, after operations like tumour extractions, or just after wear of functional elements like joints or teeth still represents a challenge for scientists, physicians, and industry.

Despite the fact that many efforts were directed into this direction in the past three decades, many problems cannot be properly addressed. The ultimate goal of regenerative medicine is the restoration of the original function of a tissue or an organ. This is clearly only partially achieved for cases like artificial joints, tooth restoration, or bone substitution. The current approaches are not biomimetic in the sense of this word.

In the last decades, the focus of research on biomaterials has shifted. 20 years ago, it was typically directed from the adaption of materials from general materials science to medicine, leading to titanium alloys, aluminium oxide, or calcium phosphate as implant materials. Cell cultures were used to demonstrate the cytocompatibility and the absence of cytotoxicity.

Today, biomaterials research has become increasingly "biological" in nature. Simple cell viability tests have been replaced by sophisticated co-cultures, cell culture tests under mechanical loading, immunological tests and other approaches.

Nanomaterials and the reaction of cells towards nanostructured surfaces came into the focus as they permit to control a cellular response without changing the chemistry of the underlying material. Nanoparticles are developed in an increasingly sophisticated way to deliver drugs, genes, or imaging moieties into cells and tissues.

Tissue engineering remains a hot topic in regenerative medicine, although many of the (probably exaggerated) promises of the 1990's have never been fulfilled. However, if we learn to understand and control the cellular functions, we might eventually be able to develop a truly regenerated tissue by extracorporal cell cultivation.

Current trends suggest increasingly complex systems for tissue regeneration. Typically, a new biomaterial involves not only the material itself, but a combination with biologically active compounds like drugs and possibly even cells. 3D printing techniques permit patient-specific geometries of implant materials, up to cell printing techniques. Increasingly advanced mathematical tools permit the analysis and the prediction of the biomechanical properties of implants.

However, it must be noted that a clinical application of a novel biomaterial is only possible after it has passed strict regulatory tests. This involves a strict quality control of synthetic procedures, including the full-scale characterization of the biomaterial with respect to its chemical composition, the dose of any bioactive molecule or drug, the fate of the biomaterial in the body, and possible immune reactions. If cell-based constructs are to be applied, high-level safety regulations must be observed. In the case of older patients who will be the recipients of many biomaterials, questions may be asked whether the extracted cells are as active as cells from a young donor and about the risk of the secondary operation. This will lead to high costs which must be borne by the health care system.

The current research trends are really exciting as they involve the accumulated knowledge of researchers from (bio-) chemistry, physics, biology, medicine, and engineering to a higher degree than 20 years ago. Biomaterials have a bright future, provided that research activities remain connected to clinical application. The eventual clinical application (including possible limitations) must always be in the focus of the researcher.

20 Years of Biomaterials Research.

Marc Bohner

RMS Foundation, Bischmattstrasse 12, 2544 Bettlach, Switzerland
http://www.rms-foundation.ch/en/contact/bohner-marc/

Twenty years ago, articles were searched for in microfilms and books, and copied or ordered physically at the library. The number of journals and articles was limited, so finding a new relevant article felt like a victory. Currently, it is almost impossible to keep track of all biomaterials journals and publications. In parallel, metrics to assess the quality of research have become extremely important and accessible, in particular the h-index, and the impact factor. Since the quality of a journal "quality" is now assessed by the IF factor, some journals have started focusing only on topics generating high citation counts. This is highly detrimental for those interested in "low-impact" topics such as ceramics and metals.

Translational research is a new expression that is used to describe research that can be translated into a product. Researchers are pushed to start their own company and/or to protect their research by patents. The paradox is that has become much more difficult to translate a research idea into a product due to increasingly tight regulations. The number of "pre-market approvals" approved in the orthopaedic field has sunk drastically in the past few years. As such, the gap between academic research and industry is increasing.

In 1995, the number of researchers and industry representatives interested in biomaterials was limited. The annual meeting of the SSB represented an opportunity to meet and exchange ideas. It was also a time when biomaterials professors were appointed. Now, hundreds of Swiss research labs publish articles in biomaterials journals, but the attendance of the meeting has barely increased, and biomaterials professors getting retired are not replaced. Also, the board of new biomaterials journals are often occupied by researchers not attending traditional biomaterials meetings. This is a paradigm shift that biomaterials societies and researchers interested in traditional biomaterials have to face.

The application of 3D hydrogel printing technology for cartilage regeneration

Jos Malda

Department of Orthopaedics, University Medical Center Utrecht

Hydrogels are attractive biomaterials for repair and potential regeneration of articular cartilage. Moreover, hydrogels are also particularly suitable as "bioinks" for biofabrication as they recapitulate several features of the natural extracellular matrix and allow cell encapsulation in a highly hydrated mechanically supportive 3D environment. Additionally, they allow for efficient and homogeneous cell seeding, can provide biologically-relevant chemical and physical signals and can be formed in various shapes and biomechanical characteristics. Optimization of – intrinsically weak – hydrogels to address the physico-chemical demands of the biofabrication process, whilst ensuring the right conditions for cell survival is currently regarded as an important research topic. Nevertheless, there exists an additional significant challenge in the biofabrication of articular cartilage tissue constructs: to address the harsh in vivo mechanical environment on the other. We have developed novel hydrogel-based bioink formulations, as well as multimaterial biofabrication approaches that allow for the construction of intricate stable 3D structures, whilst providing the cells with a biologically suitable environment.

Biomaterials in Australia

Sally McArthur

Swinburne University of Technology

The aim is to couple our knowledge of materials, surface engineering, physical science, analytical chemistry and cell-surface interactions to create novel interfaces capable of reproducing and/or controlling physical and biological function. The work reaches out from the medical devices and biosensing to colloids and surface science, composites and food processing. The research has two interlinked themes: Surface modification of materials to control biointerfacial interactions and the physicochemical characterisation of biointerfaces. The ability to control protein and cellular interactions is fundamental in the development of many new biomaterials and biomedical devices. These interactions are influenced by a variety of both specific (e.g. antibody/antigen) and non-specific interactions (e.g. van der Waals, electrostatic and steric forces). The experience is in the surface modification of materials using plasma polymerisation, grafted polymers (polysaccharides, polyethylene glycol (PEG), polyelectrolytes and dendrons), self-assembled monolayers (SAMs) and biomolecules. The approach has been to manipulate the physicochemical properties of a surface and in turn, control protein and cellular interactions both in vitro and in vivo.

Should the physician try to perform tissue engineering?

Peter Frey

Experimental Pediatric Urology
Institute of Bioengineering, EPFL
peter.frey@epfl.ch

The need for regenerative medical procedures is highlighted from the physician's point of view, discussing different clinical examples, which could benefit from a tissue engineering approach. The interdisciplinary team approach is elucidated and the successes and pitfalls of tissue engineering approaches in regenerative medicine are discussed.

In particular collagen and fibrin matrix technologies for the use in the regeneration of the urinary tract are discussed. The advantages and limits of the combination of matrices and engineered growth factors are demonstrated and critically analyzed. The in vitro behavior and the in vivo application in a rabbit model of such smart matrices for tissue engineering of tubular structures for urethral or ureteral replacement are evaluated. Further their ability for in vivo use for bladder augmentation is shown in a rat model. Apart from these potentially off-the-shelf acellular matrices, cellular engineering for humanized tubular collagen matrices, based on cultured human smooth muscle cells, inducing human extracellular matrix deposition is presented. The application of these matrices after decellularization and DNA removal in a rabbit urethral regeneration model is elucidated. I addition the existence of human urothelial stem cells with the capacity to initiate growth, to self-renew and to differentiate into mature human urothelium is discussed. Further the use of bioreactors, imitating human pressure and flow profiles, for the fabrication of cellular tubes for urethral regeneration is discussed. Finally the development of novel injectable bulking agents is mentioned.

Directional Foaming of scaffolds by integration of 3D Printing and Supercritical CO_2 Foaming

M.G.M. Marascio[1], P.E. Bourban[1], J.A. Månson[1], D. Pioletti[2]

[1] *Laboratory of Polymer and Composite Technology*,

[2] *Laboratory of Biomechanical Orthopedics*,

Ecole Polytechnique Fédérale de Lausanne (EPFL), Station 12, CH-1015 Lausanne,

INTRODUCTION: Cartilage repair is a challenging clinical problem because once damaged in adults, it never regenerates and resulting defects may further lead to osteoarthritis (1). Tissue Engineering has emerged as a possible solution to the problem. One of the challenges is to produce an optimum scaffold, able to reproduce the natural ECM and to carry cartilage functions in the early stage of the implant process, while inducing the regeneration of tissue. While many techniques as applied to process biomaterials, physical methods as supercritical foaming and Additive Manufacturing represent a clean way to control the exact composition of the final construct. This work represents a first attempt to combine the advantages of the two techniques while overcoming some of the main drawbacks, producing 3D anisotropic size-controlled structures.

METHODS: An Ultimaker Original+ was used to produce the raw scaffold by fusion deposition modelling. Fibers were first created from PLA Natureworks 4043D and 2003D acquired respectively from FiloAlfa and TreeDFilament. Fibers. Three 2D structures were printed for each PLA isomer, with a dimension of 10mm x 10mm x 1mm and with inner windows of 3.5mm x 3.5mm. Then, three 3D scaffolds were produced from each PLA, (4.4mm x 4.4mm x 4.4 mm, 0.4mm fibers and 0.6mm fibers spacing). Each 2D and 3D structure was then foamed with supercritical CO_2 in a GMP medical autoclave from SITEC SIEBER Engineering AG (2).
Porosity, pore size distribution and interconnectivity were determined by µCT (Microcomputed Technologies Inc. Skyscan 1076, Belgium) and Scanning Electron Microscopy (Microscopy XLF30 microscope) (SEM). Compression behaviour was investigated with an Ultimate Tensile Strength machine (Test Machine Systeme, Germany).

RESULTS: The minimum architecture deformation and the maximum interconnected porosity were obtained by tuning the foaming parameters, offering the desired cellular architectures, with fibre directional porosity in the micro meter range (Figure 1).

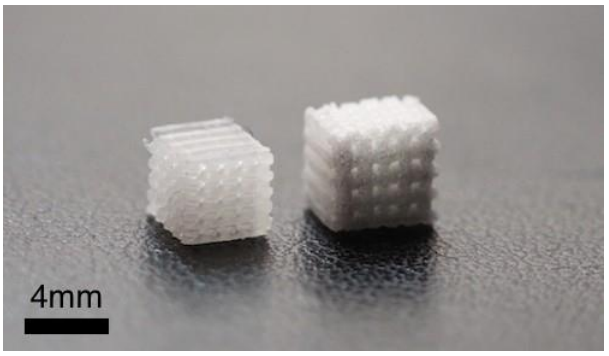

Fig. 1: Scaffold before (left) and after (right) supercritical foaming.

Mechanical properties were shown to reflect the behaviour of a foamed cellular material, reducing the stiffness of scaffolds with solid walls (2) and introducing anisotropic properties related to the orientation of the fibres.

DISCUSSION & CONCLUSIONS: The results overcome several limitations of existing scaffolds and can be now extended to different biopolymers. A controlled anisotropy, a homogeneous macro- and an oriented micro-porosity in 3D structures are obtained by combining 3D additive manufacturing and supercritical foaming, two solvent-free processes which could integrate living cells.

ACKNOWLEDGEMENTS: They go to the Swiss National Science Foundation (grant 200021_150190) which supports this research, to Dario Pizzigoni (TreeDFilament) for the kind supply of PLA fibers and to Joris Pasquale Jean for the work on printing and foaming characterization.

Designing patient specific implants fabricated by stereolithography for orbital wall reconstruction

V Varjas[1], M. Geven[2], DW Grijpma[2], X Wang[3], J Peng[3], D Eglin[1], L Kamer[1]

[1] *AO Research Institute Davos, Davos, CH; University of Twente, Enschede, NL; The Institute of Orthopaedics of the General Hospital of the People's Liberation Army, Beijing, CN.*

INTRODUCTION: The reconstruction of orbital wall defects is a complex surgical procedure. Accurate anatomical reconstruction at primary surgery is a critical step necessitating difficult implant shaping and positioning[1]. A solution might be the manufacturing of patient specific implants (PSI)[2] relying on preoperative Computed Tomography (CT). However, insufficient clinical CT image resolution leads to pseudo holes in the three-dimensional (3D) model of the orbits, incompatible with additive manufacturing. Thus, a computational workflow for patient specific orbital implant design is described.

METHODS: Five retrospective, preoperative CT scans affected by unilateral orbital defects (3 orbital floor, 2 orbital floor/medial wall fractures) were selected. An orbital mean model was available derived from 3D statistical modeling. The images were processed using Amira (FEI Visualization Sciences Group, Bordeaux, France) extended by custom modules using TCL scripting, ITK (Insight Segmentation and Registration Toolkit, U.S. National Library of Medicine) and C++ programing. The generated patient specific implants were fabricated by stereolithography. A commercial resin (Envisiontec PIC 100) was used on an Envisiontec Perfactory$^{3®}$ SXGA^{+} Standard UV system. Irradiation times of 9 s per layer and an intensity of 180 mW/dm^2 were employed.

RESULTS: The workflow consisted of the pre-processing of the CT images data by applying noise-reduction, thresholding and removal of small floating components. Preliminary 3D model of the orbits were generated, affected by pseudo holes. Using a complex, automatic method, the pseudo holes of the intact orbit were eliminated by adapting and merging the orbital mean model to it using rigid, affine and non-linear registrations. Then the reconstructed intact orbit was mirrored and adapted to the fractured side. Landmarks were manually placed on the affected side to describe the shape and location of the fracture. In a series of following steps a 3D implant template was automatically generated covering the defect and shaped as the corresponding intact region. The fabrication of the implants was successful

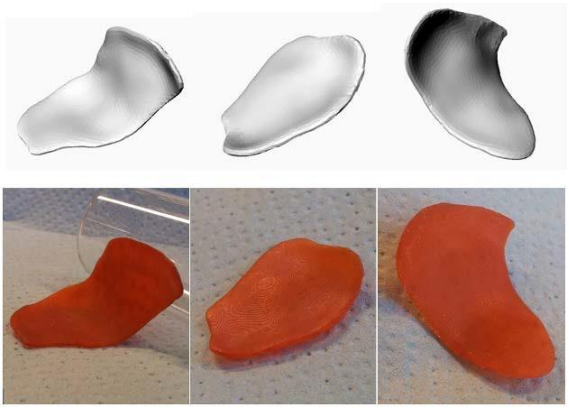

Fig. 1: Example images of the 3D PSI computer models (top row) with the corresponding implants fabricated by stereolithography (bottom row).

DISCUSSION & CONCLUSIONS: A computational workflow to generate PSIs for the reconstruction of orbital wall defects fabricated by stereolithography was developed and tested using 5 CTs. The method represents an efficient/near to automatic approach to process a given CT case. It merely requires the surgeon to place few landmarks to define the implant and the fixation pathway. It may speed up and accommodate the designing of a PSI for primary reconstruction of complex orbital wall defects. Additional design features like screw holes will be included.

ACKNOWLEDGEMENTS: The authors' acknowledge the funding by NSFC-DG-RTD Joint Scheme (Project No. 51361130034) and the European Union's 7th Framework Program under grant agreement n° NMP3-SL-2013-604517.

Fabrication of continuous $PDMS_{star}$-PEG gradients for osteochondral regeneration

BM Bailey[1], LN Nail[2], MA Grunlan[1,2]

Texas A&M University, [1]Materials Science and Engineering Program, [2] Department of Biomedical Engineering, College Station, TX, USA

INTRODUCTION: The chemical and physical properties of a 3D material scaffold influence tissue regeneration.[1] However, the undefined cell-material relationship has lead to the regeneration of insufficient, non-native like tissues.[2] Thus, we have developed a *combinatorial platform* adapted to prepare libraries of tissue engineering (TE) scaffolds in the form of continuous gradients towards the rapid characterization of cell-material relationships and as a potential scaffold for the regeneration of interfacial tissues (i.e. bone – cartilage interface). Herein, we report an initial"library" based on the gradual incorporation of hydrophobic, bioactive methacrylated star poly(dimethyl siloxane) ($PDMS_{star}$-MA) into a poly(ethylene glycol) diacrylate (PEG-DA) hydrogel using solvents of varying polarities (i.e. dichloromethane (DCM) and distilled water (DI-H_2O)) to extend and tune scaffold properties along a gradient (Fig. 1).

METHODS: Towards gradient fabrication, two precursor solutions were prepared at two different ratios [(0:100)-mixing solution and (20:80)-stock solution] of $PDMS_{star}$-MA to PEG-DA (synthesized as previously reported [3]) in either DCM or DI-H_2O and poured into the two chambers of a standard laboratory gradient maker (Hoefer SG 15, Amersham Biosciences). The gradient maker was connected in line to a peristaltic pump followed by a top-filling vertical mold (8 x 6 cm x 3 mm) consisting of two clamped glass slides separated by a Teflon spacer. After filling the mold, the cross-linked hydrogel was formed by immediate exposure to UV light. Upon removal from the mold, the DCM based sheets were rinsed with DCM then air dried for 30 min to permit evaporation of DCM (leaving open pores) then (as with H_2O hydrogels) were put to soak in 60 mL DI-H_2O for 72 hr. Swelling, morphology, mechanical properties, and bioactivity were investigated by analyzing discs from 4 "zones" within the gradient scaffold.

RESULTS: Previous work established that $PDMS_{star}$ distribution and porosity can be enhanced when hydrogels are fabricated in DCM versus DI-H_2O and subsequently hydrated.[4] As $PDMS_{star}$ is bioactive and osteoinductive [5], its

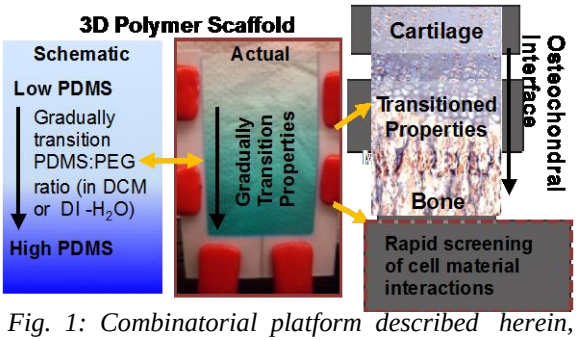

Fig. 1: Combinatorial platform described herein, verified by the fabrication of $PDMS_{star}$-PEG gradient scaffolds possessing a continuous change in bioactive, osteoinductive $PDMS_{star}$.

incorporation into a PEG hydrogel scaffold along a gradient permitted the ability to spatially control bioactivity and osteoinductivity throughout the scaffold. Swelling ratios for hydrogel scaffolds fabricated in DCM were significantly lower and varied more broadly than corresponding DI-H_2O scaffolds due to the dissolution and homogenous distribution of $PDMS_{star}$ in DCM. Also noteworthy, are the high modulus values achieved with the $PDMS_{star}$:PEG scaffold fabricated in DCM, which increased linearly up to 350 kPa corresponding to an increase in $PDMS_{star}$ content. Such high values were attributed to increased pore size resulting in increased pore wall thickness.

DISCUSSION & CONCLUSIONS: Herein, we describe a *combinatorial platform* for the fabrication of TE scaffolds. Utilizing two polymers with relevant properties in terms of TE as well as fabrication solvent, we proved the ability to expand and spatially control relevant properties throughout a single TE scaffold. This could be a potential regenerative method for a native-like osteochondral interface, which is characterized by a gradual transition in mechanical and chemical properties.

ACKNOWLEDGEMENTS: *Funding from NIH/NIBIB (1R21HL089964-01 and 1R03EB015202-1) is gratefully acknowledged.*

Elastic, biocompatible and biodegradable electrospun scaffold delivering growth factors for tendon repair

Olivera Evrova[1,2], Maurizio Calcagni[1], Eliana Bonavoglia[3], Manfred Welti[1], Pietro Giovanoli[1], Viola Vogel[2], Johanna Buschmann[1]

[1] *Division of Plastic Surgery and Hand Surgery, University Hospital Zürich, CH.*
[2] *Laboratory of Applied Mechanobiology, ETH Zürich, CH.* [3] *Ab Medica, Lainate, Milan, Italy.*

INTRODUCTION: For tendon repair applications, combinations of biomaterials with biological factors have been considered as a viable option for improved healing. Here, we explore electrospun scaffold made from elastic and biodegradable material, DegraPol® (DP), carrying PDGF-BB as a biological cue for tendon healing after rupture. Release kinetics and bioactivity of the delivered growth factor are of high importance as well as the cell-material interactions happening at the implant interface. Thus, we focus on understanding these objectives.

METHODS: Emulsion electrospinning was used for production of bioactive DP scaffolds, carrying rhPDGF-BB. Water-in-oil emulsion of the polymer solution and aqueous solution with biomolecule was produced by short magnetic stirring and ultrasonication (50 % power) for 2 min. The produced emulsion was directly electrospun using in-house built electrospinning device. Changes in fiber morphology and diameter as a function of different electrospinning parameters were determined. The mechanical properties (Young's modulus and strain at break [%]) were determined from stress/strain curves of the bioactive DP scaffolds and compared to pure DP scaffolds. Initially, release kinetics of two model molecules, fluorescein and FITC-BSA were studied and later the delivery of rhPDGF-BB was assessed and analysed using ELISA. The bioactivity of the released growth factor *in vitro* was tested on rabbit tenocytes and its capability to increase cell proliferation and migration. In addition, tenocyte adhesion and proliferation were assessed on the bioactive DP scaffolds.

RESULTS: Emulsion electrospinning allowed for dispersed incorporation of biomolecules within the DP fibers. No blob formation on the fibers was visible. The fiber diameter was significantly smaller for emulsion electrospun DP fibers when compared to pure DP fibers. In terms of mechanical properties, no significant differences were observed in the Young's modulus, but bioactive scaffolds experienced 2-fold decrease in strain at break [%]. However, the elasticity was still high enough for surgeon friendly handling and easy stretching. In contrast to FITC-BSA and PDGF-BB having a sustained release within 14 days, fluorescein experienced a burst release within 2 days. On the other hand, the rhPDGF-BB release was a more sustained one in a period of 14 days. Rabbit tenocytes were able to adhere and proliferate on the DP scaffolds. Tenocyte proliferation and migration are stimulated by PDGF-BB were a dose dependent manner.

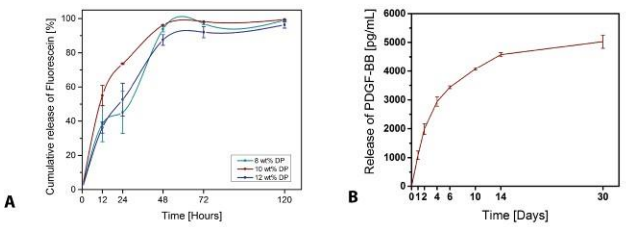

Fig. 1: Release kinetics of fluorescein (A) and PDGF-BB (B) from DP scaffolds

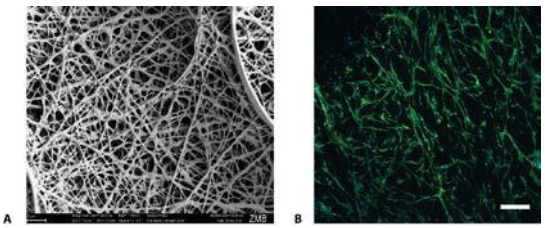

Fig. 2: Morphology of electrospun DP scaffolds (SEM) (A) and tenocytes cultured on DP scaffolds (F-actin and nucleus staining) (B)

DISCUSSION & CONCLUSIONS: Emulsion electrospinning allows for easy production of bioactive scaffolds. Bioactive DP scaffolds show sustained release of PDGF-BB and their mechanical properties are still good for surgeon handling and application. They provide a good carrier system for biomolecules and allow tenocyte adhesion and proliferation.

ACKNOWLEDGEMENTS: This work was supported with scientific fellowship by *ab medica*, Lainate, Milan, Italy, for O.E.

HiPIMS titanium metallization of PEEK for improved osseointegration

K Thorwarth[1], G Thorwarth[2], C Voisard[2], M Kraft[2], L. Bernard[1] and J Patscheider[1]

[1] *Empa, Swiss Federal Laboratories for Materials Science and Technology, Überlandstrasse 129, CH-8600 Dübendorf, Switzerland,*

[2] *DePuy Synthes GmbH, Luzernstrasse 21, CH-4528 Zuchwil, Switzerland*

INTRODUCTION: An increasing number of implants and instruments are made from PEEK (Polyetheretherketone) due to the material's mechanical strength and chemical stability and low elastic modulus. However, the osseointegration of PEEK was found to be comparably poor, requiring surface modification to warrant good bone apposition[1]. We present a novel method to deposit thin, 3D conformal and highly adherent titanium layers over the whole implant surface to facilitate osseointegration while maintaining the substrate's favourable mechanical properties.

METHODS: 500 nm thick dense titanium coatings were deposited on test coupons and implant prototypes by means of an unipolar chopped HiPIMS setup. Prior to deposition, a plasma activation step was applied to increase the PEEK surface reactivity.

Relevant coating properties such as composition, adhesion and biocompatibility were tested according to established standards, employing methods such as ToF-SIMS, XPS, compression shear,insertion and tensile testing, cytotoxicity testing, and GC-MS .

RESULTS: High adhesion strength values (>30 MPa) could be obtained with c-HiPIMS[2] including penetration into narrow trenches and to surfaces with a high inclination towards the sputter target. XPS and ToF-SIMS measurements confirm film qualities compliant to commercially pure grade II Titanium (ISO 5832-2). The layers did not significantly roughen the implant surface, thus preserving primary stability features of the design

Excellent film adhesion to PEEK substrates led to layer loss in impaction and compression shear tests only in regions where the PEEK substrate failed due to decohesion.

Cytotoxicity and GC-MS analysis of extracts revealed excellent biocompatibility of the HiPIMS coated PEEK prototypes comparable to commercially pure titanium grade II.

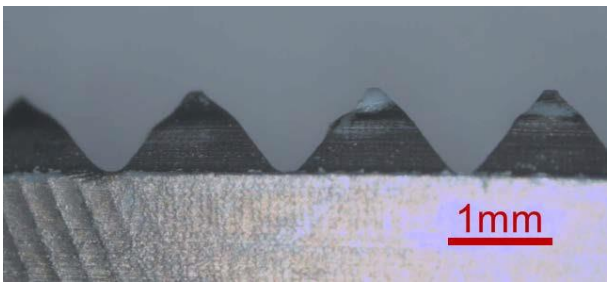

Fig. 1: Side view image of the coated primary fixation features of an implant prototype after compression shear test (ASTM F2077 2011). The titanium layer is only removed in places of excessive abrasion.

DISCUSSION & CONCLUSIONS: In comparison to established and routinely applied coating techniques (VPS, APS), the presented process features a much thinner and denser pure metal coating. Based on the results, the osseointegration is expected to equal pure titanium. A transfer of the HiPIMS process to industrial setups seems straightforward as several advanced commercial HiPIMS systems are nowadays available.

A further enhancement of the HiPIMS coated Ti surface by subsequent processes like spark anodization is likely to provide even better osseointegrative properties.

ACKNOWLEDGEMENTS: Financial support provided by the Swiss innovation promotion agency CTI is gratefully acknowledged.

Calcium deficiency in β-TCP platelets produced in organic media

C Stähli[1], J Thüring[1,2], L Galea[1], M Bohner[1], N Döbelin[1]

[1]*RMS Foundation, Bettlach, Switzerland.* [2]*ETHZ, Department of Materials, Zürich, Switzerland.*

INTRODUCTION: Sub-micrometric hexagonal β-tricalcium phosphate (TCP, $Ca_3(PO_4)_2$) platelets with controllable geometry and aspect ratios up to 15 (Fig. 1) were recently produced by precipitation in ethylene glycol at high temperature.[1,2] These materials are of great interest as fillers in nano-structured composites, potentially offering load bearing bone substitute materials by combining high tensile strength and toughness. Moreover, the platelets are non-agglomerated and, at lower aspect ratios, may thus provide promising additives to improve the injectability of pastes or cements. Interestingly, x-ray diffraction (XRD) spectra obtained on these platelets could not be precisely fitted with the known β-TCP crystal structure. Therefore, the obtained β-TCP phase was analysed in more detail.

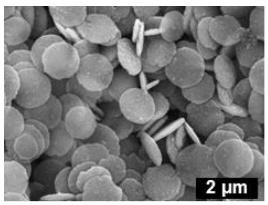

Fig. 1: β-TCP crystals produced in ethylene glycol

METHODS: β-TCP platelets were produced by mixing a $CaCl_2$-ethylene glycol solution with a H_3PO_4 or Na_2HPO_4-ethylene glycol solution where the pH was adjusted by adding either HCl or NaOH. The reaction was kept at constant temperatures (90 to 170°C) for at least 30 minutes in order to allow for precipitation and particle growth. The phase composition and β-TCP crystal structure were analysed by XRD and Rietveld refinement in order to fit the spectra with either stoichiometric β-TCP or a with structure where Ca4 and O2 occupancies were variably determined according to the best fit (while ensuring charge balance).

RESULTS: XRD spectra obtained on β-TCP platelets yielded poor fits when refined with the stoichiometric β-TCP structure. In particular, electron density difference (EDD) maps (Fig. 2a) revealed an occupancy mismatch of the Ca4 (and O2) position along with position discrepancies. In contrast, a refinement with variable Ca4 and O2 occupancies allowed for better fits and resulted in a flat EDD map (Fig. 2b). The Ca/P ratio at optimal refinement was approximately 1.45. Following calcination of the platelets at 1000°C, phase separation into stoichiometric β-TCP (Ca/P = 1.5) and β-calcium pyrophosphate (CPP, $Ca_2P_2O_7$; Ca/P = 1) was demonstrated, and quantification of the phase fractions confirmed the overall Ca/P ratio of 1.45. Moreover, platelets produced at different temperature and pH as well as in a different solvent (glycerol) all exhibited a Ca/P ratio of 1.45±0.01, despite the profound effects of these parameters on the platelet geometry and on the fraction of other precipitated phases (predominantly monetite).

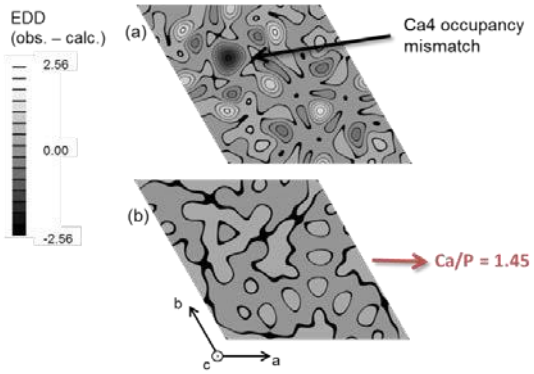

Fig. 2: Electron density difference (EDD) maps on a cross section through the β-TCP unit cell. (a) EDD between the platelet crystal structure observed by XRD and the structure calculated in stoichiometric β-TCP. (b) EDD between the observed structure and a refined β-TCP structure with partially occupied Ca4 and O2 positions.

DISCUSSION & CONCLUSIONS: This study demonstrates a consistent non-stoichiometric Ca/P ratio in β-TCP platelets precipitated in ethylene glycol (and glycerol). The origin of the Ca- and O-deficiency in the synthesis, in particular possible phosphate condensation, is subject of ongoing investigation. Future work will examine the effect of the non-stoichiometry on the solubility of the platelets. In particular, a material with a slightly higher solubility than currently available β-TCP, and without the inconvenience of acidic pH changes related to monetite and brushite dissolution, would be of clinical interest for bone substitute materials.

ACKNOWLEDGEMENTS: Swiss National Science Foundation (SNF; 200021_13758).

Fibre composite hydrogels: towards a load-bearing implant for nucleus pulposus replacement

A Khoushabi[1], PE Bourban[1], A Schmocker[2], D Pioletti[3], C Schizas[4], C Moser[2], JA Månson[1]

[1] *Laboratory of composite and polymer technology*, [2] *Laboratory of applied photonics devices*, [3]*Laboratory of biomechanical orthopedics*, *Ecole Polytechnique Fédérale de Lausanne (EPFL), CH-1015 Lausanne,* [4] *Neuro-orthopedic Spine Unit, Clinic Cecil, CH-1003 Lausanne, Switzerland*

INTRODUCTION: Replacing a gel like central part of the intervertebral disc, so-called nucleus pulposus (NP) via minimally invasive surgery is one of the most recent approaches in low-back pain treatment (1). An ideal biomaterial for NP replacement should mimic the cyclic mechanical and swelling properties of the native tissue. Additionally, it should be injectable, biocompatible and stable in the intervertebral disc environment. In this work, a novel injectable, biocompatible, photo-curable composite hydrogel based on a poly(ethylene glycol)dimethacrylate (PEGDM) matrix and a nano fibrillated cellulose (NFC)reinforcement is designed and characterized.

METHODS: Hydrogel precursors containing PEGDM (molecular weights of 6 and 20 kDa), NFC (different concentrations up to 0.7 %vol), photo-initiator and phosphate buffer saline were prepared. Photo-curing was performed by 30 min irradiation of a 365nm light to the moulded hydrogel precursors. A native NP tissue was isolated from a bovine tail disc for performance comparison. The swollen hydrogel and the bovine NP samples were loaded in unconfined compression. The elastic moduli and fracture strengths were evaluated from the measured stress-strain curves. Hydrogels swelling ratio (SR) were calculated based on Archimedes' buoyancy principle. The photo-curing kinetics of hydrogels was evaluated by photo-rheology measurements.

RESULTS: The mechanical and swelling test results show that PEGDM 6 kDa and native NP tissue have approximately the same modulus and SR. However, the native tissue is intact until 80% of compression strain whereas the PEGDM 6 kDa hydrogel fails at approximately 60% compression strain. In order to address such an issue, another PEGDM hydrogel with higher molecular weight, i.e. lower crosslink density, was synthesised. As shown by solid lines in Figure 1, the PEGDM 20 kDa hydrogel sustains more than 80% compression with the elastic modulus (43 kPa) significantly lower than 6 kDa PEGDM (150 kPa) owing to the reduction in the crosslink density

As shown by the dashed line in Figure 1, the addition of NFCs, significantly compensates the softening of the hydrogel matrix. Furthermore, this composite hydrogel shows the same strain as the neat 20 kDa hydrogel and the native NP.

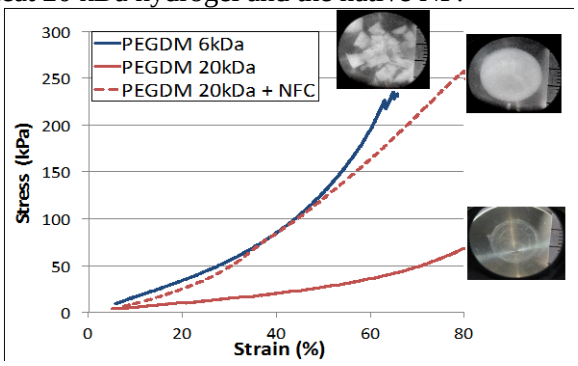

Fig. 1: stress-strain curves of the PEGDM 6 kDa, PEGDM 20 kDa without and with 0.5 %v NFC. The inserted images show 6 and 20kDa hydrogels under 60% and 80% compression respectively.

As expected, the hydrogel SR was increased from 8% to 100% by decreasing the hydrogel crosslink density. The high SR of 50% is preserved in 20k Da PEGDM hydrogel reinforced with 0.5%vol NFCs. Curing kinetics indicate that the NFC fibres scatter the UV light and accelerate the curing time up to 20% when compared to the neat hydrogel.

DISCUSSION & CONCLUSIONS: Simultaneous reduction of crosslink density and addition of fibres are efficient in the studied hydrogels for concurrent improvement of stiffness and strength, while providing desired swelling ratios. It was also shown that such an approach accelerates curing kinetics. Currently, performance of bovine discs implanted with developed hydrogels is evaluated in ex vivo condition.

ACKNOWLEDGEMENTS: The SNSF (grant 10024003165465) is acknowledged as well as the group of T. Zimmermann and P. Tingaut at EMPA Dubendorf, Switzerland, for advices and supply of the NFC.

An injectable formulation of thermo-responsive hyaluronic acid-pNIPAm loaded with gentamicin for infection prophylaxis in an *in vivo* contaminated fracture model in rabbits

G-JA ter Boo[1,2], D Arens[1], I Keller-Stoddart[1], W-J Metsemakers[1,3], T Schmid[1], S Zeiter[1], RG Richards[1], DW Grijpma[2], TF Moriarty[1], D Eglin[1]

[1] *AO Research Institute Davos, Davos, CH.* [2]*Department of Biomaterials Science and Technology, University of Twente, Enschede, NL.* [3]*Department of Trauma Surgery, University Hospitals Leuven, Leuven, BE*

INTRODUCTION: Infection remains a major challenge in traumatology. On average, 5% of patients receiving internal fracture fixation devices develop an infection, although in the case of severe (grade 3) open fractures this can increase to >30%. Antibiotic loaded biomaterials (ALBs) may offer additional antimicrobial protection beyond that provided by systemically delivered antibiotics. In this study, the efficacy of a thermo-responsive hyaluronic acid-pNIPAm composition loaded with gentamicin was tested in a rabbit contaminated humeral fracture model with internal fixation and compared to gentamicin loaded collagen-fleece.

METHODS: HApNIPAm was synthesized by a direct amidation reaction of HATBA with amine-terminated pNIPAm. The sol-gel transition was screened for the HApNIPAm composition at 15 w/v% in PBS with or without addition of 1 w/v% gentamicin-sulphate (GS). Storage and loss moduli were measured as function of the temperature during a temperature sweep with 5% oscillatory strain at 1 Hz during heating at 1°C/min. In the *in vivo* study, 30 rabbits received a defined inoculum of *Staphylococcus aureus* into an osteotomy of the humerus that was fixed with steel fixation plates. Rabbits were then treated with HApNIPAm or collagen fleece loaded with gentamicin, or no intervention. 1 Wk post-OP, rabbits were euthanized and humuri were dissected. Bacterial cultures determined if the bone (B), soft tissues (ST) or implant (IM) were culture positive.

RESULTS: At 20°C both the HApNIPAm gel with and without 1% gentamicin-sulphate added have low elastic and viscous moduli. Upon heating to 37°C, G' increases 3 orders of magnitude for the HApNIPAm composition. Onset of gelation starts at lower temperature for the gentamicin loaded HApNIPAM compared to the unloaded one. This could be assigned to interactions between charges on free carboxylate (HA) and amine groups (GS) (Fig. 1). All rabbits treated with the HApNIPAm gels with gentamicin stayed free of infection, whereas without treatment 100% of the rabbits were infected (Fig. 2). In the collagen-sponge treated group, 1 rabbit was infected with a *Streptococcus salivarius*.

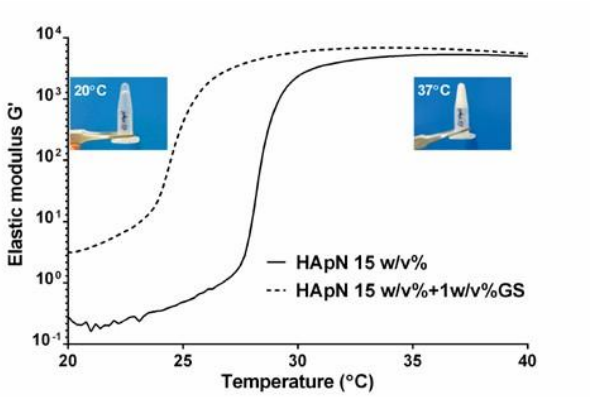

Fig. 1: HApNIPam (15w/v%) and HApNIPAm (15w/v%)-gentamicin (1w/v%) temperature sweep

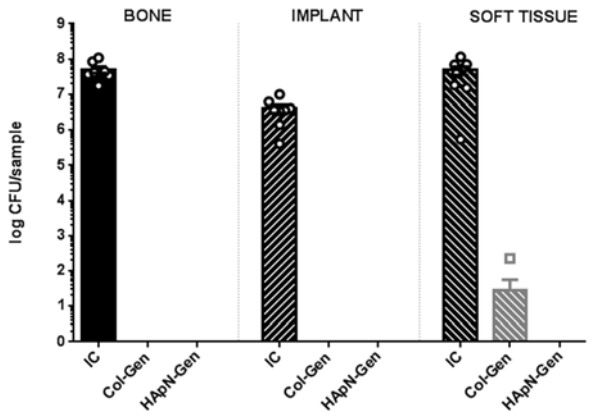

Fig. 2: Bacterial quantification in B, ST and on the IM surface in infected control (IC), collagen sponge (8 mg GS), and HApNIPAm gel (8 mg GS)

DISCUSSION & CONCLUSIONS: The HApNIPAm hydrogel loaded with gentamicin proved to be effective in preventing infection in a contaminated fracture model in rabbits and a promising alternative for currently used ALBs.

Bisphosphonate-loaded *in situ*-mineralizing hydrogel for peri-implant bone augmentation

U Kettenberger[1], P Procter[2], DP Pioletti[1]

[1] *Laboratory of Biomechanical Orthopedics, Swiss Federal Institute of Technology Lausanne (EPFL), Switzerland.* [2] *Applied Materials Science, Uppsala University, Sweden.*

INTRODUCTION: Locally delivered bisphosphonates such as Zoledronate have been shown in several studies to inhibit peri-implant bone resorption and recently also to enhance peri-implant bone formation [1]. Other studies have demonstrated positive effects of hydroxyapatite particles on peri-implant bone regeneration [2] and an enhancement of the anti-resorptive effect of bisphosphonates by the presence of calcium [3]. In the here presented study, we evaluated the bone augmenting properties of locally applied hyaluronic acid hydrogel containing both substances, nano-sized hydroxyapatite particles and Zoledronate.

METHODS: Eight female Wistar rats were ovariectomized to induce estrogen-deficiency caused bone loss and were implanted five weeks after OVX with miniature screws in both femoral condyles. The pre-drilled pilot holes of the screws were filled with either a hydrogel containing pure hydroxyapatite particles (nHA-Gel-group) or particles loaded with the bisphosphonate Zoledronate (nHA-Zol-Gel-group). The peri-implant bone remodelling was monitored with microCT-based dynamic histomorphometry [1]. Therefore the rats were scanned 3, 10, 17, 31, 45 and 58 days after screw implantation. Histological slides were prepared from the extracted bone samples after sacrifice of the animals at day 58.

RESULTS: Dynamic histomorphometry and histology revealed for both experimental groups an unexpected rapid mineralization of the hydrogel *in vivo* through formation of granules that served as scaffold for new bone formation (Fig. 1/2). The delivery of Zoledronate from the hydroxyapatite particles in the nHA-Zol-group inhibited efficiently a degradation of the mineralized hydrogel as well as a resorption of the peri-implant bone. The differences in demineralization rate were significant during the whole study and resulted in a significantly enhanced mineralized tissue fraction already 17 days after screw implantation. This effect was visible throughout the whole analyzed region that included bone up to a distance of 1.5 mm from the screw surface.

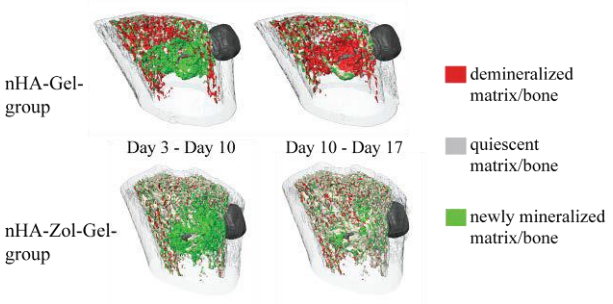

Fig. 1: 3D rendering of paired microCT scans indicating zones of bone / material mineralization and demineralization in the trabecular bone.

DISCUSSION & CONCLUSIONS: This study showed that hyaluronic acid hydrogel loaded with hydroxyapatite particles mineralizes *in vivo* within 10 days after implantation. These unique *in situ*-scaffold-forming properties combined with the anti-resorptive effect of Zoledronate and the injectability of the material make it very promising for local bone augmentation and the repair of non-load bearing and difficult-to-access bone defects.

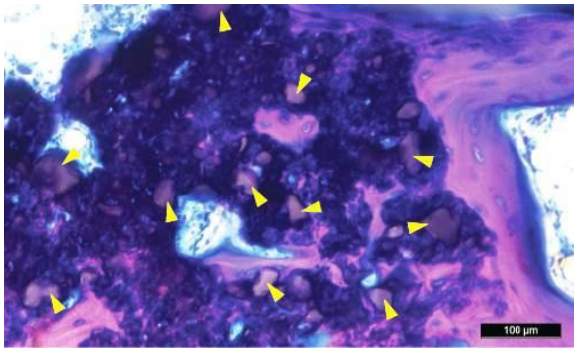

Fig. 2: Giemsa stained ground section of one sample from the nHA-Gel-group showing mineralized granules (yellow arrows) embedded in newly formed bone (pink).

ACKNOWLEDGEMENTS: This project was partly sponsored by a CTI grant (no. 11098.1).

Tuning the properties of alginate hydrogels for cell microencapsulation

François Noverraz, Solène Passemard, Virginia Crivelli, Redouan Mahou, Françoise Borcard, Sandrine Gerber-Lemaire*, Christine Wandrey

Ecole Polytechnique Fédérale de Lausanne, ISIC, CH-1015 Lausanne, Switzerland

INTRODUCTION: Cells microencapsulation is a promising technology allowing the treatment of various diseases through cells transplantation. Capsules are made of biocompatible hydrogels which require specific physical properties[1]. Lifetime of the microspheres (MS) is given from their stabilities in physiological media. Therefore investigation of several chemical modifications were done on alginate(alg)-based hydrogels with the conjugation of poly(ethylene glycol) PEG 1000 and 2000 either on hydroxyl or carboxylic groups of the alg backbone (**Scheme 1**). Physical properties of the resulting MS are reported and compared between the different systems investigated.

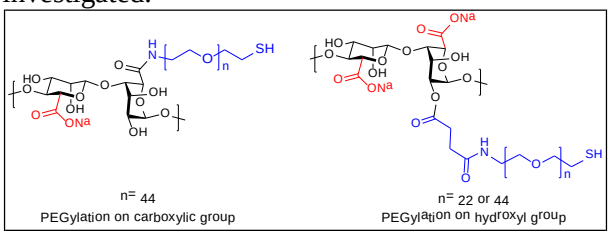

Scheme 1: PEGylated Na-alg with two different systems.

METHODS:

Synthesis of α-amino-ω-mercapto PEG1000

- α-Amino-ω-mercapto PEG derivatives were synthesized starting from commercially available PEG 1000 and 2000. The unsymmetric alteration was performed through mono-Staudinger reduction as a key step[2]. Thiol functionality was then introduced by copper click reaction.

Modification of Na-alginate

- Na-alg was modified by grafting linear α-amino-ω-thiol PEG 1000 and 2000 either to the carboxyl or hydroxyl groups up to 5 % of grafting. Different types of covalent linkages were investigated for the grafting step.

Microsphere formation

- A BÜCHI Encapsulator B-395 Pro (BÜCHI Labortechnik AG, Switzerland) was used to extrude the polymer solutions into a gelation bath containing $CaCl_2$.

Characterization of the polymer solutions

- All polymer solutions were prepared at defined concentrations and characterized by their dynamic viscosity. The osmolality and the pH were adjusted to physiological conditions.

Physical characterization of microspheres

- The size of the MS, swelling in different media, and stability were observed by optical microscopy. Water uptake was gravimetrically determined. Mechanical stability, deformability and mechanical resistance to compression were analysed using a TA-XT2i (Stable Micro Systems, Godalming, UK). Ingress diffusion experiments using fluorescence labelled dextran standards (40, 70, 150 kg/mol) served to estimate permselectivity.

RESULTS: Drastic changes of physical properties of the MS were observed depending on the grafting sites, degree of grafting and PEG chain length. Inserting PEG on carboxyl functional groups decreased the available sites needed for electrostatic crosslinking with calcium ions. Grafting on hydroxyl groups was thus investigated to preserve the integrity of the electrostatic crosslinking. Both systems exhibit covalent crosslinking through disulfide bond formation. Enhanced mechanical resistance to compression and higher stability over time were observed when grafting was done on the hydroxyl groups. The PEG chain length displayed strong impact on the hydrogel network density and also influenced the permeability and the mechanical resistance of the resulting MS.

DISCUSSION & CONCLUSIONS: Alginate-based MS with tunable physical properties were developed to answer the various needs for microencapsulation of specific cell types. Reinforcement of the electrostatic network is provided by chemical crosslinking using thiols as reactive functionalities. In addition, the grafting of heterobifunctional PEG derivatives on the alg backbone offers the possibility for further fuctionalization with bioactive agents to be released after transplantation. Biocompatibility of all MS systems was confirmed *in vitro* with different cell types.

ACKNOWLEDGEMENTS: The SNSF, the CTI and BÜCHI Labortechnik AG, Switzerland supported this research.

Optimization of silk mesh for soft tissue reinforcements: preliminary *in vitro* investigations toward cell-based therapy

Guillaume O.[1,3], Park J.[1], Monforte X.[2], Redl H.[1], Petter-Puchner A.[1], Gruber-Blum S.[1] and Teuschl A .[1,2]
1-Ludwig Boltzmann Institute for Experimental and Clinical Traumatology, Vienna, AUT. 2- University of Applied Sciences Technikum, Vienna. 3- AO Research Institute, AO Foundation, Davos, CH.

INTRODUCTION: Abdominal wall hernia is a recurrent problem in our society and requires the implantation of over one million of meshes every year. Recently, hernia regeneration using advanced cell-based therapies have shown great potential [1]. Indeed, covering the mesh with cells prior to the implantation improves the tissue integration and the rate of recurrence. However, the main limitation is the extensive *in vitro* cultivation period required. The aim of this work is to modify the surface of degradable mesh made of silk in order to enhance *in vitro* the ability of the cells to attach and to colonize the material.

METHODS: Silk meshes were manufactured using a Silver Reed knitting machine. Covalent immobilization of pro-adhesive glycoprotein (i.e. lectin) on the silk was performed using carbodiimide chemistry [2]. As a proof of concept, we investigated *in vitro* how fibroblasts attach and proliferate on the surface of the modified silk. Quantification of cell adhesion and proliferation was assessed using MTT and DNA test. The cells were evaluated using Live/Dead staining and SEM observation. In parallel, we investigated the inflammatory response of the modified silk on peripheral blood mononuclear cells (PBMC).

RESULTS: Our preliminary experiments realized on fibroblasts demonstrated that grafting lectin to the surface of silk meshes significantly enhanced cell attachment and accelerated the proliferation. Indeed, within a short-term incubation period, the modified silk meshes were covered by cells (Fig 1). In comparison, the controls (PP and native silk) did not promote similar response. In addition, investigations performed on PBMC revealed that the modification of silk by lectin immobilization did not exacerbate the pro-inflammatory reaction in comparison to standard biomaterials.

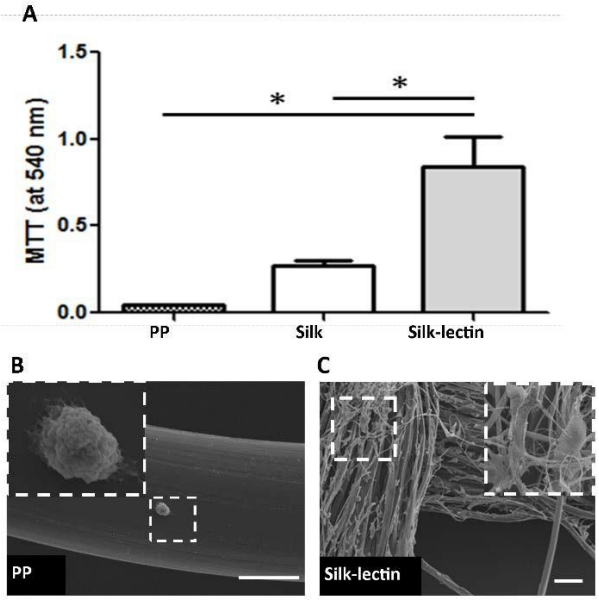

Figure 1: Quantification of fibroblast adhesion on meshes after 4 days of incubation (**A**) and SEM observations of cells on control polypropylene (PP) mesh (**B**) compared to silk-lectin (**C**).

DISCUSSION & CONCLUSIONS:

Developing a new material suitable for cell-based therapy would bring remarkable benefit for soft tissue repair. In this study, we successfully grafted pro-adhesive plant-derived molecule that promotes the attachment of cells onto the mesh.

The second advantage is the utilization of silk fibres, a promising candidate for various tissue engineering applications. We hypothesize that the creation of a long-term biodegradable mesh should prevent major post-implantation complications observed during the utilization of permanent meshes. Further investigations are required to clarify how cell-seeded meshes perform in animal model and how other cells will attach to this new bioactive mesh.

ACKNOWLEDGEMENTS: The financial support by the City of Vienna (MA 27, Project 12-06) is gratefully acknowledged.

Material degradation mechanism and wear modeling of metal-on-metal artificial hip joints

S Cao, S Mischler

Tribology and Interfacial Chemistry Group, Swiss Federal Institute of Technology Lausanne (EPFL), Switzerland

INTRODUCTION: Hip joints, involving femoral head and acetabular cup, provide the most important movement of the human body. Unfortunately, the natural hip joints sometimes lose functionality as a consequence of diseases or accidents. Hip joint replacement is a common clinical solution in such events. Polymer (UHMWPE), metal (CoCrMo alloy, stainless steal, titanium alloy) and ceramics (Alumina) have been adopted for the different parts of artificial hip joints. However, wear is a major problem causing the failure and limiting the long-term performance of artificial hip joints, especially for the polymer acetabular cup. As alternative, metal-on-metal (MoM) couplings offer a unique combination of wear and impact resistance, but the continuous release of nano-sized metal particles and ions into the body is of long-term concern as it can cause allergies and other toxic reactions. In order to better control the release of metal ions, the wear mechanisms should be identified and predictive models should be developed.

METHODS: The femoral head and the acetabular cup are surrounded by synovial fluid, which act as lubricant, alleviating the wear of implants but also introduce corrosion. The interaction of mechanical wear and electrochemical corrosion, nominally tribocorrosion, has been proposed as one of the crucial degradation mechanisms of implants [1,2] and recently saw significant progress in mechanistic understanding and modeling [1-3]. However, these studies neglect lubrication effects in the overall degradation. Indeed, Dowson [4] showed a clear relation between wear and hydrodynamic lubrication of MoM artificial hip joints.

So, in this study, a wear model for passive metals undergoing plastic deformation at asperity contacts combining mechanical wear (Archard's law), chemical wear (wear accelerated corrosion) and hydrodynamic lubrication was proposed to quantitatively describe and predict material damage.

RESULTS: As applied to CoCrMo sliding tribocorrosion contacts, the model predicts remarkably well wear rates observed in tribometers and the running-in wear rate in simulators, as shown in Fig. 1. In the case of MoM hip joints, the model predictions concerning the effect of parameters such as normal load, head radius and clearance closely correlate with experimental observations.

According to the model, both mechanical and chemical wear significantly contribute to hip joint degradation. Thus predictions based on only one mechanism likely lead to erroneous conclusions. This is for example the case of head radius that while having a significant effect on mechanical wear little affects chemical wear.

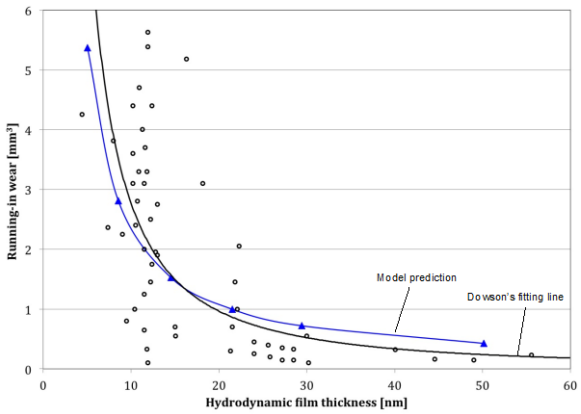

Fig. 1: The experimental running-in wear results (circular dots) with different film thicknesses and fitting line from [4] and model predicted values (triangular dots and interpolation) (R=18 mm, c_R=200 μm, 100 μm, 50 μm, 30 μm, 20 μm and 10 μm, successively)

Ag-nanoparticle formation via electron transfer through peptides

S. Kracht[1], M. Messerer[1], K. M. Fromm[1], B. Giese[1]

[1] *Department of Chemistry, University of Fribourg, CH.*

INTRODUCTION: More and more metal ions and nanoparticles with antimicrobial properties are used in medicine. Silver is known to possess good antimicrobial properties, but it is largely unknown how the organism, or on the smaller scale enzymes, peptides and amino acids, react upon that presence. With their different functional groups and heteroatoms, proteins offer many possible binding sites for metal ions. Additionally, amino acids like tyrosine can act as electron donor for the metal ion under certain conditions. In particular for silver ion, the question rises if a reduction of the metal ion to nanoparticles can occur? With the help of a model tetrapeptide chosen based on former research[1] we started investigating this question.

METHODS: The tetrapeptide Ac-L-His-L-Pro-Aib-L-Tyr-NH_2 **1** was synthesised by solid phase peptide synthesis following the Fmoc strategy. Continuous irradiation experiments were performed with a Hg-lamp attached to an irradiation bank.

RESULTS: Laser irradiation (λ=308 nm) of a peptide **1**-Ag^+ complex (Fig. 1) in aqueous solution did not show the appearance of AgNP as a reduction product. The only new UV-vis bands were due to tyrosine dimerisation products obtained after irradiation.

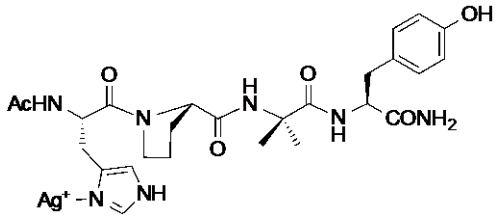

*Fig. 1: Model peptide **1** bound to silver ion.*

However, as soon as chloride ions are added to this solution, the formation of nanoparticles (NPs) occurs within minutes. Two different species **NP-2** and **NP-3** were formed, of which **NP-2** transforms into **NP-3** as irradiation goes on. This is indicated by the isosbestic point shown in Fig. 2. EDX-TEM and powder X-ray diffraction revealed the composition of **NP-2** (Ag@AgCl nanocomposites) and **NP-3** (AgNPs).

Control experiments using peptides without tyrosine revealed that the two species **NP-2** and **NP-3** were only formed in the presence of tyrosine. The reaction kinetic is furthermore dependent on the pH and the chloride concentration. The exchange of histidine as the silver-binding amino acid by different amino acids showed mostly only the formation of **NP-3**.

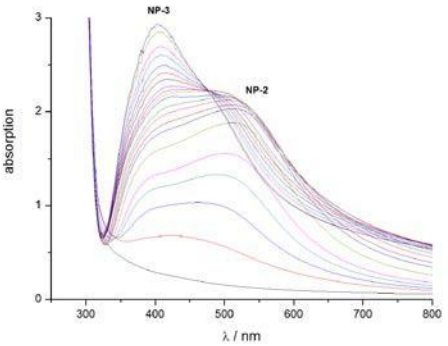

*Fig. 2: Time resolved UV-vis spectra of **1**-Ag^+ irradiated in the presence of Cl^- at pH 12.5.*

DISCUSSION & CONCLUSIONS: Our results[2] can be explained by the action of tyrosine as an electron donor upon irradiation and a following electron transfer through the peptide to reduce the histidine-bound Ag^+ to Ag^0. The AgNP formation however only occurs when Ag^+ is preorganized in the form of AgCl because the redox potentials of the Ag^0 formation on the atomic level and in bulk are very different. Hence, only in cases were the produced Ag^0 are in close proximity to each other, they live long enough to combine and form AgNP which then are identified by their characteristic plasmon resonance bands in UV-vis measurements.

ACKNOWLEDGEMENTS: We thank the University of Fribourg, the NCCR for Bioinspired Materials and FriMat for generous funding.

Improvement of mechanical properties of 3D printed hydroxyapatite scaffolds by culture of osteoblast-like cells under perfusion flow

N Rimmer[1], F Burgio[1], A Rohner[1], P. Chavanne[1], S Zimmermann[1], P Gruner[2], R Schumacher[1], M de Wild[1], A Papadimitropoulos[3,4], I Martin[3], M Beaufils-Hugot[1], U Pieles[1]

[1]FHNW, University of Applied Sciences and Arts of Northwestern Switzerland, Muttenz CH, [2]Medicoat AG, Mägenwil CH, [3]DBM, Department of Biomedicine, University Hospital Basel CH, [4]Cellec Biotek AG, Basel CH

INTRODUCTION: 3D-printed hydroxyapatite (HA) scaffolds with defined macro porosity have emerged as attractive biomaterials in tissue engineering. However their brittleness restricts their practical applications. In this study, we aimed at improving their mechanical properties by (i) surface treatment (oxygen-plasma) during the production, and (ii) deposition of extracellular matrix (ECM) by human osteoblastic cells (MG-63) during culture under perfusion flow. Mechanical compression tests were performed to measure the stiffness of the resulting materials.

METHODS: Untreated and plasma-treated 3D printed HA scaffolds (diameter 10mm, thickness 4mm, Z-510 3D-Systems, HA powder Medicoat AG) were seeded with 1Mio MG-63 with the use of a perfusion bioreactor device (U-CUP; Cellec Biotek AG) in complete medium. Following 3 days of culture, the medium was supplemented with osteoblast stimulators to induce differentiation for up to 28 days. Samples were analysed at different time points by scanning electron microscopy, MTT and DNA content assays to evaluate cell attachment, distribution and proliferation. Quantitative real-time PCR and alkaline phosphatase (ALP) activity assay were performed to assess osteoblast differentiation. Mechanical tests were done on scaffolds in wet state after 28 days of culture. Constructs in static conditions and empty scaffolds were used as controls.

RESULTS: Under dynamic conditions, cells were found to be uniformly distributed within the pores of the scaffolds (MTT; Fig.1A) following an 18 hours seeding process, while cell numbers were found to be significantly higher at each time point (DNA content; Fig.1B), as compared to the static conditions. Hydrophilic surface modification by oxygen-plasma treatment contributed also to accelerate the on-set of ECM deposition, as indicated by the earlier (i) saturation of proliferation (Fig.1B, red), and (ii) up-regulation of osteoblastic-related genes, as compared to un-treated scaffolds (ALP mRNA up-regulation at Day7 (4.5-fold)). Importantly, the elastic gradient of this cell-enhanced biomaterial generated in perfusion bioreactors (n=3) increased from 14.3 ± 0.08 to 19.3 ± 0.03 MPa from empty to matrix deposition scaffolds.

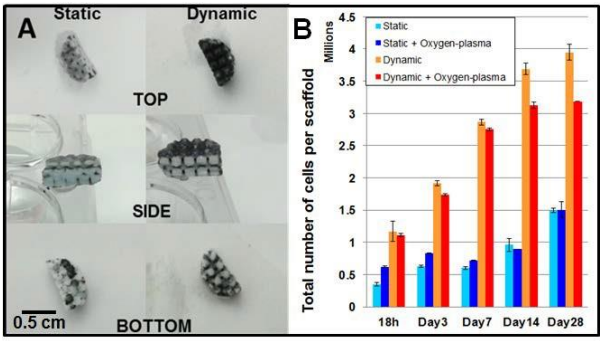

Fig. 1: MG-63 proliferation on 3D-printed HA scaffold. (A) MTT staining after 18 hours seeding in static (left) and dynamic (right) conditions. (B) DNA content assay of cells seeded on untreated (light blue and orange) or plasma-treated (dark blue and red) scaffolds for up to 28 days of culture under static (blue) and dynamic (red) conditions.

DISCUSSION & CONCLUSIONS: Plasma-treated 3D-printed porous HA scaffolds (cell-enhanced biomaterials) seeded with human osteoblast-like cells cultured dynamically in perfusion bioreactor showed clearly a mechanical improvement in terms of stiffness. This experimental setup shall be assessed by using stem cells, which typically have a higher potential of ECM deposition than MG-63 cells.

ACKNOWLEDGEMENTS: This work is supported by a grant from the Schweizerischer Nationalfonds (SNF) (Grant number: 51NF40-144618).

From the laboratory to the clinic: a revolutionary surface treatment for bone-anchored implants

S Buchini[1], R Curno[1], P Péchy[1], B-O Aronsson[1]

[1] *Nano Bridging Molecules SA, Rte de Cité Ouest, Gland, CH.*

INTRODUCTION: SurfLink® is a novel surface treatment for metallic and ceramic implants, consisting of a monolayer of phosphorous-rich molecules permanently bound to the implant surface. The treatment has been shown to promote osseointegration. This abstract will present an overview of the SurfLink® development from the pre-clinical proof of concept testing to the application in the clinics.

METHODS: *Biomechanical rat study*: 22 rats were implanted with either SurfLink® treated or control titanium rods in each proximal tibial metaphysis. The rats were sacrificed after 6 weeks and implant pull-out strength was recorded. *Ectopic bone rat study*: SurfLink® treated were compared to control cylinders in an ectopic bone rat model. After 5 weeks osteoid formation was assessed by histological analysis. *Sheep study*: Roughened dental implants (SPI® Element, Thommen Medical) with either SurfLink® treatment or no treatment (control) were placed in the pelvis of 24 sheep. Animals were sacrificed after 2, 8 and 52 weeks. Osseointegration was assessed by histological, biomechanical and SEM analyses. *Clinical study*: Dental implants (SPI® Element, Thommen Medical) with either SurfLink® treatment or no treatment (control) were placed in 21 patients requiring at least 2 single implant-supported crowns. Split-mouth, prospective, randomised design was followed. Outcome measures: implant success, marginal bone level changes, complications and adverse events, and marginal bleeding.

RESULTS: Biomechanical rat study[1]: SurfLink® treated implants showed a statistically significant increase in the mean pull-out strength (+38%) compared to control implants ($p<0.01$).

Ectopic bone rat study[1]: faster and increased osseointegration was observed with SurfLink® treated implants. The gap between the bone and implant surface was eliminated (Fig. 1).

Sheep study[2]: SurfLink® treated implants significantly improved early and long-term implant fixation and promoted faster osseointegration (Fig. 2).

Clinical study[3,4]: SurfLink® dental implants have been placed in more than 100 patients, demonstrating safety and efficacy of the treatment. One year post-loading data from the first group of 21 patients suggested a significant reduction in peri-implant bone loss with SurfLink® treated compared to control implants (Fig. 3).

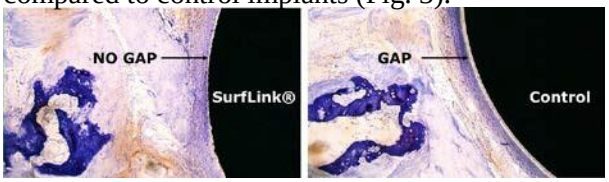

Fig. 1: Rats histological cross section, 5 weeks.

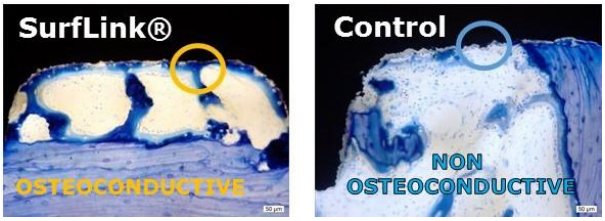

Fig. 2: Sheep histological cross sections, 2 weeks.

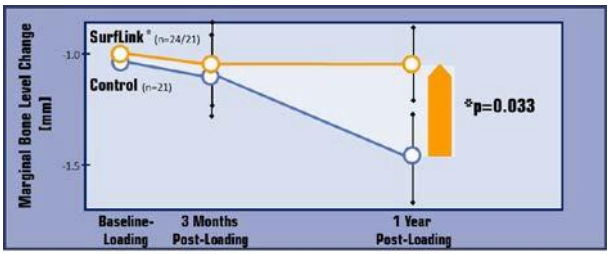

*Fig. 3: Marginal bone level change. *n=21. Three patients had 1 additional SurfLink® treated implant each: average values of the two SurfLink® treated implants were used in the statistics.*

DISCUSSION & CONCLUSIONS: From the initial bench and pre-clinical testing, the SurfLink® technology has successfully reached the clinics. Both pre-clinical and clinical data suggest that SurfLink® treated implants heal and osseointegrate quicker and remain stable in the long term.

Histology-validated, phase-contrast tomography for visualizing the cerebellum

Christos N. Bikis, Georg Schulz, Bert Müller, and Simone E. Hieber

Biomaterials Science Center, University of Basel, Basel, Switzerland

INTRODUCTION: Located at the bottom of the brain, the cerebellum plays a pivotal role in motor function and is also involved in navigation, speech, and gaze control. Recently, it has been linked to cognitive tasks such as working memory, linguistic and social skills, as well as emotional experience. In terms of clinical manifestation, cerebellum disease is most commonly associated with hypotonia, ataxia, and equilibrium or gait disorders.[1] Investigating the spectrum of the cerebellum's functions in health and disease is thus a contemporary area of neuroscience research. The remarkably uniform cerebellar cyto-architecture and its distinct cortex layering, compared to the cerebral cortex, make the cerebellum a prime target for research based on microanatomy. Towards that direction, phase-contrast, hard X-ray computed tomography was used to scan human cerebellum tissue with isotropic resolution *post mortem*. The grating-based configuration is known to yield superior contrast. Validated by and complementing conventional histology, this non-destructive visualization should provide information on the three-dimensional arrangement of cerebellar layers and on the neuronal pathways involved in brain function and regeneration capacity.

METHODS: The cerebellum of a donor was extracted *post mortem*. Subsequent to formalin fixation and paraffin embedding, a cylindrical part was extracted. This cylinder about 6 mm in diameter was scanned at the beamline ID19 of the European Synchrotron Radiation Facility (ESRF), Grenoble, France. The photon energy was 19.5 keV and the grating-based phase imaging resulted in an effective pixel size of 5 µm. Subsequently, selected haematoxylin/eosin–stained histological slices were also prepared.

RESULTS: In the cerebellar cortex, the molecular layer, the granular layer, and the white matter were clearly distinguished, with a contrast high enough for intensity-based segmentation, as indicated in Figure 1. The comparison of the anatomical features found in histology and grating-based phase tomography validates that the volume of each layer can accurately be measured within the cerebellum tissue.

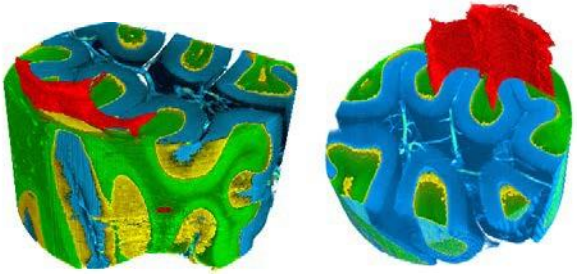

Fig. 1: Intensity-based segmentation of grating-based hard X-ray tomography data allows for the three-dimensional visualization of the cerebellar features: molecular layer (blue), granular layer (green), white matter (red), vessels (turquoise). First two layers have been partially removed digitally to depict white matter arborisation.

DISCUSSION & CONCLUSIONS: Grating-based, hard X-ray phase tomography holds considerable promise for the visualization of brain microanatomy. Especially for the cerebellum, being able to accurately quantify both the whole tissue volume as well as the thickness of each layer helps investigate the cases of cerebellar pathology. In the diseased state, one finds a characteristic reduction of total volume and/or specific layer thickness. Grating-based phase tomography has yielded sufficient contrast for segmentation by simple thresholding, but because of the limited spatial resolution only a number of the large Purkinje cells could be identified, as reported previously.[2] Since the in-line phase tomography reaches a weaker contrast but a better spatial resolution,[3] research should be directed towards the visualization of individual cells to clearly identify pathological conditions with reduced cell density and cell morphology changes.

ACKNOWLEDGEMENTS: The authors thank S. Frank, J. Hench and G. Schweighauser from the Department of Neuropathology (University Hospital of Basel) for the histology sections and the valuable discussion on brain anatomy.

Injectable and memory shape 3D scaffolds for tissue engineering applications

A Béduer[1]*, T. Braschler[1]*, S. Mosser [1], P. Fraering [1], S. Bencherif[2], D.J . Mooney [2] and P. Renaud [1]
[1] *EPFL, LMIS4-CMSN Station 17, 1015 Lausanne, Switzerland,* [2] *Mooneylab, 60 Oxford St, Harvard University, 02138 Cambridge MA, USA*

INTRODUCTION: Scaffolds made from various hydrogels have been proposed in order to support and protect the transplanted cells, guide graft growth and facilitate its integration with the host tissue. However, the transplantation of such scaffolds remains a surgical challenge. One proposed solution consists in minimally invasive delivery of in-situ gelling formulations or scaffold suspensions [2] through narrow-bore needles. However, without the guidance of a large-scale organized scaffold, the transplanted cells typically build disorganized structures rather than repairing the native tissue architecture as desired. The scaffolds developed here are both: organized at a large size scale, and nevertheless injectable through narrow bore needle thanks to their compressibility and memory shape properties. To the best of our knowledge, the injectable neuronal scaffolds reported here are the first to combine macroscopic scaffold size and injectability through a narrow-bore conduit.

METHODS: Cryogels were synthesized based on established carbodiimide chemistry [3]. Autoclave-sterilized cryogels were coated prior to cell culture with poly-L-ornithine and laminin. Mouse primary cortical neurons were seeded onto cryogel and control substrates at a density of 4000 cells/mm^3. Actin cytoskeleton and cell nuclei were stained. Cell density and neurite length were quantified and measured based on confocal images. For cell survival analysis, samples were incubated in a trypan blue solution (0.4% in HBS).

RESULTS: After neurons seeding and 7 days in vitro (DIV), we observe a complex network of neurites with a homogeneous cell density throughout the 1mm thick scaffold. Cell densities was above 40.10^6 cells/mL. It approaches the ones found in the mouse cortex (92*10^6 cells/mL[4]), and are 10 times higher than the densities that can be obtained with homogeneous gels. Mean neurites length increased with time also showing the compatibility of the developed scaffolds with long term neuronal culture (21 DIV). The main interest of the developed scaffolds is that they are designed to be highly compressible. The scaffolds can be partially dehydrated, reducing the size of the scaffold and allowing to perform injection through a syringe needle (1a). After injection, scaffolds retrieve their initial shape and volume. We thus investigated cell survival to the injection of the 3D cellular construct through a 16Gauge needle (volume reduction of 90%) performed after 7 days of culture. The injection step does not affect the viability of primary neurons (1c) and even the developed long neurites did not suffered from the injection (1d).

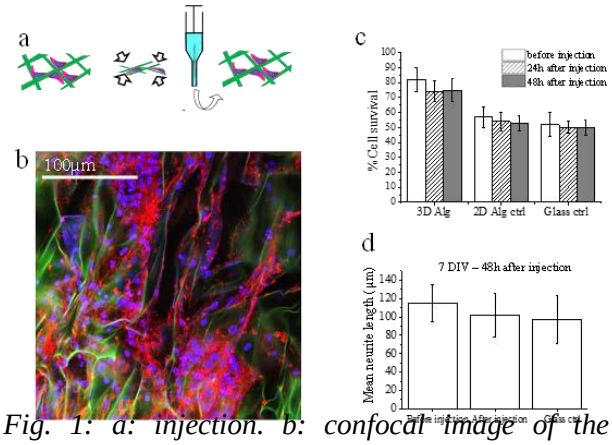

Fig. 1: a: injection. b: confocal image of the scaffold after its injection. c: cell survival scores before and after the injection step. d: effect of the injection step on neurites length.

DISCUSSION & CONCLUSIONS: The 3D structure, with its high available surface area and high pore space for nutrient diffusion is responsible for sustaining high viability at these high cell densities. The gels are soft at the macroscopic scale, enabling syringe injection and potentially good cellular scaffold integration in the target tissues. At the same time, the scaffold material has a high local Young modulus, allowing to protect the neurons during injection.

The scaffolds will thus allow to transfer *in vivo* not only the cells, but also their precise spatial organization in a minimal invasive way, without damaging the neighboring tissues.

.

Explanted tendons remain viable only under in vitro mechanical stimulus

S Wunderli[1,2], J Widmer[1,2], U Silván[1,2], JG Snedeker[1,2]

[1] *Department of Orthopaedics, Universitätsklinik Balgrist, University of Zürich, CH.* [2] *Institute for Biomechanics, D-HEST, ETH Zürich, CH.*

INTRODUCTION: The mechanisms by which mechanical loading affect the outcome of injured tendons remain unclear, such as how the extracellular matrix may act as a transducer of mechanical signals that guide tissue remodelling through tendon cells [1]. In the present study we have established an experimental baseline for modelling tendon matrix regeneration as a function of cell-perceived mechanical stimulus. A custom-designed tendon explant bioreactor allows the simultaneous mechanical loading of tendon explants under controlled conditions. Future results obtained by the introduced platform are expected to contribute to basic tendon research and therapeutic developments that may shape the future of orthopaedic medicine.

METHODS: In our pilot study tendon fascicles were isolated from wild-type B6 mouse tails and randomly assigned to the untreated control group (UC) or one of the treatment groups. Explants in the treatment groups were cultured for 6 days under either free floating unloaded (FU) or dynamic loading (DL) conditions in serum-free nutrient medium at 29°C in a CO_2 incubator. DL samples were exposed to interval cyclic stretch to 0.25%L_0 in a custom-built bioreactor (Fig. 1). The initial length (L_0) was manually set at crimp disappearance of each probe.

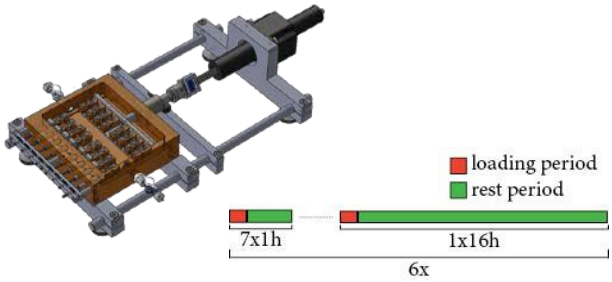

Fig. 1: Eight mouse tail tendon explants were stretched for 138h in the scalable bioreactor unit

Following treatment FU and DL were formalin fixed for immunofluorescent staining of actin and nuclei or ramped to failure on a material testing machine. UC samples were fixed and mechanically tested right after isolation from the mouse tail. All material properties were evaluated as previously described by Fessel and Cadby [2].

RESULTS: Preliminary data showed no significant differences in e-modulus and failure stress of treated fascicles compared to UC (Table 1). Failure strain was reduced in dynamically loaded explants. The continuous cytoskeletal network was disrupted in the FU treatment group, while the cells in the dynamically loaded sample showed parallel alignment to the stretch axis (Fig. 2). In both treatment groups the nuclei were rounded compared to the untreated control.

Table 1: Mechanical properties of tendon explants

	UC (n = 6)	FU (n = 6)	DL (n = 3)
E-Modulus [MPa]	1149 ± 190	1352 ± 207	1356 ± 220
Failure stress [MPa]	63 ± 11	75 ± 13	64 ± 10
Failure strain [%]	12.7 ± 1.6	12.8 ± 2.3	8.4 ± 0.8

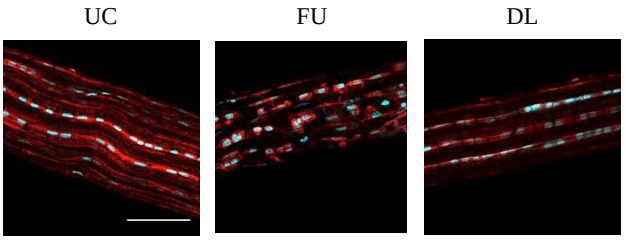

Fig. 2: Immunofluorescent staining of actin cytoskeleton (red) and cell nuclei (blue). Scale bar 100μm

DISCUSSION & CONCLUSIONS: Our pilot study indicates that mechanical load is necessary to maintain tendon cell alignment in *ex vivo* tissue models. It is probable that cellular alignment does not influence the mechanical properties of tendon explant and that failure properties of the tissue might change due to prolonged clamping. The established platform can be used to mechanically condition connective tissues and to study mechanics-driven evolution of their structure and function. In the future this scalable platform should enable high throughput studies of cell-matrix response in damaged and healing tendons.

ACKNOWLEDGEMENTS: *We gratefully acknowledge the invaluable support of Mr. Hansrudolf Sommer in device design and construction. This study was funded by ETH Grant ETH-1213-2.*

In-situ crosslinkable, extracellular matrix based scaffold for cartilage repair

Emma Cavalli[1], Claudia Loebel[1,2], David Eglin[2], Marcy Zenobi-Wong[1]

[1]*Cartilage Engineering + Regeneration, ETH Zürich, Zürich, Switzerland,* [2]*AO Research Institute, Foundation, Davos, Switzerland*

INTRODUCTION: In this study we present a novel scaffold for cartilage repair based on cartilage extracellular matrix (ECM) fragments and tyramine modified hyaluronic acid (HA-tyr). Cartilage fragments have been used to improve the tissue quality after bone marrow stimulation and to promote chondrogenesis of MSCs. They are FDA approve and commercialized by Arthrex as Biocartilage®. HA-tyr is an injectable hydrogel that can undergo in situ crosslinking in the presence of horseradish peroxidase (HRP) and hydrogen peroxide (H_2O_2). Its mechanical, swelling and degradation behaviour can be precisely controlled by tuning the degree of substitution. In addition the crosslinking reaction is based on the formation of covalent bonds between hydroxyphenyl groups that are present both in HA-tyr and in tyrosine residues of cartilage matrix proteins[2]. Hence, the HA-tyr can be enzymatically crosslinked to both the cartilage fragments and to the cartilage defect promoting initial adhesion and integration of the scaffold (Fig.1).

METHODS: HA-tyr was synthetized according to a newly established protocol which uses DMTMM as a coupling agent[1]. Cartilage particles were obtained by cryomilling calf articular cartilage. Push-out tests were performed at 0.5 mm/s with a 3 mm rod on gels that were either "crosslinked" in cartilage rings (8mm outer diameter, 4mm inner diameter) or pressfit in similar rings. Cell activity was studied by performing MTS assay on bovine chondrocytes (bCh) encapsulated in HA-tyr gels with and without cartilage particles. Growth factors release from the particles was investigated with ELISA assays.

RESULTS: Initial bond strength of HA-tyr gel crosslinked to cartilage rings was 714 Pa: 5 times the bond strength of a non-adhesive gel (alginate). Encapsulation of cells in HA-tyr gels increases the bond strength to 2053 Pa after 5 weeks of culturing. In addition the digestion of GAGs by chondroitinase and the subsequent exposure of the tyrosine groups of collagen yielded a bond strength of 5480Pa, 4 times higher than the bond strength of an adhesive gel (fibrin glue) (Fig.2, left). The cartilage fragments contain the key components of cartilage, including collagen 2, proteoglycans and growth factors (eg. IGF-1 and FGF-2) and induced cell proliferation as shown by the MTS assay (Fig.2, right).

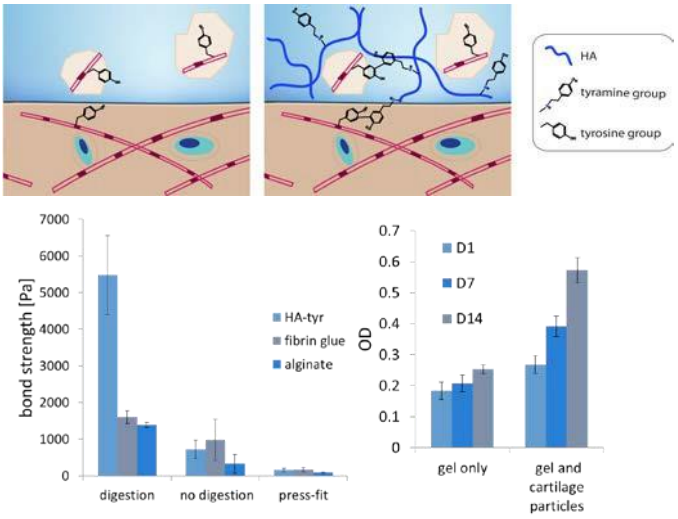

Fig. 2: Left, Initial bond strength of HA-tyr, fibrin glue and alginate. The gels were either pressfit in the cartilage rings, or crosslinked in the ring with- or without digestion. Right: MTS assay of bCh encapsulated in HA-tyr gels with and without cartilage particles.

DISCUSSION & CONCLUSIONS: This study presents a novel ECM-based scaffold whose crosslinking is initiated by enzymatic reactions between tyramine groups. Cartilage fragments were used as bioactive filler as they contain large amounts of GAGs, collagen 2 and other key biological cues, while HA tyr was used as the biological glue which converted the individual particles into a mechanically intact and stable scaffolds. Push-out tests indicate that HA-tyr can be enzymatically crosslinked to both the cartilage fragments and to the cartilage defect.

ACKNOWLEDGEMENTS: This project was funded by the ETH Foundation (Grant ETH-50 13-1)

In vitro lymph node to study stromal cell-mediated T cell migration

Cara F. Buchanan[1] and Melody A. Swartz[1]

[1]*Institute of Bioengineering, École Polytechnique Fédérale de Lausanne, Lausanne, CH*

INTRODUCTION: Fibroblastic reticular cells (FRCs) are the primary stromal cell type of lymph nodes (LNs), forming an interconnected network that guides the interaction of T lymphocytes and antigen presenting cells[1]. During inflammation, FRC proliferation and lymphatic vessel dilation occurs, leading to increased flow and changes in the cytokine milieu that further promote guided lymphocyte-antigen encounters. While this suggests that LN stromal cells direct the quality and type of immune response, the physical mechanisms by which the stromal network regulates adaptive immunity are largely unknown. To address this issue, we developed an in vitro model of the LN paracortex to investigate the interdependence of T cell migration and activation on stromal cell-derived microenvironmental cues. The model will be used to study how stromal cell-lymphocyte interactions help prime T cells under simulated naïve or inflammed conditions.

METHODS: A multi-level PDMS microdevice was fabricated by soft lithography and bonded to APTES treated TCPS by oxygen plasma. FRCs and dendritic cells (DCs) harvested from LNs and bone marrow of C57BL/6 mice[2] were mixed in 0.02% collagen and injected in the center shallow region of the device (3D), while lymphatic endothelial cells (LECs) were seeded in the deep side channels (2D). Cell viability and expression of phenotypic markers were assessed to validate the model. Then, fluorescently labeled $CD8^+$ OT-I cells, which specifically recognize the antigen ovalbumin (OVA), were added to track velocity, migration and interaction using live microscopy. Stromal cells were primed with OVA peptide in the presence or absence of IFNγ and TNFα.

RESULTS: LN stromal cell viability and a phenotypically distinct LEC ($gp38^+CD31^+CD45^-$) and FRC ($gp38^+CD31^-CD45^-$) morphology is maintained up to 3 days. Under inflammatory conditions, FRCs increase matrix contractility as measured by confocal reflectance microscopy, as well as expression of MMP-3, MMP-9, and adhesion molecules ICAM-1 and VCAM-1. T cell velocity, directed migration, and interaction time was greatest during co-culture with FRCs, LECs, and DCs primed with IFNγ or TNFα, compared to that of DCs alone or T cells alone, thereby suggesting that during inflamation, matrix remodeling and adhesion molecule expression by LN stromal cells generates a path of least resistance to guide T cell migration.

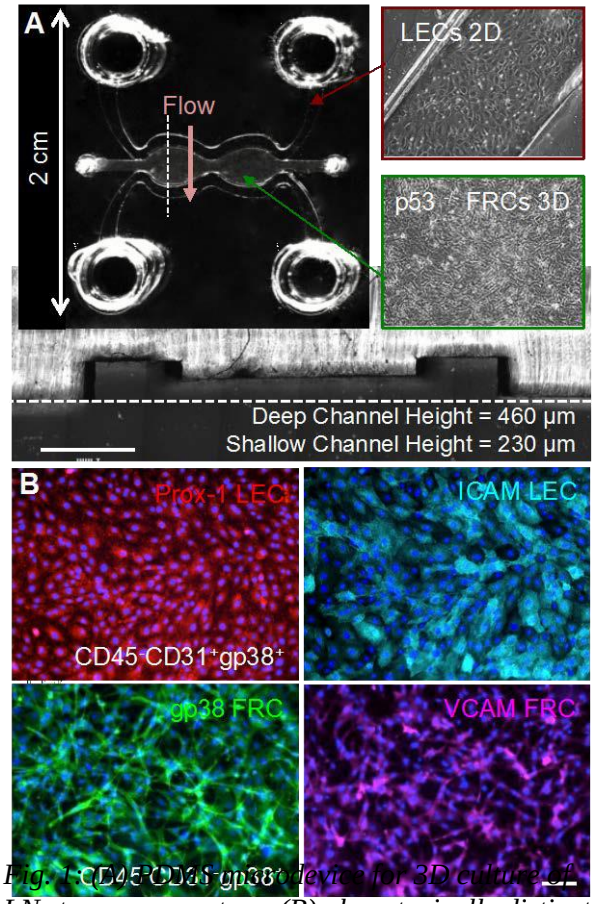

Fig. 1: CD45-CD31-gp38- device for 3D culture of LN stroma generates a (B) phenotypically distinct compartment to track T cell interactions in vitro

DISCUSSION & CONCLUSIONS: The development of a functionally relevant in vitro LN model can drive important and complimentary insights compared to that of either traditional cell culture or animal models alone. With the ability to quantify and differentiate contributions of specific cell types, as well as precicely modulate parameters such as flow rate, cytokine or antigen delivery, the tissue-engineered LN has the potential to enhance our understanding of how the LN stroma modulates adaptive immunity.

Texture and shape quantification to characterize angiogenesis in tumour tissue

Marco D. Dominietto, Peter Thalmann, Sabrina Lang, Simone E. Hieber, Georg Schulz, and Bert Müller

Biomaterials Science Center, University of Basel, Switzerland.

INTRODUCTION: Derivation of quantitative information descripting tissue morphology and physiology is critical for the detection and staging of a disease, as well as for treatment follow-up.[1] The aim of this work is to present a mathematical framework that explicitly considers the spatial variability within data sets. Such framework consists of two classes of geometrical estimators[2]. The texture class allows estimating the fractal dimension (FD), a measure of the self-similarity at lengths from 50 µm to 10 mm, and the lacunarity (L), which quantifies the relative distribution of substructures within the tissue. The shape class yields measures of the compactness, which describes the deviation of a mass from spherical symmetry, and the signature, which is a measure of the branching (or infiltration) of the tumor into the surrounded healthy tissue.

METHODS: The analysis was applied to tissues of twelve mice injected with C51 tumor cells: Six mice were treated with a pro-angiogenic drug (dimethyloxalylglycine, DMOG) and six with a placebo (saline). We analyzed physiological parameters describing the tumor vasculature derived from magnetic resonance imaging: i) vascular permeability, ii) blood volume distribution, iii) blood flow, and iv) vascular size index (VSI). This analysis was complemented by a detailed study of the vascular architecture using synchrotron radiation-based micro computed tomography (SRµCT).

RESULTS & DISCUSSION: We found significant differences in the FD and L values between treated and non-treated group for both the permeability and perfusion maps (Table 1).

*Table 1: Quantification of treatment effects on FD and L. Values are given as mean±SD; * indicates significant difference between the two groups*

		DMOG	Placebo
FD	pre	2.16±0.18	2.00±0.17
	post	2.58±0.04*	2.07±0.22
L	pre	7.70±4.61	7.86±3.35
	post	6.81±0.37*	3.22±1.06

The FD values increased significantly in response to treatment. A higher level of FD means smaller self-similarity and therefore more chaotic structure, which may reflect angiogenesis, i.e. an expansion of the chaotic capillary network. The L values remained unchanged in the DMOG group and significantly decreased in placebo treated mice. Interestingly, no effect of drug treatment has been found comparing volume averaged values: this illustrates the superior sensitivity of the texture analysis in identifying morphological differences.

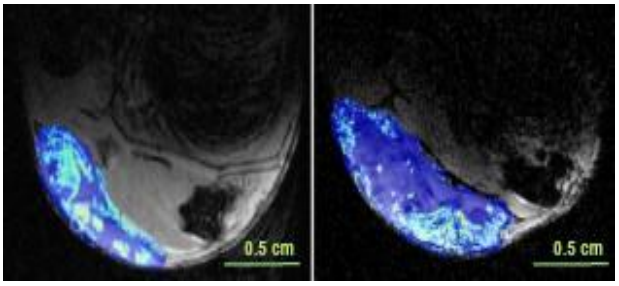

Fig. 1: Blood volume distribution (high value in red, low value in blue) for a mouse treated with drug (L = 6.5, left) and with placebo (L=3.11, right).

The increase in FD values is corroborated by the structural analysis of the tumor vasculature: VSI showed a persistent predominance of capillaries during tumor growth, but no formation of bigger vessels indicating the absence of hierarchical organization. This is in line with the SRµCT results, which reveal a high number of highly tortuous capillaries in C51.

CONCLUSIONS: The use of non-biased mathematical methods enables the quantification of changes in tissue heterogeneity. Such changes can be masked when analyzing volume averaged data sets.

This approach can be easily applied to monitor angiogenic cascade in regenerative treatment of damaged tissues.

ACKNOWLEDGEMENTS: The authors thank M. Rudin, S. Lehmann, and R. Keist for their support.

Synthetic extracellular microenvironments for neuroepithelial differentiation

A Ranga[1], A Meinhardt[2], D. Eberle[2], E. Tanaka[2], MP Lutolf[1]

[1] Laboratory of Stem Cell Bioengineering, Institute of Bioengineering, EPFL, Lausanne,Switzerland. [2] CRTD, Dresden,Germany.

INTRODUCTION: Complex three-dimensional (3D) multicellular constructs grown in-vitro, termed organoids, have in recent years become important models for studying developmental processes and morphogenesis, and have shown promise as increasingly biomimetic test beds for drug screening and regenerative medicine applications. Thus far, such organoids have been generated exclusively within Matrigel, a naturally derived proteinaceous extracellular matrix (ECM) with variable and poorly controllable properties. This has limited our ability to understand the extrinsic microenvironmental factors responsible for morphogenesis. Here, we develop an in-vitro three-dimensional model of the neural tube within a synthetic poly-(ethylene) glycol (PEG)-based matrix, and explore how extracellular matrix properties, including mechanical properties, degradability and ECM protein composition influence morphogenesis.

METHODS:

In order to rapidly and systematically assess the effects of the extracellular matrix on 3D neural differentiation, we adapted a high-throughput screening platform previously developed by our group. A library of molecular building blocks were independently mixed and then cross-linked in the presence of cells to form a large diversity of 3D cell environments with distinct and independently controllable properties. We assessed the neural differentiation potential of embryonic stem cells by image-based monitoring of the expression levels of the Sox1-GFP reporter as a marker of early neural commitment. We also evaluated proliferation and apico-basal polarity via a quantification of colony size and presence of an organized actin cytoskeleton, respectively. We utilized a generalized linear model (GLM)–based approach to systematically assess the effects of matrix stiffness and degradability as well as a set of relevant ECM proteins, including those previously reported to be present in Matrigel. We then validated the key findings of this screen by assessing the influence of a set of selected parameters on dorso-ventral patterning of the cysts, as assessed by polarized expression of sonic hedgehog.

RESULTS:

Our screening approach, combined with GLM-based analysis, allowed us to determine an optimal matrix leading to efficient neuroepithelial differentiation and apico-basal polarization. This matrix was characterized by an intermediate stiffness and a lack of degradability. This analysis also allowed us to identify laminin as a key ECM component involved in the establishment of apico-basal polarity. The further use of this optimized matrix, along with treatment of the developing cysts with retinoic acid (RA), resulted in efficient dorso-ventral patterning, as well as the establishment of neural-tube-like architecture within the cysts.

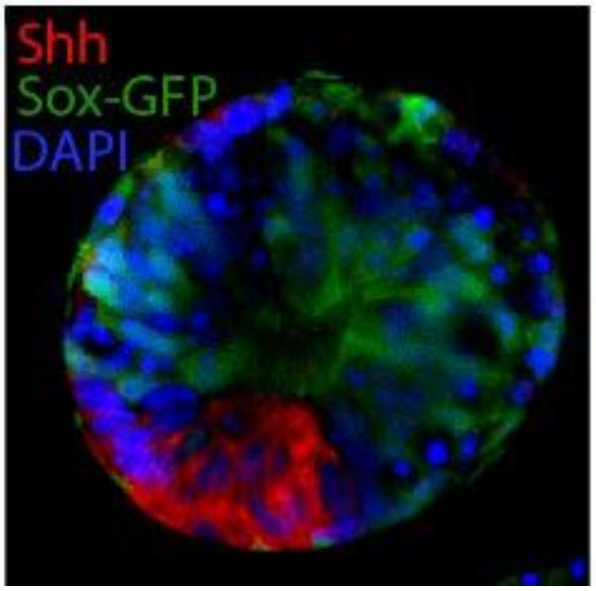

Fig. 1: Immunohistochemistry demonstrating dorso-ventral patterning of neuroepithelial cysts within optimized synthetic matrix.

DISCUSSION & CONCLUSIONS:

This study demonstrates how a systematic screening-based approach using synthetic matrix components can be used to efficiently derive a "signature of differentiation" for 3D neuroepithelial differentiation. This study also demonstrates for the first time the role of the extracellular microenvironment in establishing complex morphogenetic in an in-vitro organoid system and offers the promise of a fully synthetic recapitulation of developmental processes.

Using a Computer-Assisted and Robot-guided Laser Osteotome (CARLO) in bone surgery - considerations on ergonomics, system accuracy and biological response

M Augello[1], KW Beck[1], P Cattin[2], A Bruno[3], P Jürgens[1]

[1] *Clinic for oral and maxillofacial surgery ,University Hospital Basel.* [2] *Medical Imaging Analysis Center, University Basel.* [3] *AOT AG Basel*

INTRODUCTION: Major advantages of cutting bone with laser are absolute freedom in cutting geometries, minimal damage to the bone and the surrounding tissues and the high accuracy. These advantages can be effective only when the system is coupled to a robotic guidance, as operating hand does not reach the required accuracy. Due to the size of laser systems and surgical robots a merge leads to an unergonomic setup hindering surgeon's space in the operation room[1].

METHODS: An Er:YAG laser[2] and the accompanying optical system was set up in a miniaturized composite box. This laser system was mounted on a surgical lightweight robotic arm with 7 joints which has 270° of range or motion. Whole robot-guided laser system is integrated with computer-assisted pre-operative planning station and an intraoperative navigation system. An in vivo study was carried out where several osteotomy patterns were performed in minipigs mandibles using an intraoral approach comparing CARLO with the gold standard Piezosurgery.

RESULTS: The CARLO device with the compact construction can be easily integrated into an operation room (OR) environment.

Fig. 1: Setup of CARLO in the OR S/PA Surgeons, ST Nurse, CN navigation/tracking camera.

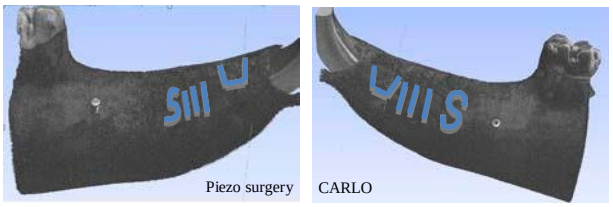

Fig. 2: Nanotom scans show more precision in cutting geometries and shapes with CARLO.

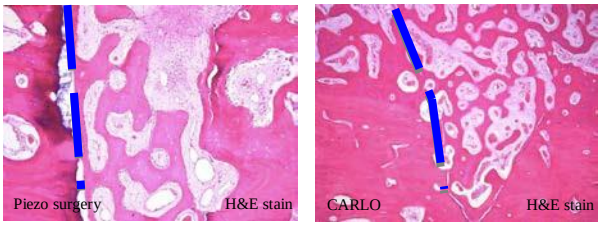

Fig. 3: Bone healing after 8 weeks showed no inflammatory or degenerative changes. Cuts by Piezosurgery show still a gap or even a slight bone resorption. Osteotomies by laser were almost covered by darker stained newly formed bone.

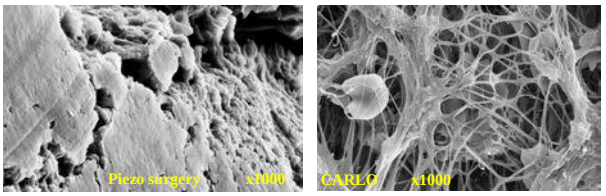

Fig. 4: Bone after ultrasonic cutting shows a smooth surface due to bone debris on cortical and cancellous surfaces, micro fractures and furrows in contrast to the bone surface after laser osteotomy which shows a comparable roughness like untreated bone (Scanning Electron Microscopy).

DISCUSSION & CONCLUSIONS: The miniaturized and robot-guided laser system can be successfully applied to perform osteotomies delivering all the advantages of laser osteotomy without hindering the range of motion of two surgeons around OR setup. Laser osteotomies show a better and faster bone healing tendency compared to Piezosurgery, due to a missing closure of bone vascular canals, which likely occurs by the compression of bone debris into the trabecular architecture.

The ceramic ZircaPore® implant surface - in vitro / in vivo experiences

F. Berghänel, C. Strehler
Metoxit AG, Thayngen, Switzerland

INTRODUCTION: Introducing hot isostaticially post compacted (HIP) ceramics with their favourable mechanic behaviours into dentistry, the full ceramic implant supported restorations got matter of interest. The ability to osseointegrate was critical endpoint of certain studies. The application of a technical feasible roughness is limited due to the undesired reduction of mechanical strength. Ziraldent® Implants (ATZ) with the additive microporous ZircaPore® surface (Fig. 1) show beneficial mechanical reliability and favourable tissue friendliness. The 3 years follow up of a prospective cohort study confirms a successful fullceramic implant treatment so far.

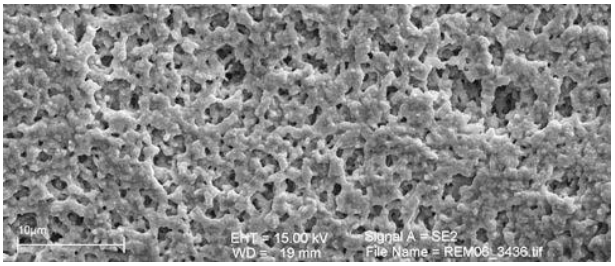

Fig. 1: ZircaPore® Surface

METHODS: In preclinical testings the biological behaviours are compared by using osteoblast-like CAL72 cell cultures [1] but also human osteoblasts [2]. Included in the comparison are different surface modifications of ceramic substrates and SLA® versus polystyrene controls. An animal study compares quantitative and qualitative controls of osseointegration of the modified Zirconia surface versus an anodised titanium surface and machined Ti- and ZrO_2 references. The bone-implant-contact (BIC) is assessed histomorphometricially, the biomechanical strength is indicated by the Push-In forces[3]. 40 patients and 57 implants are included in a 5 years prospective clinical cohort study. Beside the survival rate the bone level behaviour and gingiva attachment are primary success criteria.

RESULTS: The Zicapore® surface shows a roughness of R_a/P_{p-v} von 0.286µm/2.73µm compared with R_a 0.38µm of the anodised titanium surface. There is no significant difference of proliferation versus the control obvious. The status of gene expression is assessed by RT-PCR during 28 days. Quantity of those genes differencing osteoblasts increases faster in the titanium group, however at day 28 there is no more a significant difference compared with control group. The animal study assessing the osseointegration shows 24% BIC of ZircaPore® at day 28 and therefore delayed in difference to the 54.8% of the anodised titanium implants. However the biomechanical data of the Push-In-Test comparing ATZ (24.5N (SD 26.94)) vs. Ti (39.49N (SD 5.44)) show no statistical significance. The published data of the clinical 3 years follow up report 2 implant losses during early healing period prior prosthetic restoration. Measurement of gingiva attachment express a beneficial soft tissue behaviour, finally the endpoint bone loss is reported as an increase of the bone level compared with the data of year one p.i. [4].

DISCUSSION & CONCLUSION: Ziraldent® implants with ZircaPore® surface show promising success and are outstanding related to mechanical safety and biocompatibility. The supposed moderate stimuli for cell proliferation and differentiation demands an implant macro design to ensure necessary primary stability. Concerning that ZircaPore® further development for orthopaedic applications is ongoing.

Tribo-electrochemical wear resistance against bone of biomedical alloys

A Bermúdez[1], A Esguerra-Arce[2], J. Esguerra-Arce[2], S Mischler[1]

[1] *Groupe de Tribologie et chimie des interfaces, EPFL, CH.* [2] *TPMR, School of Materials, Universidad del Valle, Colombia*

INTRODUCTION: Micromovements occur at the bone-stem interface of orthopedic implants even after osseointegration [**1**]. These micromovements can be harmful when their amplitude exceeds 70 µm, however below this threshold micromotion are thought to favor osteoconductivity of implants interface [**2**]. Nevertheless small micromovements can still induce adverse fretting corrosion phenomena. Friction process involving amplitude displacements smaller than the contact width are referred as fretting. The presence of a corrosive medium contributes to accelerate wear and is known as fretting-corrosion [**3**]. Fretting-corrosion is one of the main causes of reintervention [**4**] and generation of debris from bone and metals devices [**5**]. In the present study, fretting-corrosion of biomedical alloys against bone is studied.

METHODS: 304ss, Co-Cr-Mo and Ti6Al4V biomedical alloys were tested in a fretting machine described previously [**6**]. The tests were carried out in Hank´s solution (Sigma Aldrich®) as simulated body fluid at 37 °C. A normal load of 2 N was used (close to the maximum stress applied *in vivo*) using an animal-bone ball as the wear counterpart. The amplitude used was 60 µm and the frequency value was 1 Hz **(**as the human gait**)**. A three-electrode electrochemical cell was integrated in to the system to perform the fretting corrosion test. The working electrode, i. e. the biomedical alloys, the counter electrode made of platinum wire and the reference electrode of Ag/AgCl were connected to a Wenking LB 95L potentiostat. The wear tracks were studied by optical profilometry (Smart WLI basic ®).

RESULTS: The OCP measurements are shown in Fig. 1 (A-B, period before fretting; B-C, during fretting; C-D, after fretting). When fretting started, the potential of the alloys remains constant until several cycles, when the potential slumped towards in the cathodic domain, due to the equilibrium between the mechanical depassivation and electrochemical repassivation. Once the fretting was stopped, the OCP recovered towards more positive values indicating repassivation of the materials. Wear was observed in bone and the disks. Disk wear track profiles are shown in Fig. 2. The wear scar observed in the case of Ti6Al4V and Co-Cr-Mo was smaller than that of 304ss.

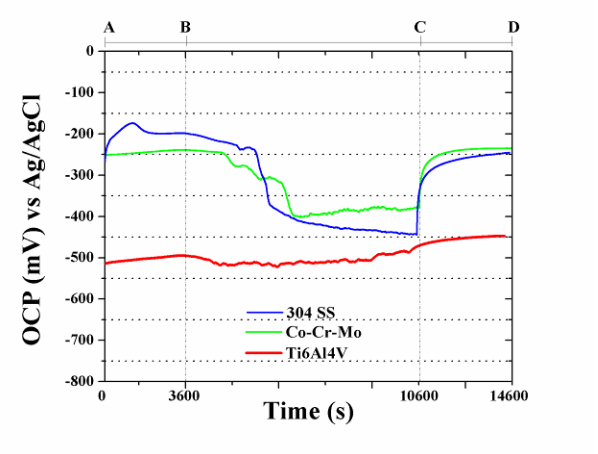

Fig. 1: Effect of fretting on the OCP of 304ss, Co-Cr-Mo and Ti6Al4V in Hank's solution against bone

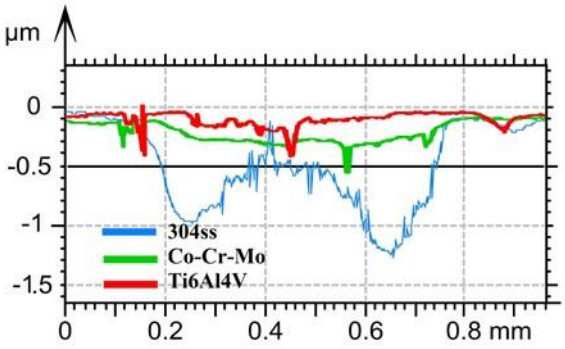

Fig. 2: Wear profile of 304ss, Co-Cr-Mo and Ti6Al4V in Hank's solution against bone

DISCUSSION & CONCLUSIONS: The protective oxide film can be damaged when rubbed against bone in 304ss, Co-Cr-Mo and Ti6Al4V alloys, however, Ti6Al4V showed the less wear.

Development of an extracellular matrix (ECM)-mimetic nanoparticle-based platform to deliver growth factors for inner ear regeneration

PS Briquez[1], A de Titta[1], C Takeda[1], JA Hubbell[1,3]

[1]Institute of Bioengineering, School of Life Sciences, Ecole Polytechnique Fédérale de Lausanne, Lausanne Switzerland. [2]Massachusetts Eye and Ear, Massachusetts General Hospital and Harvard Medical School, Boston MA USA. [3]Institute for Molecular Engineering, University of Chicago, Chicago, IL USA.

INTRODUCTION: About 10% people worldwide suffer from hearing impairment, due to aging, noise overexposure and ototoxic drugs. In contrast to human adults, some species such as birds are naturally able to regenerate hair cells and restore hearing loss. Although not completely understood, this process has been partially associated with the effect of some specific growth factors (GFs) [1]. GFs are key molecules in regenerative medicine, in that they have the ability to control cell behavior and tissue morphogenetic processes. In this study, we aim to evaluate *in vitro* the therapeutic effects of growth factors (not detailed in this abstract) and to develop a GF delivery system suitable for applications in the inner ear.

METHODS: 35 nm diameter polyethylene glycol (PEG)-polypropylene sulphide (PPS) nanoparticles synthesis and peptide conjugations were made as described in previous publications [2]. Conjugated nanoparticles were purified by size exclusion chromatography. Peptides were either chemically synthesized by GenScript USA Inc, or expressed in E.coli BL21 [3]. Engineered GFs have been modified by polymerase chain reactions, expressed in human embryonic kidney (HEK-293E) cells as previously described [4]. Protein purifications were performed by affinity and size exclusion chromatographies.

RESULTS: We functionalized the surface of PEG-PPS nanoparticles with a growth factor-binding domain from fibrinogen (Fg-GFBD) that we recently identified and characterized in our laboratory [4]. After conjugation, western blot analyses confirm the presence of Fg-GFBD conjugation on nanoparticles *(Figure 1C)*. Growth factors engineered with PlGF-$2_{123-144}$ for super-affinity to the ECM domains, in particular Fg-GFBD, are much better retained on the nanoparticles surface than their corresponding wild-type low affinity GFs *(Figure 1B, 1D)*.

DISCUSSION & CONCLUSIONS: The extremely small size and highly sensitive structure of the inner ear make it a challenging environment to deliver drugs. We take inspiration from the natural affinities between GFs and ECM domains, and the advantage of nano-sized particles to engineer a delivery platform that retain growth factors on nanoparticle surface and protect them from fast diffusion and rapid clearance, in order to control their sustainable delivery and improve their therapeutic efficacy. We are currently studying the mechanisms of GFs release from nanoparticles in adult mice cochleae.

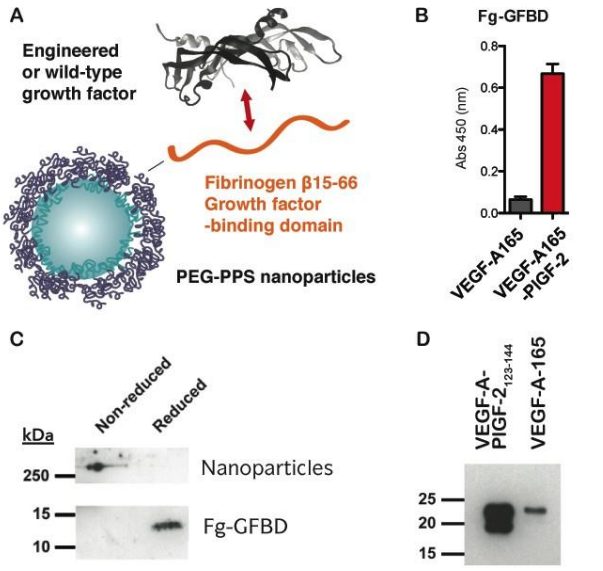

Figure. 1: *(A) Conceptual representation of the nanoparticle-based growth factor delivery system. (B) Relative affinity of PlGF-$2_{123-144}$ engineered vs. wild-type vascular endothelial growth factor-A (VEGF-A) to Fg-GFBD domain. (C) Western blot analysis detecting Fg-GFBD on nanoparticle after conjugation. (D) Relative retention of VEGF-A variants on nanoparticle detected by western blot analysis.*

ACKNOWLEDGEMENTS: This study was funded by the Fondation Bertarelli.

Understanding shear-stress sensitive nano-containers for targeted drug delivery

Marzia Buscema[1], Andreas Zumbuehl[2], Thomas Pfohl[3], Jörg Huwyler[4], Bert Müller[1]

[1]Biomaterials Science Center, University of Basel, Basel, CH. [2]Department of Chemistry, University of Fribourg, Fribourg, CH. [3]Department of Chemistry, University of Basel, Basel,CH. [4]Department of Pharmaceutical Sciences, University of Basel, Basel, CH.

INTRODUCTION: A shear-sensitive nano-container formulation for the treatment of myocardial infarction through the release of vasodilatatory drugs has recently been discovered [1]. The mechanical properties of the phospholipid nanometer-sized vesicles should be tailored to ensure a local drug release in constricted human coronary arteries. Dynamic Light Scattering (DLS) technique provides the required size control while Small Angle X-ray Scattering (SAXS) combined with microfluidic devices is a promising tool for the investigation of vesicles behavior in terms of membrane deformation as well as rupture under selected shear stresses. Complementary studies on human coronary diseased arteries have been performed by means of micro-CT experiments [2, 3] as a basis for flow simulations used to determine the shear stress range in healthy and constricted regions.

METHODS: Two phospholipid formulations have been tested: the mechano-sensitive 1,3-diamide Pad-PC-Pad synthetized as described [1] and the 1,2-diester DPPC (Lipoid, Zug, Switzerland) used as a control, both prepared in aqueous solution. After several cycles of freeze thawing, extrusion by means of polycarbonate filters is performed to obtain unilamellar vesicles. The vesicle preparation is followed by light scattering analysis using a Delsa Nano C (Beckman Coulter, USA) to check vesicles size distribution essential for SAXS measurements. Micro-channels pattern mimicking healthy and diseased regions of blood vessels are molded from Kapton films and NOA81 glue [4]. Preliminary SAXS measurements in microfluidic devices were carried out at Paul Scherrer Institute (SLS, Villigen, Switzerland) scanning the micro-channel through an energy of 12.4 keV, using a focused spot size of 40 μm^2 and a sample-detector distance of 2.2 m.

RESULTS: Extruding through 50 nm diameter filter leads to a solution containing unilamellar vesicles with a diameter distribution centered on 75.3 nm with a FWHM of 70.6 nm (Fig.1). SAXS measurements of DPPC vesicles solution have already shown a reasonable scattering signal.

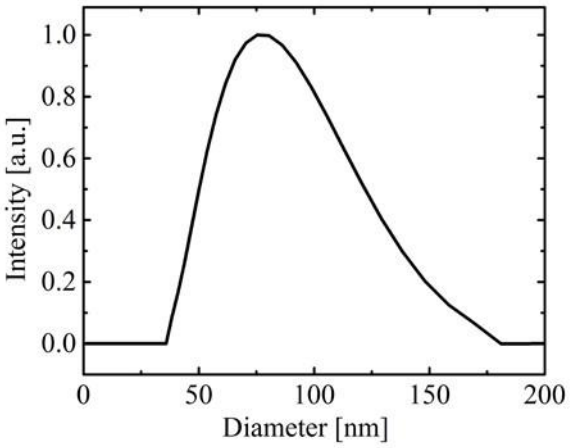

Fig. 1: DPPC vesicles size distribution determined by light scattering

DISCUSSION & CONCLUSIONS: 100 nm phospholipid vesicles sensitive to shear variation have already shown promising results. Here, we pointed out how important is to control the sample size after the preparation to set accurately the parameters in further experiments. Microfluidics combined with SAXS technique will be the main technique used to determine the range where the drug carriers locally release their cargo avoiding not desired side effects.

ACKNOWLEDGEMENTS: This work was funded by Swiss National Science Foundation via the program NRP 62 'Smart Materials'. We acknowledge Dr. Fabiola Porta for helpful discussions.

Density improvement of selective laser melting titanium structures for regenerative medicine

P.Chavanne[1], O.Bill[1], R.Schumacher[1]

[1]*FHNW – University of Applied Sciences and Arts, School of Life Sciences, Institute for Medical- and Analytical Technologies, Muttenz, CH.*

INTRODUCTION: Continuous improvement of generative fabrication technologies such as selective laser melting (SLM) has made these techniques very attractive for applications in personalized regenerative medicine. Yet, mechanical performance of SLM produced titanium parts are still minor compared to traditional fabrication techniques due to material defects and stresses [1]. This paper deals with laser parameter optimization of SLM processing using design of experiments methods in order to achieve dense parts with homogenous and flaw-less micro structure.

METHODS: Design of Experiments (DoE) methodology was used to optimize specific SLM process parameters for titanium grade 2 material. Density (Archimedes, cuboid parts, s = 10 mm) was chosen as optimization goal. In a first step 15 SLM parameters were considered as potential influential on density and chosen as input factors for initial screening round. A two level fractional factorial screening design with a total of 16 tests was implemented. Parameter levels were set to extreme values based on own process know-how and on scientific publications [1-2]. Specimens were produced using a SLM 250 HL system (SLM Solutions, Luebeck). Density measurement was conducted with a tensiometer (K100, KRÜSS, Germany) according to ISO 3369:2010. In a second step, parameters with a significant influence on density were optimized in a three-stage Box-Behnken test design consisting of 54 samples. The resulted parameter optimum prognosis was finally verified during a third test round with twelve samples.

RESULTS: Screening test unveiled an influence of both geometrical parameters (e.g. laser distance) as well as performance parameters (e.g. laser speed). In total, only six relevant laser parameters like speed, focus, contours and hatching were selected for second optimization. Both laser speed in volume and contour as well as hatching distance were again found to have a significantly strong influence on the density.

Best parameter combination during the second optimization round yielded test parts with a relative density of 99.953% (n = 5, s = 0.0027) compared to density of wrought grade 2 titanium.

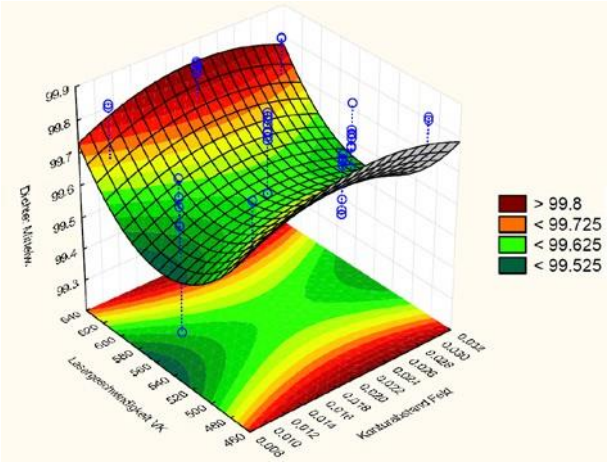

Fig. 1: Interaction plot of laser speed and hatch contour distance parameter showing their influence on SLM part density with two optima.

DISCUSSION & CONCLUSIONS: Parameter optimization of SLM process is challenging since a multitude of parameters do not converge at one single optimum. Nevertheless, by means of DoE a relative density improvement from initial 99.87% to 99.95% could be achieved. As an outlook, the effect of this density focused optimization on static and mainly dynamic material properties will be investigated. It can be concluded that it is very unlikely to reach 100% dense parts by means of SLM parameter optimization. For achieving this, elaborated post fabrication techniques such as hot isostatic pressing (HIP) should be considered.

ACKNOWLEDGEMENTS: The RMS Foundation is gratefully acknowledged for the support of this project (Proj.Nr.E11_0001). .

Automatic matching of grating-based phase tomography dataset with histology

N Chicherova[12], PC Cattin[2] , G Schulz[1], K Fundana[2] , B Müller[1], SE Hieber[1]

[1] *Biomaterials Science Center, University of Basel, Basel, CH.* [2] *Medical Image Analysis Center, University of Basel, Basel, CH*

INTRODUCTION: Identifying a histological slice in a three-dimensional dataset corresponds to a challenging 2D-3D matching problem. Recently, we developed an automatic algorithm that was successfully applied to micro computed tomography (μCT) data acquired in absorption contrast mode and histology images of the jaw bone biopsy.[2] To explore how the method generalizes, here we evaluated its performance on another modality for tissue, namely grating-based phase contrast tomography of the human cerebellum.

METHODS: The sample data used for this study originates from a human cerebellum extracted post mortem. The 3D volume scan of the specimen was acquired using grating-based phase tomography at the beamline ID 19 (ESRF, Grenoble, France) at a photon energy of 19.5 keV and an effective pixel size of 5 μm. The diameter of the specimen is 6 mm. Our automatic algorithm is based on the rotation- and scale-invariant edge detector SURF (Speeded Up Robust Features[3]). In a first step corresponding feature points are detected between each slice in the 3D data set and the histology image using SURF. The coordinates of all matching points from 3D data are subconsequently saved relative to its axial position. Based on these coordinates, we build a 3D point cloud, where the third dimension corresponds to the slice number in the dataset. Finally, to find the best matching tomography slice to histology, we filter the points based on their density distribution and use RANSAC algorithm to robustly fit a plane in a noisy point cloud. For this particular dataset, we added an additional parameter for robustness, namely filter radius for matched keypoints. The specimen borders usually produce high edge response. To remove it, we cropped the points by taking only those lying inside a circle with a radius less than the radius of the specimen. Other parameters were the same as in the previous study[1].

RESULTS: We observed reasonable performance of the method for four histology slices. Thus, the method shows a potential for generalization to other imaging modalities. The figure shows the results for the best found match of a histological slice in the tomography data. The high similarity between the two images indicates that the algorithm performed well in this case. In total we analysed four histology slices and visually evaluated the similarity between the automatically found images. The algorithm found good matching pairs in all four cases.

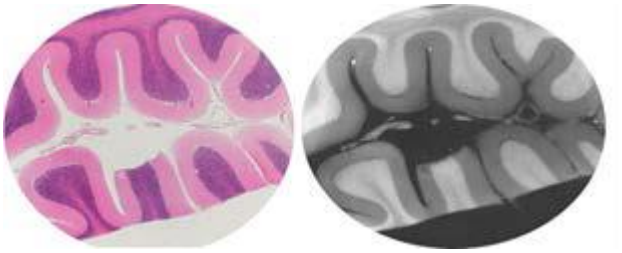

Fig. 1: Automatically registered slice from the 3D tomography dataset (right) and the reference histology image (left).

DISCUSSION & CONCLUSIONS: The results indicate that our method can be applied to datasets of other modalities. Even though the SURF descriptor is usually not considered to be multi-modal, it shows good performance when applied to this density problem. The main advantage of the detector is a property of detecting borders of two images for matching. Therefore, we believe that our approach will work with other modalities with high intensity contrast and corresponding tissue borders. However, this property is also a limitation which can potentially lead to incorrect registration. Currently, we are working on improving the method using sparse modality invariant descriptors.

ACKNOWLEDGEMENTS: The authors thank G. Schweighauser and J. Hench for the tissue preparation and the histological sectioning. The project was supported by the ESRF (proposal MD-861) and funded by SNSF project 150164.

Encapsulation of adipose-derived stem cells in fibrin gels for transplantation at a nerve injury site

AC de Luca[1], PG di Summa[2], W Raffoul[2], SP Lacour[1]

[1] *Centre for Neuroprosthetics, Laboratory for Soft Bioelectronic Interfaces, EPFL, Lausanne, CH.*
[2] *Department of Plastic, Reconstructive and Hand Surgery, University Hospital of Lausanne (CHUV), Lausanne, CH*

INTRODUCTION: Adipose-derived stem cells (ASC) have been demonstrated to be a valid alternative to Schwann cells (SC) for peripheral nerve applications. ASC are in facts able to differentiate into a SC phenotype [1], prevent neuron apoptosis [2] and support nerve regeneration [3]. Due to its degradability and biocompatibility, fibrin is a suitable matrix for cell transplantation. Therefore the interaction between ASC and fibrin was studied in order to create a suitable environment for ASC encapsulation.

METHODS: ASC were derived from inguinal and visceral rat using a previously established protocol [4], in accordance with the local veterinary commission of the canton of Vaud (Lausanne, Switzerland).

Cells were encapsulated in fibrin gels before gelation in order to obtain a cell-hybrid gel. Fibrinogen (8 mg/mL) was converted in fibrin by adding an enzymatic solution containing thrombin (2 U/mL), factor XIIIa (4 U/ml) and $CaCl_2$ (5 mM).

After 24 hours cells were fixed in 10% formalin and stained for F-actin to investigate their morphology in the 3D gels. Cell viability was observed by using a two-colour live/dead cell viability kit. In addition, cell metabolic activity was monitored over 3 days using the AlamarBlue assay solution until gel degradation (n=3). Tissue culture plastic (TCP) was used as positive control. Results are expressed as mean ± standard error of the mean (SEM). Significant differences between data were evaluated using a *t*-test (***$p < 0.001$).

RESULTS: ASC were homogeneously distributed across the whole volume, as shown in Fig. 1. Very few dead cells were observed in the gels after 24 hours. Degradation of the gel was then observed and cells migrated at the bottom of the plate, keeping proliferating. Cells cultured directly on tissue culture plates expressed higher proliferation rates compared to those in the gels (Fig. 2). However, the cells maintain their proliferative potential while encapsulated.

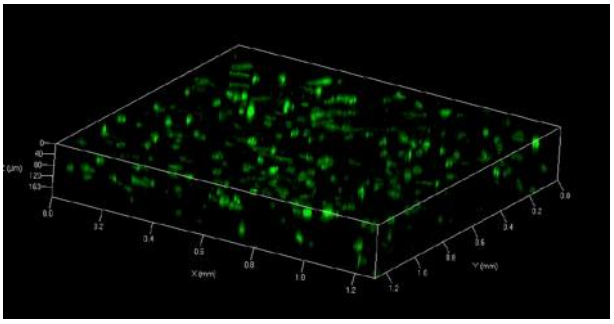

Fig. 1: 3D confocal image of ASC encapsulated in fibrin gels and fixed after 24 hs.

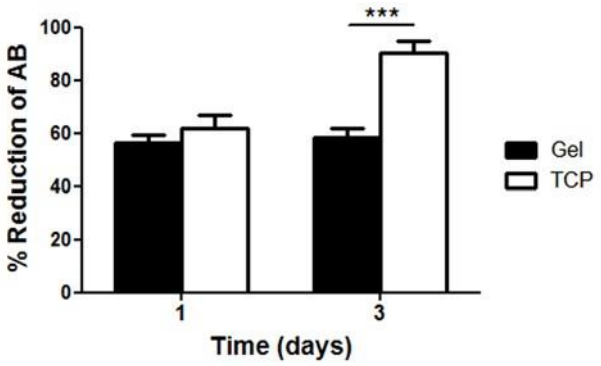

Fig. 2: ASC metabolic activity in gels and TCP over 3 days is expressed as % of reduction of AlamarBlue.

DISCUSSION & CONCLUSIONS: ASC maintained their proliferative ability once released in the confining environment. Together with the fast degradation of the fibrin gels, this hybrid system can be possibly used to transplant ASC at a nerve injury site.

ACKNOWLEDGEMENTS: The authors would like to acknowledge the Swiss National Science Foundation for funding this research project.

Micro computed tomography for the investigation of tooth hard tissues

Hans Deyhle[1], Peter Thalmann[1], Iwona Dziadowiec[1], Felix Beckmann[2], Georg Schulz[1], and Bert Müller[1]

[1] *Biomaterials Science Center, University of Basel, Basel, Switzerland.* [2] *Helmholtz-Zentrum Geesthacht, Institute of Materials Research, Geesthacht, Germany*

INTRODUCTION: Absorption-based X-ray micro computed tomography is a well-established technique for the investigation of human crown's density.[1-3] The reconstructed tomograms yield the local X-ray attenuation coefficients μ. Since μ depends on the X-ray energy as well as linearly on the material density, measurements performed with monochromatic X rays, as performed at synchrotron radiation facilities, provide quantitative results about tissue density. Conversely, the attenuation coefficients obtained with a polychromatic X-ray spectrum, as found e.g. in advanced laboratory sources, are only of semi-quantitative nature. It is, therefore, of significant interest to correlate the results from the two facilities.

METHODS: The crown of a human tooth, extracted for reasons unrelated to the study, was used for the investigation. Lab-source micro computed tomography was performed with a nanotom® m (General Electric, Wunstorf, Germany) with an acceleration voltage of 90 kV. The pixel size of the 1200 equiangular projections corresponded to 4.8 µm. Synchrotron radiation-based tomograms were acquired at the beamline P07 operated by HZG at PETRA III (DESY, Hamburg, Germany) with a photon energy of 45 keV and a pixel size of 4.8 µm. 2400 equiangular projections were acquired over 180°.

RESULTS: The images in Figure 1 display a selected slice from the datasets obtained with monochromatic and polychromatic X rays, respectively. Dentin and enamel as well as the lesions can clearly be identified in both datasets. Figure 2 shows the joint histogram of the two datasets. Here, the grey values obtained by the nanotom setup are compared with the local X-ray absorption values obtained with monochromatic radiation. The attenuation values scale almost linearly, indicating that the data acquired with the chosen settings for the laboratory source reasonably reflect the density of the tooth crown.

DISCUSSION & CONCLUSIONS: Quantitative synchrotron X-ray tomography allows for the calibration of the grey values obtained with lab-sources.

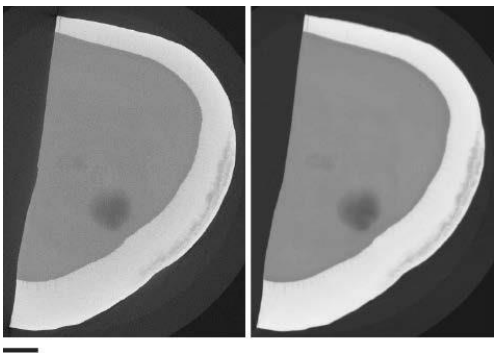

Fig. 1: Selected slices from laboratory- (left) and synchrotron radiation-based (right) CT data. The length bar corresponds to 1 mm.

The beam time at synchrotron radiation sources is limited. Our approach enables us to derive local densities from data of laboratory-based systems for the quantification of tooth hard tissues in health and disease.

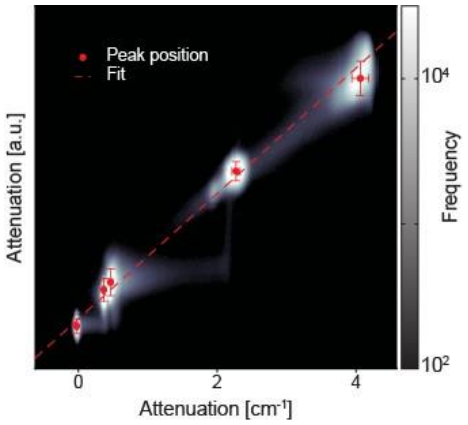

Fig. 2: Joint histograms of the two datasets. Abscissa – SR data, ordinate – nanotom data.

ACKNOWLEDGEMENTS: The support of L. Kind for specimen preparation is gratefully acknowledged. Project funded via SNF grant #51NF40-144617.

Division-linked phenotypic changes and chondrogenic potential of chondrocytes

R Duhr[1], I Martin[1], D Wendt[1]

[1]*Departments of Surgery and of Biomedicine, University Hospital Basel, University of Basel, Basel, Switzerland*

INTRODUCTION: The production of engineered cartilage using primary chondrocytes typically requires an initial *in vitro* proliferation phase, during which cells lose their native phenotype and chondrogenic potential with cumulative population doublings[1]. Despite numerous efforts, chondrocytes with superior regenerative capacities have not been identified so far, possibly because of heterogeneous growth rates causing a domination of the expanded population by rapidly proliferating cells[2]. We hypothesized here that selecting chondrocytes based on their number of cell divisions reveals differences in the progression of de-differentiation and chondrogenic potential of subpopulations.

METHODS: Freshly isolated human chondrocytes were stained with the cell division tracking dye carboxyfluorescein succinimidyl ester (CFSE) and cultured in 2D polystyrene dishes with or without growth factors. At different time points, expression of cell surface markers was assessed by flow cytometry or cells were FACS sorted according to their prior divisions to assess gene expression and re-differentiation potential.

RESULTS: CFSE labelling allowed the identification of distinct subpopulations of proliferating chondrocytes. Changes in the expression of CD54, CD90 and CD166 as well as of extracellular matrix genes collagen type I and collagen type II (figure 1), aggrecan and versican clearly progressed with cell divisions. Different culture conditions influenced cell doubling rates but not the link to phenotypic alterations. Interestingly the highest chondrogenic potential was measured for chondrocytes that were growing slowly, as compared to non-dividing or rapidly dividing cells (figure 2).

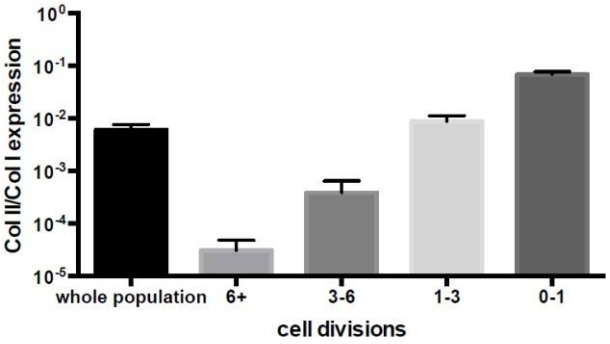

Fig. 1: Gene expression ratio of collagen type II to collagen type I. Cells sorted according to number of divisions after 1 week of proliferation.

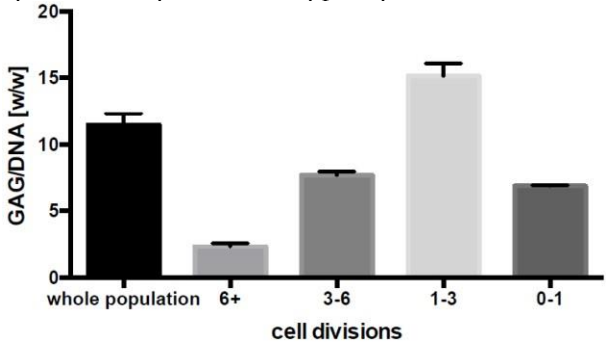

Fig. 2: GAG/DNA ratio of cells sorted after 1 week of proliferation and re-differentiated as micromass pellets for 3 weeks in chondrogenic medium.

DISCUSSION & CONCLUSIONS: The correlation between high cell proliferation rate and low re-differentiation capacity constitutes an important challenge for cartilage tissue engineering applications. Future studies will have to show in how far slower dividing cells have an intrinsically higher chondrogenic potential and need to reveal the underlying molecular mechanisms for the coupling between phenotypic changes and cell divisions in chondrocytes.

ACKNOWLEDGEMENTS: Supported by the Fonds National de la Recherche, Luxembourg (4090751).

Fretting corrosion of coatings against bone

J. Esguerra-Arce[1], A. Esguerra-Arce[1], S. Mischler[2], Y. Aguilar[1], O. Gutiérrez[3]

[1] *TPMR, School of Materials, Universidad del Valle, Colombia,* [2] *Groupe de Tribologie et chimie des interfaces, EPFL, CH,* [3] *Pharmacology Group, Universidad del Valle, Colombia*

INTRODUCTION: In surfaces that are meant to be fixed to each other, as in the case of bone-artificial material or bone-cement interfaces in orthopaedic implants, can occur fretting corrosion [1], which is a particular form of tribocorrosion involving a small amplitude relative displacement or vibration. The aim of this work is to evaluate fretting behaviour of AISI 304 coated with calcium phosphate/calcium titanate (CP/CT) and with Ti-Al-N against bone emphasizing in the influence of the presence of an electrolyte simulating human body fluids. Before fretting assays cytotoxicity of the materials was measured.

METHODS: Mirror finished AISI 304 was used as a substrate. CP/CT coating was obtained by R.F magnetron sputtering (M.S) from a target composed by 25% of hydroxyapatite and 75% calcium titanate. Ti-Al-N coating was obtained by reactive M. S from 2 targets (one of alumina and one of titanium) with N_2 gas. Cytotoxicity of the coatings was examined with the LDH kit from Roche™. To reproduce fretting-corrosion phenomenon a ball-on-flat fretting tribometer [2] was used. The femoral stem was modeled by a plane coated AISI 304. The bone around the stem was modeled by a spherical animal bone (6,2 mm in diameter), prepared from a bovine metacarpal diaphysis. The applied normal load was 2 N and the amplitude of displacement was 60 μm; the displacement was triangular and the frequency was 1 Hz. The tests were carried out in dry conditions and in Hank´s solution at 37 °C. A 3D laser scanning profilometer (UBM Telefokus UBC14) was used to characterize the surface topography before and after the fretting experiments.

RESULTS: The hardness of the CP/CT and Ti-Al-N coatings were 17 GPa and 30 GPa, respectively. Both coatings showed no cytotoxicity. Fig. 1 shows the wear track of the coatings after fretting test. In dry conditions CP/CT coating suffered wear without reaching the substrate and Ti-Al-N coating did not suffer any wear. Instead, in Hank´s solution, CP/CT coating exhibits a high adhesion of bone and Ti-Al-N coating showed detachment from the substrate. The OCP measurements are shown in Fig. 2.

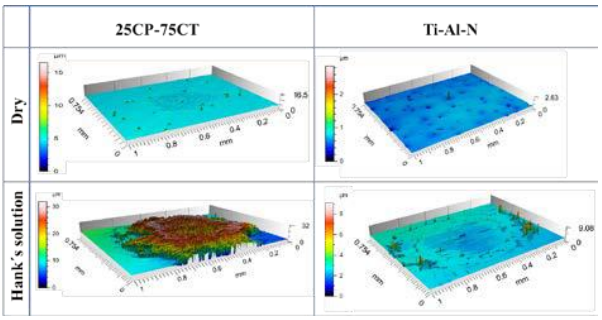

Fig. 1: Effect of dry and wet conditions in fretting on CP/CT and Ti-Al-N coatings growth onto AISI 304

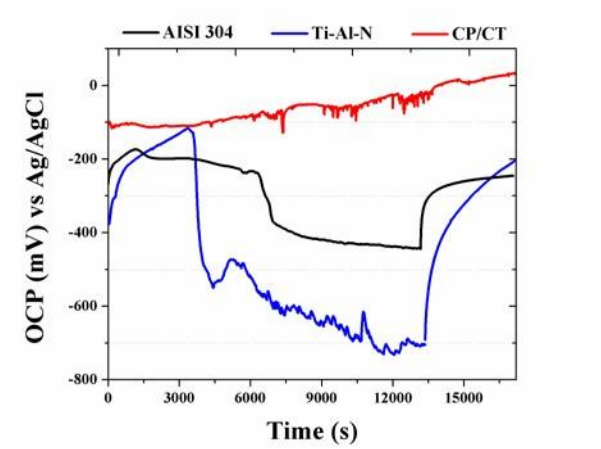

Fig. 2: Effect of fretting on the OCP of 304ss, CP/CT and Ti-Al-N in Hank's solution against bone

DISCUSSION & CONCLUSIONS: In dry conditions the hardest coating (Ti-Al-N) did not suffer any wear. In wet conditions the response of the coatings is explained because of their electrochemical characteristics. The OCP in CP/CT coating did not show shift towards cathodic potentials, because of the adherence of the bone. On the contrary, the Ti-Al-N coating did show a shift toward cathodic potentials because of the detachment of the coating. It can be seen that in fretting regime not only the hardness but also the electrochemical characteristics are important in the behaviour of the coatings.

Optimization of fibrin gels for cell encapsulation.

C Fonta[1], AC de Luca[1], SP Lacour[1]

[1] *Centre for Neuroprosthetics, Laboratory for Soft Bioelectronic Interfaces, EPFL, Lausanne, CH*

INTRODUCTION: Fibrin gels are commonly used for cell encapsulation for tissue engineering applications[1]. However, some biochemical cues are required in order to make the gels more suitable for nerve engineering. Previous studies have demonstrated the beneficial effects of Laminin in the regeneration process, enhancing neurites growth and Schwann cells proliferation[2]. Hereby, the action of Laminin was assessed by comparing the viability of encapsulated cells in fibrin gels.

METHODS: Fibrin gels were prepared from two separate solutions: an enzymatic solution containing Thrombin (2U/ml), $CaCl_2$ (10mM) and Fibrinogramm (8U/ml), and a fibrinogen solution containing Fibrinogen (16mg/ml), Aprotinin (34µg/ml) and Laminin at different concentrations (ranging from 1µg/ml to 100 µg/ml). Finally, the gels were formed by mixing the two solutions and incubating the plates for 1 hour at 37°C.
Rat adipose-derived stem cells (ASC) were cultured in growth medium (90% α-MEM, 10% FBS, 1% PS) at 37°C, 5 % CO_2 until needed. Cells were then encapsulated in the gels before gelation and cultured in the incubator for further tests.
Cells viability was tested with live/dead assay after one day of culture in the gels and their proliferation was assessed at day 1 and day 4 by using the Alamar Blue assay according to the manufacturer's protocol. Cell morphology was assessed by immunocytochemistry after four days: the samples were fixed with 10% formalin, permeabilized and stained against DAPI for the nuclei and Phalloidin for the cytoskeleton.
Results are expressed as mean ± standard error of the mean (SEM) and were considered statistically different for $p < 0.5$.

RESULTS: Cell viability was not remarkably affected after encapsulation in the gels, as shown by the live/dead assay. The Alamar Blue experiment (Fig. 1) demonstrated an enhanced cell proliferation in fibrin gels supplemented with 1µg/ml of Laminin compared to the other conditions (absence and different Laminin concentrations).

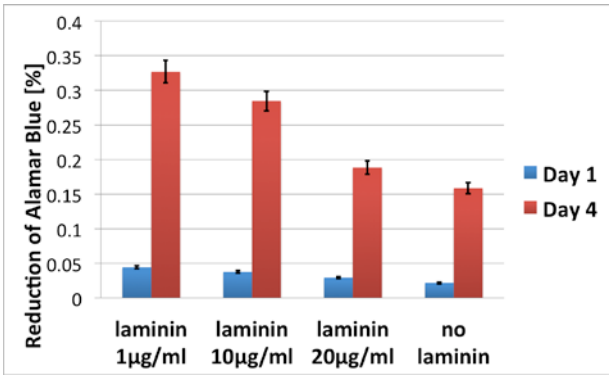

Figure 1: Percentage of Alamar Blue reduction for gels supplemented with different concentrations of Laminin.

Confocal imaging (Fig. 2) showed an increased cell spreading in the gels containing 1µg/ml Laminin, confirming the AlamarBlue results.

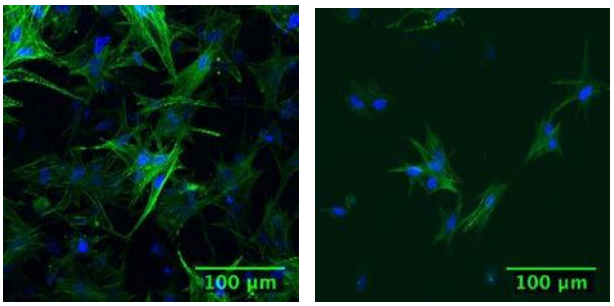

Figure 2: Composite images of cells distribution and spreading in 1µg/ml Laminin-supplemented gels (left) and in gels without Laminin (right). Blue: nuclei, Green: f-actin (cytoskeleton).

DISCUSSION & CONCLUSIONS: The beneficial effect of Laminin in creating a good regenerative environment is here confirmed by the improvement of cell viability and proliferation in Laminin-supplemented gels compared to control gels. Small protein concentrations (just 1µg/ml) are enough to provide an optimal environment for cell survival and proliferation. These results are promising for future application in nerve regeneration.

Silk membrane-fleece in combination with genipin-enhanced fibrin hydrogel for annulus fibrosus repair

DA Frauchiger[1], SCW Chan[1,2], LM Benneker[3], B Gantenbein[1]

[1]*Tissue & Organ Mechanobiology Group, Institute for Surgical Technology and Biomechanics, University of Bern, Bern, CH.* [2] *Biointerfaces, EMPA, Swiss Federal Laboratories for Materials Science and Technology, St. Gallen, CH.* [3]*Department for Orthopedic Surgery and Traumatology, Inselspital, University of Bern, Switzerland.*

INTRODUCTION: Low back pain is affecting a high number of people and is often caused by trauma causing disc herniation and/or disc degeneration. Apart from some promising approaches for nucleus pulposus repair, so far no treatment or repair is available for the outer fibrous tissue, annulus fibrosus (AF). Hence we aimed first to develop a reproducible AF injury model that in a later step was both sealed and repaired in a bovine organ culture model *in vitro*. For this purpose a silk fleece composite and a genipin-enhanced hydrogel was used on bovine intervertebral discs (bIVD), which were subjected to different loading profiles over a culture period of two weeks.

METHODS: Coccygeal bIVD were harvested under aseptic conditions from 12-17 month old animals and kept in free swelling conditions for 24h in *Dulbecco's Modified Eagle's medium* with 4.5 g/L glucose containing 5% serum for equilibration [1]. Then a circular 2mm biopsy punch (Polymed, Switzerland) was used to form a reproducible defect in the AF. A human-derived fibrin gel (Baxter Tisseel, Switzerland) enhanced with 4.2 mg/ml of the cross linker genipin (Wako Chemicals GmbH, Germany) was used to fill the defect. The silk composite consists of sericin free *bombyx mori* silk and possesses a mesh- and a membrane side (Spintec Engineering GmbH, Germany); the membrane is facing outwards to form a seal. bIVDs were cultured *in vitro* for 14 days either under complex load in a custom-built bioreactor (0.2MPa load and ±2° torsion at 0.2Hz for 8h/day), static diurnal load of 0.2MPa or free swelling [2]. At the end of culture discs were checked for seal failure, disc height, metabolic activity (alamar blue), cell death by necrosis (LDH assay), DNA and GAG content, expression of typical IVD anabolic and catabolic genes.

RESULTS: Throughout the 14 days of culture the silk composite and fibrin hydrogel maintained its position in the AF regardless of the loading profile applied in all discs (n=6) and no leakage could be observed. Disc height decreased in all discs, except free swelling condition (2-way ANOVA, P = <0.0001), and can be referred to the loading profile rather than applied treatment (Figure 1). Cell activity of repaired discs did not differ relative to control whereas injured discs showed a decrease in metabolic activity, apart from free swelling. Furthermore, repaired discs contain GAG and DNA in the range of unaltered control discs except static diurnal load.

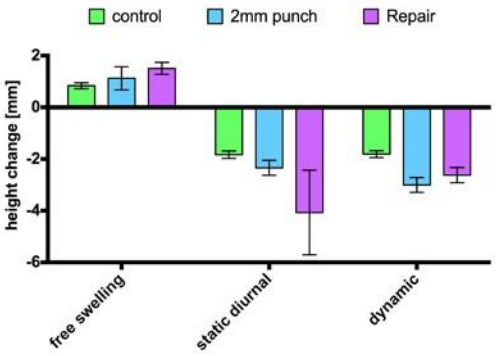

Fig. 1: C
culture relative to initial height after harvest.

DISCUSSION & CONCLUSIONS: First tests suggest that silk-genipin-fibrin reinforced hydrogel might be a possible approach to close AF defects even when subjected to compression and torsion. Also parameters tested for were showing promising results. Further tests have to be done as well as cytocompatibility has to be investigated.

ACKNOWLEDGEMENTS: This project is funded by the Gerbert Rüf Stiftung project # GRS-028/13 and the Swiss National Science Foundation SNF #310030_153411.

Absorption-based micro computed tomography measurements of a human knee joint

Christian Götz[1], Hans Deyhle[1], Magdalena Müller-Gerbl[2], Bert Müller[1] and Georg Schulz[1]

[1] Biomaterials Science Center (BMC), University of Basel, Switzerland. [2] Department of Biomedicine, University of Basel, Switzerland

INTRODUCTION: High-resolution three-dimensional imaging of soft and hard tissue plays an increasing role in the understanding of the function of joints in health and disease. Micro-computed tomography (µCT) is of special interest because of its high spatial resolution. In particular, it overreaches the resolution of magnetic resonance imaging, which is considered golden standard in clinical imaging of soft tissue, even for post-mortem specimen by far.[1] Its non-destructive nature is often a selection criteria for µCT.

METHODS: The focus of this study is a post mortem human knee joint. Within 24 hours of death the knee of an 87 year-old female was fixed in formalin following the standard protocol of the Institute of Anatomy of the University of Basel. After fixation, the skin, fat and muscle tissue was removed. The goal of this study is producing high resolution images displaying not only bony tissue but also soft tissues including cartilage, tendons and ligaments with reasonable contrast. Absorption contrast based µCT experiments were performed with the nanotom® m holding the knee joint in a polyethylene container filled with the formalin solution to prevent the tissue from drying. The acceleration voltage was 150 kV and the beam current 50 µA using an additional 0.3 mm thin Cu-filter to reduce beam hardening. 2000 projections were recorded over 360 degrees. For each projection angle, the average of 10 single projections was chosen. The exposure per projection was set to 0.5 s. The resulting isotropic pixel size was 30 µm.

RESULTS: The bones are clearly represented with a high contrast allowing insights in the subarticular bone structure. The surrounding cartilage layer on the artificial surface of the femoral condyles and on the tibial plateau can be clearly distinguished along its tissue border demarcation. Also the quadriceps and patellar tendon is visualized with micro meter resolution giving a view on its fibrous strands. The cruciate ligaments and menisci are distinguishable but only partly seen on the selected image (Fig. 1).

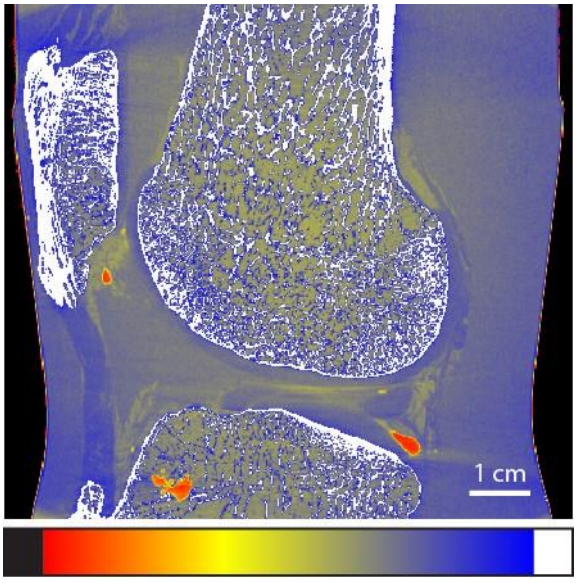

Fig. 1: Sagittal section through medial femur condyle of left knee.

DISCUSSION & CONCLUSIONS: Further preparation of the knee, in particular segmentation into smaller pieces will allow for a resolution down to a few microns. Not entirely satisfying is the contrast of the soft tissue, e.g. menisci and cruciate ligaments. Also artefacts shown in red color interfere with the actual image information. Measurements using phase-contrast modes will have the power to improve contrast for soft tissues and to reduce artefacts in the vicinity of bones.[2] Therefore, further measurements using grating-based phase contrast method promise more detailed imaging of soft and hard tissue.[3]

Enhanced blood coagulation on ceramic versus titanium implant surfaces

S. Guimond[1], M.Rottmar[1], U. Tobler[1], S. Berner[2], K. Maniura-Weber[1]

[1]*Laboratory for Biointerfaces, Empa, Lerchenfeldstr.5, 9014 St.Gallen, CH*

[2]*Institute Straumann AG, Peter Merian-Weg 12, 4002 Basel, CH*

INTRODUCTION: Titanium has been used as an implant material since the early 1970s[1] and is nowadays the gold standard material for dental applications[2]. However, the grey colour of such an implant might compromise the esthetical outcome[3]. Due to superior esthetical properties and established biocompatibility of zirconia-based materials, such implants are of great interest for dental applications[4]. Early and effective bone tissue integration of dental implants is of crucial importance for their long-term stability. Directly upon implantation, the material surfaces come into contact with the patient's blood. As the topography and chemistry of the implant surfaces plays a crucial role in the interaction of blood components with the material[5], it is important to understand these early events and it's implications for osseointegration. In this study, we therefore investigated blood-surface interaction and blood coagulation on titanium and zirconium-based materials.

METHODS: Titanium samples SLActive® (hydrophilic, sandblasted and acid-etched surface) and ceramic samples ZLA™ (hydrophobic, sandblasted and acid-etched surface) were supplied by Institute Straumann AG. Implant surfaces were incubated with partially heparinized (0.5 IU/ml) human whole blood or platelet-rich plasma from healthy volunteers (with ethical approval) for different time points (10, 20 and 30 min). Blood coagulation on the surfaces was analysed by SEM and total protein content was determined by Pierce™ BCA Protein Assay Kit.

RESULTS: Incubation of SLActive® and ZLA™ with both, whole blood and platelet-rich plasma showed enhanced protein amounts on ZLA™ compared to SLActive®, as determined by BCA protein assay and SEM imaging. Evaluation of blood coagulation at time points of 10, 20 and 30 min showed that the fibrin network develops faster on ZLA™ compared to SLActive®. Interestingly, samples that were incubated in whole human blood showed the same trend as the samples incubated in platelet-rich plasma, but the discrimination between the samples was better with platelet-rich plasma.

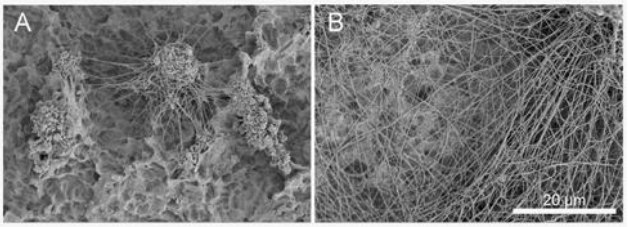

Fig.1: Fibrin network formation on (A) SLActive® and (B) ZLA™ after incubation with platelet-rich plasma for 20 min.

DISCUSSION & CONCLUSIONS: It could previously be shown that HBCs display an enhanced osteogenic differentiation when cultivated on SLActive® surfaces compared to SLA® upon pre-inbubation with human whole blood[6,7]. In this study, enhanced blood coagulation could be observed on the zirconium-based implant surface even when compared to SLActive®. It is therefore of great interest to further evaluate whether the enhanced blood coagulation observed on ZLA™ also promotes the osteogenic differentiation of primary human bone cells (HBCs) and if this is relevant for in vivo osseointegration.

ACKNOWLEDGEMENTS:

We thank the Swiss Commission for Technology and Innovation CTI (Grant no: 16873.2) for financial support.

Effect of a mechanical loading coupled with cell therapy in a bone tissue-engineering scaffold

TC Hausherr[1], LA Applegate[2], DP Pioletti[2]

[1] *Laboratroy of Biomechanical Orthopedics, Institute of Bioengineering, Ecole Polytechnique Fédérale Lausanne, Lausanne, Switzerland.* [2] *Department of Musculoskeletal Medicine, Service of Plastic and Reconstructive Surgery, Regenerative Therapy Unit, University Hospital of Lausanne, Lausanne, Switzerland*

INTRODUCTION: Biomaterials play a crucial role in bone replacement. The main challenge is to combine them with cells, growth factors and an applied mechanical loading. In this study, we combine an external mechanical loading with cell therapy and we analyse their effect on bone growth inside a scaffold implanted in femoral condyles of rats.

METHODS: 2 groups of female rats (6 per group) were implanted in each femoral condyle with a PLA/5% ß-CTP scaffold. One group was implanted with cell-free scaffold while the other one was implanted with scaffold seeded with fetal bone progenitor cells [1]. An external mechanical loading (10 N at 4 Hz for 5 min, 5 times every 2 days, starting 2 days post-implantation) was applied on one leg of each animal while the contra-lateral leg was free of an external mechanical loading. MicroCT images at 6 different time points were used to evaluate the bone volume density (BV/TV) of bone-scaffold construct. The statistical analysis was done using a general additive mixed (GAM) model [2]. The confidence interval of each modeled curve is calculated based on the t-test with $\alpha = 0.05$. The 4 different conditions have been compared pairwise.

RESULTS: The BV/TV of the cell-free and cell-seeded scaffolds over 12 weeks are reported in Figure 1. For each condition, the external (dashed red line) and no external mechanical loading (blue line) conditions are compared. Based on the results obtained by the GAM model (figures not shown), BV/TV of the cell-seeded groups with or without loading is significantly lower compared to the cell-free group for all time points. In particular, for the cell-seeded groups, after 12 weeks of implantation, the BV/TV is 36% and 57.6% lower for an external mechanical loading and for no external loading respectively compared to the cell-free scaffold. This difference in BV/TV between cell-seeded scaffold and cell-free scaffold observed in Figure 1 could be explained by cell migration out of the scaffold towards the vascularized tissue. Through their migration, the cells densify the surrounding

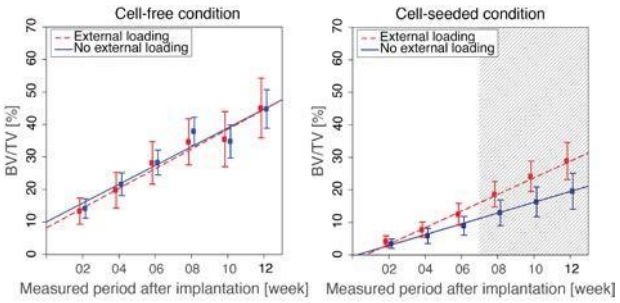

Fig. 1: Evolution of bone volume density (BV/TV) of cell-free and cell-seeded condition over 12 weeks after implantation. The hatched rectangle shows the time period where a significant difference between external mechanical loading and no loading is detected using a general additive mixed model [2].

tissue. Therefore, reduced exchange (*e.g.* nutriments, growth factors) slows down the bone growth inside the scaffold. Nevertheless, from 8 week on, the mechanical loading increased significantly the BV/TV in the cell-seeded group.

DISCUSSION & CONCLUSIONS:
The delivery of cells in the scaffold seemed to impair the bone formation compared to scaffold-free implanted materials. This result is in contrast to most studies and could be explained by the observation of a denser tissue surrounding the cell-seeded scaffold. A produced positive effect on BV/TV was observed anyway when external mechanical loading was applied. Supplemental *in vivo* cell tracking studies are necessary to better understand the cell migration and the stated observations.

Three-dimensional imaging of brain tissue by grating-based micro computed tomography using synchrotron radiation

Simone E. Hieber[1], Christos N. Bikis[1], Anna Khimchenko[1], Georg Schulz[1], Gabriel Schweighauser[2], Jürgen Hench[2], and Bert Müller[1]

[1]*Biomaterials Science Center, University of Basel, Basel, Switzerland.* [2]*Institute of Pathology, Department of Neuropathology, University Hospital Basel, Basel, Switzerland*

INTRODUCTION: Imaging the brain tissue remains a challenge for both clinical and laboratory purposes. Presently, magnetic resonance (MR) imaging is considered the method of choice for three-dimensional visualization of soft tissues, but synchrotron radiation-based micro computed tomography (SRμCT) in phase contrast mode reaches comparable contrast without the application of contrast agents and with a higher spatial resolution relative to MR microscopy.[1] Thus, human brain tissues were scanned to prove the performance of the grating-based method.

METHODS: *Post mortem* samples of the cortex were cut from a human brain of a 73 year-old male who suffered from ischemic stroke. The samples were selected to represent both healthy and diseased tissue. The specimen were fixed in 4 % histological grade buffered formalin, dehydrated in ethanol, transferred to xylenes and embedded in a paraffin/plastic polymer mixture (Surgipath Paraplast®, Leica Biosystems). Cylindrical punches measuring 6 to 9 mm in diameter were extracted from the paraffin blocks. The specimens were scanned at the beamline ID 19 (ESRF, Grenoble, France) with a photon energy of 19.5 keV using synchrotron radiation. The grating-based phase imaging resulted in an effective pixel size of 5 μm. Over a range of 360° 1199 projections with four phase-stepping images over one period of the interferometer fringe pattern.

RESULTS: The grating-based phase tomography data reveal a variety of tissue types including white and gray matter. It should be highlighted that one can distinguish between the healthy and necrotic tissue of the neocortex as demonstrated in the selected virtual slice in Fig. 1. The brain tissue, represented in the upper part of the image with a light gray color, was affected by a stroke and therefore has been degenerated. Presumably located in the gray matter, the boundary between the healthy and diseased tissues is well defined. Blood vessels visible in black could be identified in the gray (darker gray color) and the white matter (medium gray color). They are orthogonally oriented to each other.

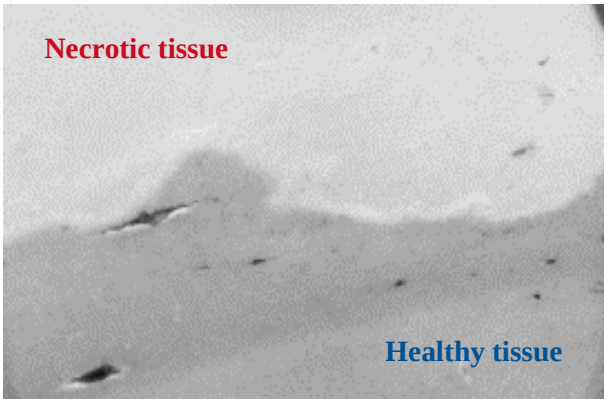

Fig. 1: Reconstructed slice of a human brain tissue scan. The upper part shows necrotic brain tissue due to a stroke that clearly separates from the healthy part represented on the bottom. The slice corresponds to an area of 4.2 mm × 2.8 mm.

DISCUSSION & CONCLUSIONS: Grating-based micro computed tomography is a powerful modality to image human brain tissue *post mortem*. The data sets feature a comparably high contrast at reasonable spatial resolution. Using propagation-based methods the spatial resolution can be further improved but the contrast becomes weaker.[2] The presented tomography data will serve for the selection of the histology slices to be prepared. As histology also yields functional information the two methods are regarded as complementary.

ACKNOWLEDGEMENTS: The project was supported by the ESRF (proposal MD-861).

Development of a novel tissue culture model for degenerative disc disease

M Hlavna[1], S Zollinger[1] and K Wuertz[1]

[1]*ETH Zürich, Department of Health Sciences and Technology, Institute For Biomechanics, Zürich, CH*

INTRODUCTION:

Chronic low back pain is strongly associated with intervertebral disc degeneration. Known and widespread models for disc degeneration have several disadvantages and are not fully convenient to cover all experimental needs (1). Furthermore, proper artificial induction of disc degeneration similar to the physiological in vivo processes in humans is challenging. Changes in mechanical loading can induce degenerative changes, but only over an extremely long time (2), hence not representing a suitable model for animal experiments.

AIMS: To establish a novel degenerative disc disease model based on a bovine nucleus pulposus (NP) tissue culture with artificial annulus fibrosus (AF) described by Prof. Dr. Ito from the TU Eindhoven (3). To enhance similarities to the clinical situation in humans, daily physiological loading, the proteolytic enzyme chondroitinase ABC as well as inflammatory factors was applied.

METHODS: The previously described NP culture system (van Dijk, 2012) was first established with a total of 40 discs from 8 cows (CC2-CC6), which were cultured for up to 21 days. Physiological loading is simulated by applying 1 MPa at 1 Hz for 1 or 2 hours. Degeneration is mimicked by 20 ul of chondroitinase ABC injection into the isolated NPs at concentrations of 1, 2, 5 and 20 U/mL.

Cell and tissue responses were analyzed by RT-PCR (Collagen I and II, Aggrecan, MMP1, 2 and 13, Interleukin 6 and 8), DMMB assay (sulphated glycosaminoglycans), Chloramin-T assay (collagen content), Picrogreen assay (DNA content) and HPLC (chondroitin content analysis). In addition, histological analysis was performed by H&E staining, Safranin-O staining (proteoglycans) and Fast Green staining (collagen).

RESULTS: RT-PCR analysis and GAG content determination of cultured NPs with artificial Annulus fibrosus showed that our NP cultures maintained the tissue matrix composition (GAG content) for up to 21 days. However, mRNA analysis of gene expressions of aggrecan, collagen I and collagen II revealed up to 5-fold down regulation in comparison with Day 0. Expression of matrix metalloproteinases 1, 3 and 13 as well as inflammatory factors Interleukin 6 and 8 in cultures were not different from Day 0. Furthermore, gene expression of collagen I and II as well as of aggrecan was significantly increased after physiological loading in comparison to NP culture samples without loading and hence reached up to 75 percent of gene expression of fresh tissue.

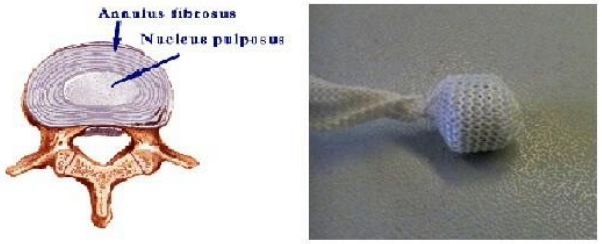

Fig. 1: Scheme of Intervertebral disc (Left). Nucleus pulposus culture in artificial annulus, explants were placed inside a semipermeable membrane and subsequently in a fiber jacket and sewn.

DISCUSSION & CONCLUSIONS: Current results indicate that the established NP culture system is suitable for further experiments with mechanical loading and induction of degradation coupled with inflammation.

ACKNOWLEDGEMENTS: This project is supported by Scientific Exchange Programme NMS.CH.

Preparation of zonal cartilage equivalents via bioprinting technology

E Hoch[1], A Weber[2], T Hirth[2], GEM Tovar[1,2], K Borchers[1,2]

[1] Institute for Interfacial Process Engineering and Plasma Technology IGVP, University of Stuttgart, D. [2] Fraunhofer Institute for Interfacial Engineering and Biotechnology IGB, Stuttgart, D

INTRODUCTION: Because of the limited capacity for spontaneous repair, articular cartilage damage is a serious problem. Cartilage tissue engineering approaches have been investigated for over two decades, but have not yet advanced to guarantee clinical success. One of the potential reasons for this is that current engineered cartilage constructs do not hold the cartilage-specific zonal structure that, however, is crucial for tissue function.

In order to develop artificial, biomimetic structures which perform as well as natural ones, we need fabrication processes that do not set any limits to the generation of shapes, such as bioprinting technology. Furthermore, we need materials that allow for tailoring of the physical, chemical, and biological tissue properties. Thereby, biomolecules from the extracellular matrix of native tissues constitute very promising materials as they hold natural signalling motifs for the stimulations of cell adhesion, migration and function.

With respect to the generation of artificial cartilage by bioprinting technology we develop printable and photo-crosslinkable material systems, based on bio-polymers derived from the native extracellular matrix (ECM). Such bioinks can be used for 3D encapsulation of cells and cell printing, thereby constituting biomimetic matrices with adjustable properties for engineering of tissue models with complex intrinsic structure.

METHODS: Photo-crosslinkable derivatives of the ECM biopolymers gelatin, chondroitin, and hyaluronan are prepared by derivatization with methacrylic anhydride.[1,2] To furthermore achieve printable and dispensable bioinks, the viscous behavior of gelatin precursor solutions is adapted to the requirements of the printing technologies by additional acetylation.[3] The developed bioinks are used for bioprinting with articular chondrocytes to proof cytocompatibility.[2] For fabrication of zonal cartilage models bioinks with appropriate biopolymer composition for replication of the three cartilage zones (superficial, middle, deep) are determined. Criteria for evaluation are the visco-elastic properties of the resulting hydrogels, such as mechanical strength, swellability, and degradability, as well as their potential to preserve cell viability and functionality. Finally, three-dimensional, zonal cartilage models were fabricated and evaluated for their quality.

RESULTS: In this study we present biopolymer-based biomaterials which are processable by inkjet printing and dispensing technology and which can be crosslinked into hydrogels with tissue-like, e.g. cartilage-like properties. Furthermore, three-dimensional cartilage equivalents with biomimetic hierarchical structure as potential cartilage substitutes are presented.

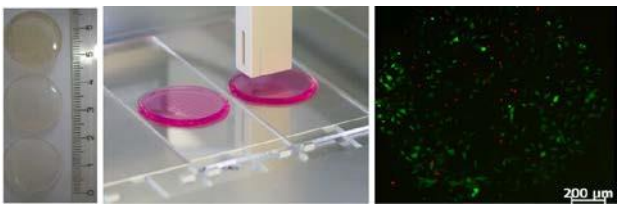

Fig. 1: Left: EZM-based hydrogels of different mechanical properties. Middle: Inkjet-printing of cell-laden biopolymer-based bioink onto hydrogel substrates. Right: Porcine chondrocytes after inkjet printing (green: viable cells, red: dead cells).

DISCUSSION & CONCLUSIONS: The paper discusses our approach to the preparation of functional, zonal cartilage equivalents as tissue substitutes for cartilage defects.

ACKNOWLEDGEMENTS: The authors kindly thank the Fraunhofer-Gesellschaft, the EU (Project 263416, Artivasc 3D), the Max-Buchner-Stiftung, and the Peter und Traudl Engelhorn Stiftung for financial funding.

Energy shift of the pink beam at the beamline ID19 measured with a grating interferometer and a liquid phantom

Anna Khimchenko, Bert Müller, and Georg Schulz

Biomaterials Science Center, University of Basel, Basel, Switzerland

INTRODUCTION: Grating-based hard X-ray phase tomography allows for the determination of the imaginary and real parts of the refractive index distribution[1] to three-dimensionally visualize soft and hard tissues.[2] Laboratory systems are easier accessible than tomography setups at synchrotron radiation facilities.[3] Therefore, conventional µCT-systems should also be equipped with a grating-based phase contrast setup. This is not as simple, because conventional X-ray sources produce a wide energy spectrum and the refractive index is energy-dependent. It is, therefore, reasonable to investigate the refractive index of phantoms at synchrotron facilities to determine the energy shift along the X-ray beam.

METHODS: For the quantitative comparison of reflective indexes a dedicated phantom containing >99.8 % ethanol and polypropylene was built and visualized using the grating-based phase tomography setup at the beamline ID 19 (European Synchrotron Radiation Facility Grenoble, France). The experiments were performed at the mean photon energy of 19.45 keV with 400 projections equiangular along 360° in four phase-steps over one period of the interference pattern.

RESULTS: The measured relative refractive index decrement $\Delta\delta$ depends on the photon energy. The comparison of the measured values $\Delta\delta_m$ with the predicted ones $\Delta\delta_c$ for each reconstructed slice of the homogeneous phantom enabled us to determine the photon energies along the rotation axis, which corresponds to the *y*-axis of the detector, see Fig. 1. The precise knowledge of the photon energy is essential to determine the electron density distribution of the objects of interest. The refractive index decrement of ethanol for the photon energy of 19.45 keV matching best the theoretical value of $-120.59 \cdot 10^{-9}$.was found in slice 301. Within a region of interest of 63 × 54 this value was $-(119.88 \pm 0.07) \cdot 10^{-9}$. To confirm the results the refractive index decrement of polypropylene of the same slice was determined to be $-(43.98 \pm 0.10) \cdot 10^{-9}$. This value fits well to the theoretical value of $-43.08 \cdot 10^{-9}$. The further data treatment is ongoing.

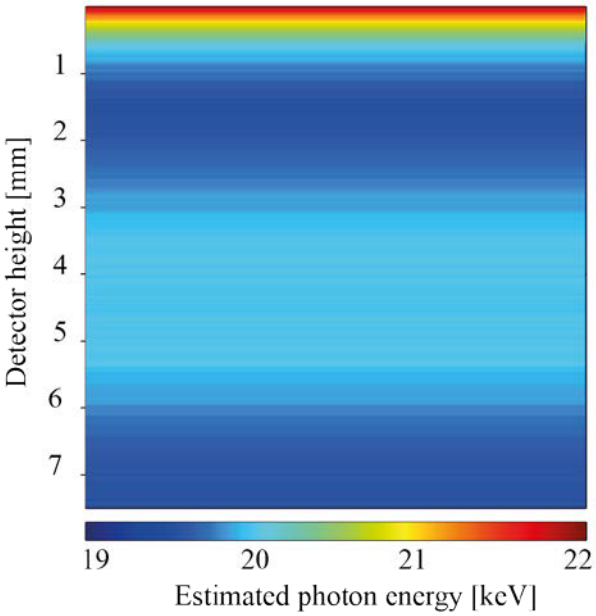

Fig. 1: Determined distribution of the photon energy along the rotation axis based on the calculation of $\Delta\delta$ of the ethanol-filled polypropylene phantom (239 × 281 pixels) measured with a mean photon energy of 19.45 keV.

DISCUSSION & CONCLUSIONS: Grating-based hard X-ray tomography of phantoms at a synchrotron radiation facility as necessary for the calibration of systems with conventional X-ray sources allows for the determination of energy shifts along the beam. Knowledge of energy shifts together with relative refractive index decrements could be used for the determination of electron densities of any material of interest more precisely. It is especially important for the visualization of soft tissues such as brain.

ACKNOWLEDGEMENTS: The authors gratefully acknowledge the active support of Irene Zanette and Alexander Rack. The project is funded by the Swiss National Science Foundation (SNSF project 147172). ESRF provided beamtime (proposal MD-860).

Dental caries: Biomimetic treatment and tooth model development

L Kind[1], C Mangeng[2], S Stevanovic[1], B Bellon[2], S Winkler[2], U Pieles[1]

[1]*Life Sciences/Institute for Chemistry and Bioanalytics, University of Applied Sciences and Arts Northwestern Switzerland (FHNW), CH,* [2]*Nanotechnology/Institute of Chemistry, University of Basel, CH*

INTRODUCTION: Commonly, carious attacks start off with sub-surface demineralization by acid secretion from bacteria. Arresting the process in early stage is crucial to avoid cavitation of the surface resulting in costly tooth restoration and replacement [1].

Biomimetic mineralization is a very promising non-invasive method to treat early caries. It is induced by a peptide (P11-4) which self-assembles into a supramolecular fibrillar 3D network that triggers the nucleation of de-novo hydroxyapatite [2]. Previous studies showed a significant increase of remineralization in artificial induced early caries lesions [3].

Additionally and due to the limited availability and great structural variety of human teeth a bioceramic tooth model (BTM) was developed mimicking natural human dental enamel. Since the peptide is diffusing into the lesion and builds a network there, properties like porosity/ density and structure of BTMs are particularly important. One big challenge in building artificial teeth is with the complex structure of natural human teeth. Enamel exhibits a hard and dense structure, whereas dentin is rather soft and porous. This study should facilitate the possibility to establish enamel-like BTM as a standardized test system for further studies in caries treatment.

METHODS:

De-/Remineralization of natural human tooth

Artificial sub-surface lesions on human enamel were induced by incubation in acidic demineralization buffer. P11-4 was directly applied on sub-surface lesion and the tooth was subsequently incubated in remineralization buffer for 2 weeks. The samples were analyzed by micro-computed tomography (micro CT).

Bioceramic tooth model (BTM)

BTMs are based on mixtures of hydroxyapatite and a porosifying agent. The ratio reflects the degree of porosity and density of BTMs. The mixtures were pressed into tablets and sintered at 1250°C. The models were characterized by micro CT, scanning electron microscopy (SEM) and Brunauer-Emmett-Teller (BET) in order to compare them with human dental enamel.

RESULTS: micro CT measurements represented a successful remineralization status *in vitro* in artificial sub-surface lesions of human enamel. Samples treated with peptide showed within 14 days an increasing growth of material in the cavity region compared to the reference, which was not treated with peptide.

Figure 1 presents micro CT images of BTMs with different hydroxyapatite (HA) : porosifier (P) ratio. Differences in grey values could be detected indicating material with different density / porosity. The demineralization procedure to introduce artificial carious lesions in BTMs is still in process.

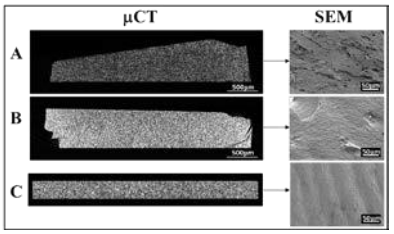

*Fig. 1: micro CT images of BTMs with different ratio (HA):(P) **A**-80(HA):20(P); **B**-100(HA) w%); **C**-human enamel slice (reference) - left: corresponding SEM images of interface.*

DISCUSSION & CONCLUSIONS: The peptide induced remineralization of carious lesion in human teeth demonstrates the non-invasive regeneration potential of this system. The use of BTMs can simplify and standardize studies of remineralization processes in caries lesions and ensure comparability of results. This standardized test system would be available to study new compounds to cure caries.

ACKNOWLEDGEMENTS: The authors would like to thank Swiss-Nanoscience Institute (SNI) and Swiss National Science Foundation (SNSF) (project no 144617) for providing financial support to this project.

A new *in vivo* MRI method to non-invasively monitor and quantify the perfusion capacity of 3D-biomaterials grown on the chorioallantoic membrane of chick embryos

F Kivrak Pfiffner[1], C Waschkies [2,3], Y Tian[3], A Woloszyk[4,5], M Calcagn[1], P Giovanoli[1], M Rudin[2] and J Buschmann[1]

[1]Plastic Surgery, University Hospital Zurich, CH. [2]Institute for Biomedical Engineering, ETHZ, CH, [3]Visceral Surgery, University Hospital Zurich, CH, [4]Institute of Oral Biology, UZH, [5]Molecular Life Sciences, University of Zurich and ETH Zurich

INTRODUCTION: Artificial engineered grafts can have different effects on vascularization. Not only the pore size, but also the size of the scaffold and the interconnectivity of the pores are important criteria for blood-vessel ingrowth after implantation. The chorioallantoic membrane (CAM) of the chick embryo is a well-established model for studying vascularization. Here, we present the application of MRI to measure the perfusion capacity of CAM-implanted scaffolds *in situ* on the CAM in the living chicken embryo.

METHODS: DegraPol® (DP) foams and silk fibroin (SF) scaffolds (either seeded with human dental pulp stem cells (hDPSCs) or cell-free) were placed on the CAM of the chick embryo at incubation day (ID) 7. At ID 14, the perfusion capacity of these tissue engineered constructs was assessed *in vivo* by MRI before and after application of a constrast agent (Dotarem®).
T_1 relaxation times were determined in three regions of interest at (i) the surface of the scaffold, (ii) in the middle, and (iii) at the interface of the scaffold on the CAM. Perfusion capacity in these three regions of interest was assessed through changes in the longitudinal relaxation rate:

$$\Delta R_1 = R_1 - R_{10}$$

with

$$R_1 = 1/T_1$$

$$R_1 = R_{10} + r_1 \cdot [Gd]$$

The longitudinal relaxation rates R_1 and R_{10} are after and before contrast agent administration; and r_1 is the molar relaxivity of the contrast agent in s^{-1} mol^{-1} L and[Gd] the concentration of Gd in $molL^{-1}$.

RESULTS: In both biomaterials, DP as well as SF (± hDPSCs), perfusion capacity declined from the interface towards the surface, in line with the scaffolds being vascularized from the CAM towards the surface (*Figure 1*). The perfusion capacity of SF scaffolds was significantly higher compared to the DP scaffolds (3 - 4 times higher, $p < 0.0001$). However, the hDPSCs did not evoke a statistically significant higher perfusion of the silk fibroin scaffolds compared to the cell-free silk fibroin scaffolds ($p > 0.1$).

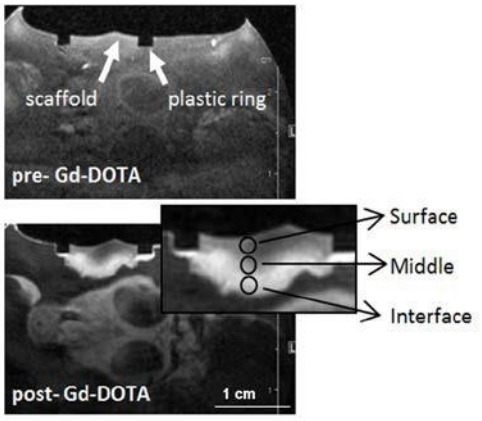

Fig. 1: In ovo T_1-weighted MRI images acquired 7 days post-implantation in an axial slice through the scaffold. (a) before, (b) 25 min after i.v. injection of Gd-DOTA. Enlarged section: scaffold with regions of interest (circles) at the interface with the CAM, in the middle and on the surface of the scaffold.

DISCUSSION & CONCLUSIONS: The CAM assay together with non-invasive MRI presents a reliable *in vivo* model for monitoring the perfusion capacity of biomaterials.

ACKNOWLEDGEMENTS: Trudel Silk Inc., Zurich, Switzerland is highly acknowledged for providing silk fibroin. We thank *ab medica*, Italy, for providing DP.

A new light comes up in the world of periodontal therapy- P11 peptides and their in vitro evaluation on human hard and soft tissue cells

Franziska Koch[1], Uwe Pieles[1], Stephanie Mathes[2], Ursula Graf[2]

[1]Institute for Chemistry and Bioanalytics, University of Applied Sciences, Switzerland
[2]Life Science and Facility Management, ICBC, ZHAW, Switzerland

INTRODUCTION: Beside caries, periodontitis is also a very common degenerative disease affecting at least every second to third people is suffering once on this disease. It is characterized by a microbial alteration which leads to a inflammation resulting in the degradation of alveolar bone, root cementum and periodontal ligament. A new treatment strategy uses different kinds of material which were placed in a defect area where progenitor/stem cells from neighbouring tissues can be recruited for in situ regeneration [1] In the present study newly synthesized peptides were produced to form hydrogels which could be applied through an injection in a periodontal defect without a surgery. The peptides, called P11-4 and P11-8, consist of 11 amino acids which could be triggered by pH and salt concentration to form beta-sheet structures. Furthermore these beta sheet structures are able to form higher ordered structures like fibrils and fibres leading to a 3D network that serve as extracellular matrix (ECM).
METHODS: To evaluate the characteristics of self-assembling peptides like P11-4 and P11-8, quartz crystal microbalance with dissipation monitoring (QCM-D) and rheology measurements were performed. Furthermore cell attachment and proliferation were studied using osteosarcoma cell line SAOS-2 and human primary periodontal fibroblast (hPDLF) in combination with different peptide hydrogels, at concentrations of 15, 20 and 30 mg/ml after 24h, 48h and 96h, respectively.
RESULTS: The viscoelastic properties of the different peptide hydrogels and the time which they need to build up, depend on the peptide sequence and their self-assembling behaviour. Furthermore as demonstrated in Figure 1, cell attachment and cell proliferation are directly depending on the net-charge of the peptide as well as on the viscoelastic properties .For example SAOS cells showed a higher cell attachment and proliferation rate on P11-4 hydrogels (Figure 1D), which are characterized by a negative net charge and a low viscoelasticity, than on P11-8 hydrogels (Figure 1C), known to have a positive net-charge with a higher viscoelasticity. On contrary hPDLF cells showed less attachement and proliferation if they were incubated on P11-4 hydrogels (Figure 1B) than on P11-8 hydrogels (Figure 1A). These results goes ahead with the different phenotypes of the cells as e.g. for hPDLF are well spreaded on P11-8 hydrogels (Figure 1A), whereas on P11-4 hydrogels, hPDLF seem to be more roundish in shape and not well spreaded.

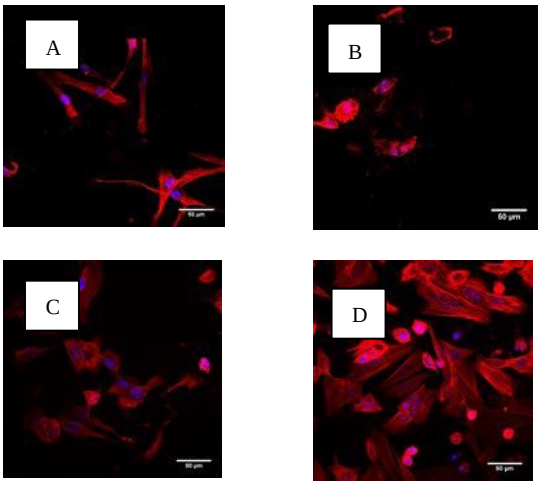

Fig. 1: show cell attachement of PDLF (1A, 1B) and SAOS (1C, 1D) on P11-8 (Figure 1A, C) and on P11-4 (Figure 1B, D) after 24 h at a concentration of 6.35 mM. PDLF cells were stained with DAPI and TRITC-conjugated Phalloidin.

DISCUSSION & CONCLUSIONS: It could be demonstrated that in consideration of the specific characteristics of the natural microenvironment like e.g. soft connective tissue for hPDLF, provide a possible scaffold where cells are able to attach, spread and proliferate into newly tissue. Therefore P11-peptides could be used as a new treatment strategy in periodontal therapy

ACKNOWLEDGEMENTS: *Credentis AG (M.Hug and D.Lysek) are greatfully acknowledged for supporting the project.*

Comparing vascular casts of murine kidneys with and without tissue corrosion

W Kuo[1], P Thalmann[2], G Schulz[2], A Marmaras[1], EP Meyer[3], A Lang[4], SE Hieber[2], U Olgaç[1], B Müller[2], V Kurtcuoglu[1]

[1] The Interface Group, Institute of Physiology, University of Zurich, Switzerland [2] Biomaterials Science Center, University of Basel, Switzerland [3] Institute of Molecular Life Sciences, University of Zurich, Switzerland [4] Institute of Anatomy, University of Zurich, Switzerland

INTRODUCTION: Vascular corrosion casting is a well-established technique for obtaining the vasculature by perfusing the blood vessels with a hardening material and then corroding the surrounding tissues. The resulting cast of the vascular lumen can be imaged using micro computed tomography (µCT) to obtain the entire 3D structure. We compared the structure of a vascular corrosion cast of a mouse kidney to that of a kidney cast with added contrast agent, but no corrosion.

METHODS: Two mice were anaesthetized with pentobarbital and perfused through the left heart ventricle with heparin 25000 u/l in PBS, 4 % formaldehyde in PBS, and the casting resin PU4ii (vasQtec, Switzerland).[1] For the corrosion, the tissue was macerated in 5-10 % KOH. The plastic casts were washed, freeze-dried, and coated with OsO_4 for enhanced contrast. For the contrast agent casting, 1,3-diiodobenzene was admixed to the PU4ii mixture to an equivalent of 90 mg iodine per ml before perfusion, and the tissue was not corroded afterwards.

Both samples were imaged on a phoenix nanotom m µCT scanner (Sensing & Inspection Technologies GmbH, Wunstorf, Germany) with a voxel size of 1.5 µm. The corroded sample was imaged in air with an accelerating voltage of 100 kV, while the non-corroded sample was measured in PBS using an accelerating voltage of 40 kV.

RESULTS: Both protocols allowed for the acquisition of the vascular (micro-)structure of the kidney. While the corroded cast had the better signal-to-noise ratio and fewer bubbles within the cast, there were some significant structural deviations. In Figure 1, roughly a quarter of a representative section of each kidney is shown. The corroded cast has a rougher surface and some large empty areas without blood vessels are visible at the image center. These features were not found in the non-corroded cast. Additionally, the vasa recta are much more tightly bundled in the latter.

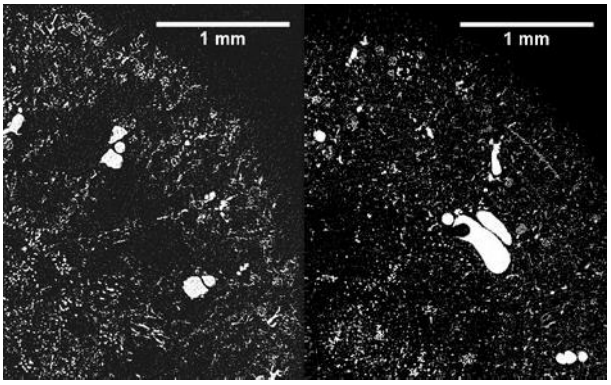

Fig. 1: µCT image slices of vascular corrosion casts after the corrosion of the surrounding tissue (left) and without corrosion (right).

DISCUSSION & CONCLUSIONS: The overall vascular structure is comparable in both cases. This observation is expected, since parameters such as blood vessel surface, volume, and connectivity depend on the casted volume and will remain unaffected by the corrosion procedure. Other parameters including the distances between vessels can change, affecting structural relationships. Depending on the research question, it may thus be necessary to image the vasculature in the perfused tissue before corrosion. Since the X-ray absorption of tissue is higher than that of air, achieving the necessary signal-to-noise ratio can prove challenging, especially when trying to resolve the microstructures close to the limit of spatial resolution. This obstacle is balanced by the possibility of performing multi-modal imaging on tissue and vascular cast when the tissue is intact and not corroded or cut into slices. Therefore, we view casting without corrosion followed by multi-modal imaging as a promising tool for 3D functional analysis of organs including the kidney.

ACKNOWLEDGEMENTS: This work was funded by the Swiss National Science Foundation through NCCR Kidney.ch and grant 205321_153523.

Development of methodology for nanoindentation testing of cartilage of rats

C Lavet[1], I Badoud-Georges[1], J Nohava[2], P Ammann[1]

[1] HUG, Geneva, Switzerland [2] Anton Paar, Peseux, Switzerland

INTRODUCTION: Osteoarthritis is widely recognized as a worldwide threat to population health. To better understand the mechanisms of cartilage degradation, it is mandatory to develop a technic dedicated to measure cartilage quality. Recently, nanoindentation of biological tissues (bioindentation) has emerged as a tool for local characterization of cartilage mechanical properties especially in small animal model. This method allows direct measurement of elastic properties of cartilage in very local areas using a spherical indenter. However, the methodology is still not entirely defined and some important issues (heterogeneous materials, spheroid surface…) have to be studied in more detail. The present work was aimed to set up the measurement protocol and to assess the sensitivity of the method.

METHODS: A new device for bioindentation named Bioindenter was used for indentation of femurs of rats. Spherical indenter with 1 mm diameter from ruby and maximum indentation depth of 15 µm was used in all experiments. The loading rate was 15 mN/min and there was a 30 seconds hold period at maximum load. The Young's modulus, maximum force reached and energy of indentation were calculated using ISO 14577 standard.

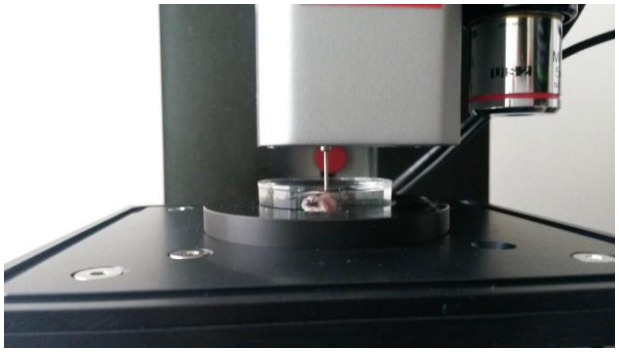

Fig. 1: Images of Bioindenter indenting femur cartilage from rat. Long shaft indenter is used to allow indentation in liquid.

All experiments were performed with the femur completely immersed in fluid. The femur specimens were obtained from 11 months old Sprague Dawley rats. There were five specimens of each type and each of them was tested in three different zones, submitted to different mechanical loading during walk. There were five indentations in each zone. The cartilage mechanical properties were evaluated in both condyles of the femur.

RESULTS: For each evaluated parameters and in each zone, the mean of individual dispersion ranged from 20 to 35%. However the mean of dispersion between the 5 rats was lower than 5-6% for almost each parameter in each zone. The most important variation was observed for force and Young's modulus in the most loaded zone (11-12%).

Independently of the zone investigated, force, Young's modulus and working energy of the lateral condyle were respectively 40, 44 and 21% lower as compared to the medial condyle. Young's modulus ranged from 4.5 to 8.03 MPa. These results are in accordance with the literature investigating other species.

In both condyles, force, Young's modulus and working energy were higher in zones submitted to the higher strain related to weight bearing during locomotion. Considering Young's modulus, this difference was higher in magnitude in medial condyle as compared to the lateral condyle (at least +50% vs +35%). In these different compartments, Young's modulus ranged from 3.94 to 11.17 MPa.

DISCUSSION & CONCLUSIONS: A new nanoindentation instrument was used for measurements of rat's femoral cartilage mechanical properties. The present study focused on the methodology and sensitivity of the method. Although relatively small number of specimens was used (5 in each group), the standard deviation of results obtained on each condyle is considerably low and hence confirms very good reliability of the bioindentation method. All the three factors compared (Young's modulus, maximum force and elastic energy of indentation) obtained by local nanoindentation give important information about mechanical properties of cartilage. Furthermore, the method is sensitive enough to reveal differences in zones of cartilage subjected to different mechanical loading. This tool could be very helpful in the field to investigate pathophysiology of osteoarthritis.

The effect of bleaching agents on the surface hardness and biological test upon composite materials

M Moldovan[1], C Prejmerean[1], V Popescu[2], I Cojocaru[3], C. Saroşi[1], D.Prodan[1], I.Baldea[4]
[1]"Babes Bolyai" University, Cluj-Napoca, Romania, [2] Technical University of Cluj-Napoca, Romania, [3] University of Craiova, Romania, [4] University of Medicine and Pharmacy "Iuliu Haţieganu", Cluj-Napoca, Romania

INTRODUCTION: The purpose of this study was to evaluate the effects of experimental natural bleaching gel G19® and commercial BrightBleach® bleaching gel on the Vickers microhardness and biological test of universal nanocomposite (Nanofill-NS), and 3 experimental nanocomposite (P1, P3, P6).
METHODS: Each type of composite resin prepared in Teflon molds (1 × 1,5 mm), was further divided into three groups [n = 5 controls were placed in distilled water for 10 days and the other two groups of n = 5 were bleached with experimental and commercial gel for 10 days]. Surface hardness of the composite resin was tested with a Vickers hardness tester, by using the universal device 270 VRSA. For cytotoxicity testing, we used both cell lines: human dermal fibroblasts (HDFa) and the dental follicle stem cells. The culture medium conditioned with the EBA was obtained as described by Cavalcanti et al (2005); and complying with the ISO 10993-12:2012 proceedings. Composite samples were prepared thin (0.5 mm) which were subjected to the bleaching process, simulating the clinical protocol standard "dentist Supervised". These samples were incubated with culture medium at 37°C, the proportion of 1ml average / 3cm2 surface composite sample for 24 and 72 hours. Viability was measured by colorimetric measurement of formazan, a colored compound generated by viable cells using CellTiter 96® AQueous Non-Radioactive Cell Proliferation Assay (Promega Corporation, Madison, USA). Untreated cultures exposed to medium were used as controls. Results are presented as OD_{490}.
RESULTS: In table 1 we have shown average value for Vickers microhardness.

Table 1. Average value for Vickers microhardness

Samples	When determining Belching	Vickers microhardness Gel CP	Gel 19
NS	Before	57.1	
	After	56	56.9
P6	Before	74.7	
	After	74.1	74.6
P1	Before	62.9	
	After	60.9	62.2
P2	Before	68.8	
	After	67.4	68.2

As show in figures 1 and 2, the compounds studied had a low cytotoxic effect on cell cultures.

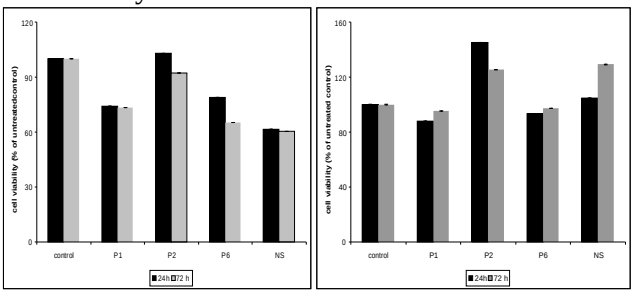

Fig. 1: The cell viability fibroblasts and dental follicle cells for samples bleached with, G19®.

For statistical analysis of viability we compared the OD490 out of every experimental group at each study period, with value initial.
DISCUSSION & CONCLUSIONS Following these studies and analyzing the results (tabel1), we could say that surface hardness of composite materials after bleaching process can increase, decrease or remain unchanged Such variations suggest that some restorative materials may be more susceptible to discoloration and some whitening agents. Although P1 composites have higher resin content than P2 and P6, would be expected to occur roughness in this group, but this did not occur in this study. This can be attributed to differences in pH bleaching agents. pH whitening gel experimentally evaluated in this study was close to neutral and had a minimal effect on surface hardness of samples. The most important effect of the decrease in viability was recorded for samples P1 and NS on fibroblasts. This effect was greatly reduced dental follicle stem cells and visible only for P1. After 10 days of bleaching treatment, there was no significant changes in the surface hardness to composite materials testing.
ACKNOWLEDGEMENTS: This work was funded by: the Romanian Ministry of Education and Research, national project PNII no: 165/2012.

Probing cell-matrix interactions in RGD-decorated macroporous PEG hydrogels for in vitro chondrocyte culture

JJ Zhang[1], A Mujeeb[1] Y Du[2,3], Z Ge[1,4]

[1]Department of Biomedical Engineering, Peking University, Beijing 100871, China. [2]Department of Biomedical Engineering, Tsinghua University, Beijing 100084, China. [3]Collaborative Innovation Centre for Diagnosis and Treatment of Infectious Diseases, Hangzhou, 310003, China. [4]Arthritis Clinic and Research Centre, Peking University People's Hospital, Beijing, China.

INTRODUCTION: Cell-matrix interactions have a profound effect on cell behaviour, in particular cell morphology, *de novo* extracellular matrix (ECM) formation and subsequent tissue growth.[1-2] Herein, macroporous hydrogels made of poly (ethylene) glycol (PEG) were fabricated, and arginine-glycine-aspartic acid (RGD) peptide was introduced to prepare PEG-G400 (with 0.4mM RGD) and PEG-G2000 (with 2mM RGD), respectively. Primary chondrocytes were encapsulated within the hydrogels and performance was evaluated based on cell distribution and morphology, proliferation, gene expression and subsequent ECM accumulation *in vitro*. This study highlights the relationship between cell adhesion and cell function within 3D macroporous scaffolds.

METHODS: Macroporous PEG hydrogels, PEG-G2000 (with 2mM RGD), PEG-G400 (with 0.4mM RGD) and PEG-RED (with 2mM RED, control group) were fabricated and subjected to primary chondrocyte culture for 5 weeks *in vitro*. Cell morphology, distribution, and viability were observed *via* fluorescein diacetate (FDA) (F7378 Sigma, China) and propidium iodide (PI) (P4170, Sigma, China) staining. Metabolism of chondrocytes was measured using MTT assay (3-(4,5-Dimethyl-2-thiazolyl)-2,5-diphenyl-2H-tetrazolium bromide) (M2128 Sigma, China). Cell-matrix interactions were evaluated *via* F-actin and integrin β1 staining. GAG deposition was quantified by DMMB assay (1, 9-dimethylmethylene blue) (341088 Sigma, China) whereas gene expression analysis was conducted using real-time PCR. Next, immunohistochemistry staining was carried out to assess the formation of cartilaginous ECM, in particular presence of collagen I, II, X and GAG molecules.

RESULTS: Encapsulated chondrocytes formed cell aggregates around the porous architectures due to RGD clustering. In comparison, a slightly stretched morphology of cell aggregates was observed in PEG-G2000 hydrogels (shown in Fig.1). Additionally, a boost in cell viability and proliferation was observed in PEG-G2000, in comparison to PEG-G400 and PEG-RED groups. GAG accumulation was found to increase with increasing RGD concentration. Elevated gene expression of collagen I and II, and aggrecan were found in groups containing 2mM RGD.

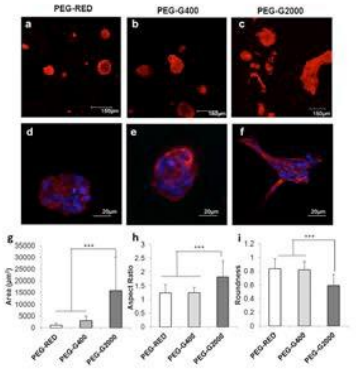

*Fig. 1: F-actin staining using rhodamine phalloidin (red) with DAPI (blue) after 3 days in culture. Confocal z-stack projections (a,d) PEG-RED, (b,e) PEG-G400, and (c,f) PEG-G2000. Morphology of cell aggregates quantified for (g) area, (h) aspect ratio, and (i) roundness. Error bar represent mean values ± S.D ***P<0.001, n=5.*

DISCUSSION & CONCLUSIONS: Hitherto, we have shown that integration of RGD in macroporous PEG hydrogels, nearing a threshold concentration of 2mM may be sufficient for improving scaffold functionality for 3D chondrocyte culture. Further investigation is underway to assess the potential application of RGD-decorated macroporous PEG hydrogels for cartilage tissue engineering.

ACKNOWLEDGEMENTS: The authors would like to acknowledge support from the National Natural Science Foundation of China grant (81471800, 81271722).

Amido, urea and thiourea ethanolamine monolayers

D Mueller, A Zumbuehl

Department of Chemistry, University of Fribourg, Fribourg, CH.

INTRODUCTION: Single chain amphiphiles such as *N*-acylethanolamines (NAEs) have a broad range of medical applications.[1] The bioactivity include anti-inflammatory effects found for *N*-palmitoyl ethanolamine or the satiating effect for *N*-oleoyl ethanolamine.[2]

Here, the NAEs serve as model system for more complex molecules such as phospholipids. We are interested in the balance of intermolecular forces such as van der Waals interactions between the hydrophobic tails and hydrogen bonding between amido, urea, and thiourea moieties.[1]

METHODS: The synthesised ethanolamines were characterised by NMR, IR and mass spectroscopy. The monolayer behaviour of the synthesised amphiphiles was investigated on a Langmuir-Pockels film balance. Additionally, the monolayers were examined by X-ray diffraction measurements.

RESULTS: Amides were synthesised by coupling ethanolamine with long-tailed acid chlorides. The urea and thiourea ethanolamines were obtained by coupling of isocyanates or thioisocyanates with ethanolamines.

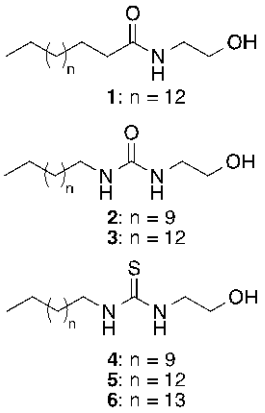

Fig. 1: Chemical structure of the synthesised amido-, urea- and thiourea amphiphiles.

Table 1. Melting points of the amido-, urea and thiourea amphiphiles with different tail lengths.

Tails	Amide	Urea	Thiourea
C14	90-91 °C [3]	103-105 °C	66-68 °C
C17	99-101 °C	112-113 °C	75-77 °C
C18	106-108 °C [4]		80-81 °C

DISCUSSION & CONCLUSIONS: The structural organisation and the behaviour of the monolayer of the synthesised amido- urea- and thiourea amphiphiles is guided both by van der Waals interactions and hydrogen bonding in the headgroup region.

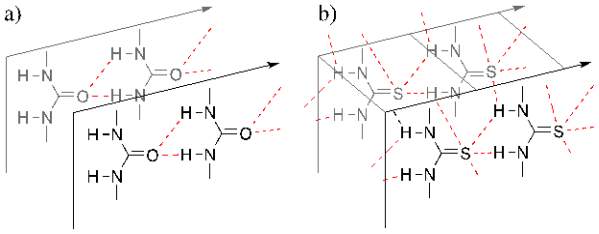

Fig. 2: Molecular organisation in the urea (a) and the thiourea (b) monolayer. Ureas form planes of hydrogen bonded moieties, thioureas form 2D networks of hydrogen bonds (drawn in red).

The hydrogen bonding gets stronger going from amide to urea and thiourea amphiphiles (see table 1). Compared to the van der Waals forces, the hydrogen bonds get the dominant force for urea ethanolamines. 3D urea crystallites form already during the spreading process on the Langmuir-Pockels through. During compression the urea aligns in a planar network with gliding planes so that the structure can adapt to the compression. The thiourea molecules orient themselves in a two-dimensional network of hydrogen bonds that has the ability to self-heal after breaking during monolayer compression. The thiourea amphiphiles represent an intermediate case between amido and urea amphiphiles and might serve as an interesting starting point for future responsive biomaterials.

ACKNOWLEDGEMENTS: This work was supported by the Swiss National Science Foundation and the NCCR for Chemical Biology.

Nanomechanical characterization of polydimethylsiloxane films

Bekim Osmani[1], Tino Töpper[1], Florian Weiss[1], Fabian Wohlfender[1], Vanessa Leung[1], Christian Bippes[2], and Bert Müller[1]

[1]*Biomaterials Science Center, University of Basel, c/o University Hospital, 4031 Basel, Switzerland,* [2]*Nanosurf AG, Gräubernstrasse 12-14, 4410 Liestal, Switzerland*

INTRODUCTION: Polydimethylsiloxane (PDMS) is the most widely used silicon-based organic polymer. Its applications range from cochlear implants for the inner ear to microfluidic chips. They are also often referred as the dielectric layer of choice for electrically activated polymer actuators (EAP). EAPs show millisecond response times and have a specific continuous power up to 10 times higher than human skeletal muscles [1]. PDMS films have to be below 1 µm in thickness for actuations below 42 V and strains above 20% [2]. A proper determination of the Young's modulus is therefore crucial.

METHODS: PDMS films were prepared, see Table 1, by mixing a siloxane base/cross linking agent (Dow Corning® 184 Silicone Elastomer Kit, Dow Corning Europe S.A, Belgium) with a methylsiloxane based solvent (Dow Corning® OS-20 Fluid, Dow Corning Europe S.A, Belgium).

Table 1. Preparation parameters of PDMS films.

Sample	PDMS/OS20	RPM	Film thickness
1	1:0	1000	192 ± 10 µm
2	1:0	6000	8.5 ± 1.0 µm
3	1:1	6000	2.4 ± 0.5 µm
4	1:5	6000	0.9 ± 0.2 µm

The mixtures were stirred for 1 minute, spin-coated on 3-inch Si-wafers (Si-Mat Silicon Materials, thickness 381 ± 25 µm) and thermally cross-linked at a temperature of 75 °C for a period of 24 h. After curing, 400 indentations were performed on a 60 × 60 µm^2 array at loads of 12, 24, 36 and 48 nN. A cantilever with a spring constant of 0.16 N/m and a spherical tip (B150_CONTR, Nanotools, Germany) with a radius of 144 nm was mounted on a AFM Scan Head (FlexAFM C3000, Nanosurf Liestal, Switzerland). Calculations based on the Hertzian contact theory were performed using the ARTIDIS® software (Automated Reliable Tissue DIagnosticS). The film thicknesses were measured using a 3D Laser Microscope with a spatial resolution of 0.5 nm in z-direction (Keyence VK-X200, Keyence International, Belgium).

RESULTS: The calculated Young's moduli for the 6'400 nanoindentations are visualized in Figure 1. The results were well reproducible indicated by the statistical error. There is an increase of the Young's modulus for thinner films. It is getting lower for higher loads exhibiting a softer 'bulk' of the film.

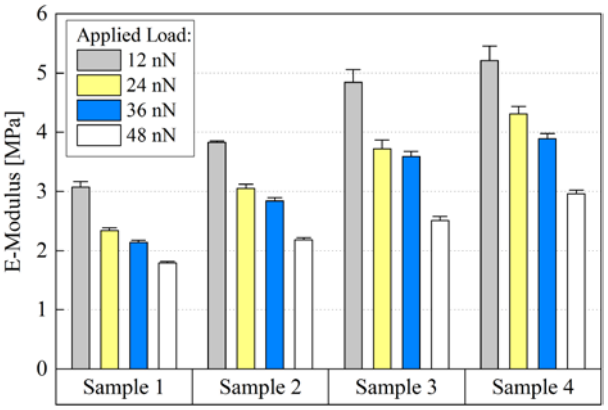

Fig. 1: Young's modulus of PDMS films.

DISCUSSION & CONCLUSIONS: The decrease of the Young's modulus at higher loads reveals a possible heterogeneity of the PDMS film, with an increased modulus at the surface. These results are in agreement with previously obtained data [3, 4]. Substrate effects can be excluded, since the modulus is decreasing at higher loads and indentations depths were below 60 nm. A Hertz model taking into consideration the interfacial adhesive forces is supposed to be more appropriate, but is not implemented in the software yet. Nanoindentations in liquid could also reduce the thermodynamic work of adhesion.

ACKNOWLEDGEMENTS: The financial support of the Swiss National Science Foundation (Project 200021-135496) and the nano-tera.ch initiative *SmartSphincter* is gratefully acknowledged.

Bioprinting of three-dimensional sulfated polysaccharide structures for local growth factors delivery

G Pagliccia[1], M Kesti[1], F Formica[1], G Gelardi[2], M Zenobi-Wong[1]
[1] *Cartilage Engineering + Regeneration, ETH Zürich, Zürich, Switzerland.*
[2] *Physical Chemistry of Building Materials, ETH Zürich, Zürich, Switzerland.*

INTRODUCTION: The ultimate goal of bioprinting is the creation of organs with precise 3D architectures which, one day, will overcome the shortage of donors for transplantation. The success of 3D bioprinting relies on the development of engineered bioinks capable of mimicking the complex nature of native tissues. Freeman et al. [1] determined the interactions between sulfate groups and several heparin-binding proteins. Inspired by this, we developed a sulfated polysaccharide capable of growth factor binding and local delivery.

METHODS: Gellan gum sulfate (GG-S) was prepared via a chemical reaction with chlorosulfonic acid in formamide [2]. The outcome of the sulfation reaction was assessed via elemental analysis, NMR and FTIR. The molecular weight (Mw) distributions after reaction were measured using SEC-MALLS. Sulfated gellan gum was added into our previously-developed bioink and the printability of the mixture was assessed via rheology. The sulfated bioink was printed into a standard dumbbell-shaped construct (Fig.2) using the Biofactory® bioprinter (RegenHU, Switzerland) to further characterize its mechanical properties. Cytotoxicity of GG-S was assessed with Live/Dead assay on hASCs encapsulated into 3D hydrogels over 21 days.

RESULTS: The degree of sulfation (DS) per monosaccharide unit is shown in Fig. 1. ^{13}C-NMR spectra confirmed that sulfation is achieved preferentially on the secondary alcohols of the glucose units, followed by the primary alcohols on the rhamnose units. Mw distribution measured with SEC-MALLS reveals a considerable degradation of the polysaccharide chains comparable to that found in literature [3]. Rheology data collected from cation-crosslinked hydrogels containing different amounts of several sulfated polysaccharides shows highly tunable mechanical properties without considerably affecting the printability of the original bioink. The Live/Dead assay of hASC encapsulated into bioink and bioink+GG-S (5% w/v.) hydrogels reveals good viability comparable to the 1% alginate control.

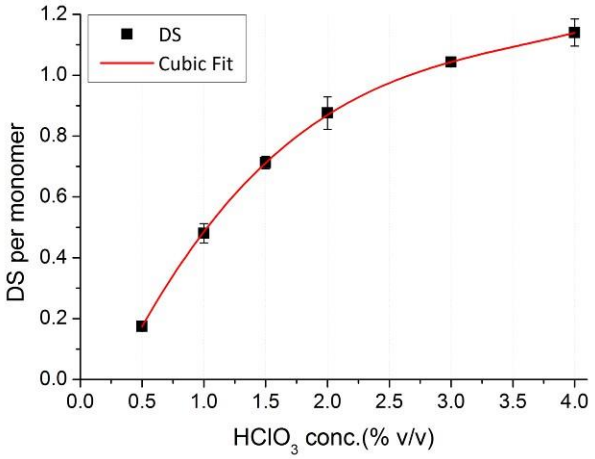

Fig.1: Degree of sulfation (DS) of modified gellan gum measured with elemental analysis (n=2)

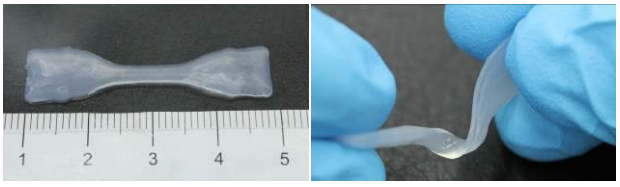

Fig.2: Bioprinted 3-layered dumbbell-shaped construct using bioink+1% w/v GG-S.

DISCUSSION & CONCLUSIONS: Gellan gum is a natural, FDA approved polysaccharide which allows a wide range of chemical modifications. In this project we present a highly-reproducible method to prepare sulfated gellan gum with precise DS and Mw distribution. This material was designed to improve our previously-developed bioink by adding the ability to bind growth factors in order to better mimic the native ECM.

ACKNOWLEDGEMENTS: The work was funded by the Swiss National Science Foundation (CR32I3_146338 /1) and FIFA F-MARC.

A method compensating for ICP-MS signal instabilities to accurately determine calcium phosphate

D Pasche[1], C Stähli[1], N Döbelin[1], M Bohner[1]

[1] *Skeletal Substitutes Group, RMS Foundation, Bettlach, CH*

INTRODUCTION: Calcium phosphates (CaP) are commonly used as biodegradable bone substitutes. Their exact composition highly influences their in vivo degradation rate which can be studied through in vitro dissolution tests. Inductively coupled plasma–mass spectrometry (ICP-MS) is a powerful tool to quantify ions in solutions, but the measurement accuracy was observed to be ±15% and limited to 30 minutes following calibration. The aim of this study was to develop a method for the precise quantification of CaP composition. The first step was to use standard solutions of known compositions. The second step was to use calcium phosphate powders that had been characterized by Rietveld refinement of x-ray diffraction (XRD) data.

METHODS: Ca-P-Mg (10:5:1wt ratio) calibration standards were made by serially diluting standard solutions (Inorganic Ventures) to desired concentrations. A 40 ppm Indium (In) solution was combined with these solutions and used as an internal standard. For the second step, eight known CaP powders (~0.1g) consisting of different phases (β-Ca2(P2O7), β-Ca3(PO4)2, Ca5(PO4)3(OH), Ca(OH)2) were dissolved in 10mL 70% HNO3 and diluted 1:1000 in 3% HNO3. Ca-P-Mg calibration standards were measured using ICP-MS (7700x, Agilent Technologies) 10 times in a row, twice, to evaluate the measurement stability over time. The variation of the concentrations was compared to the fluctuation of the In signal. For dissolved CaP powder measurements, a Ca-P-Mg calibration standard was measured every 6th sample. XRD spectra were obtained on a Brucker D8 Advanced.

RESULTS: The evolution of Ca, P and Mg concentrations over time was similar to the variation of the In concentration (Fig 1a). Thus the latter was used to correct the values, which reduced the standard deviation from 4.3% to 1.6%. Since the Ca, P, Mg and In concentrations tended to diverge over time, they were corrected with the changes of the measured concentrations of the Ca-P-Mg calibration standard. The resulting values were even closer to the nominal concentrations (Fig 1b).

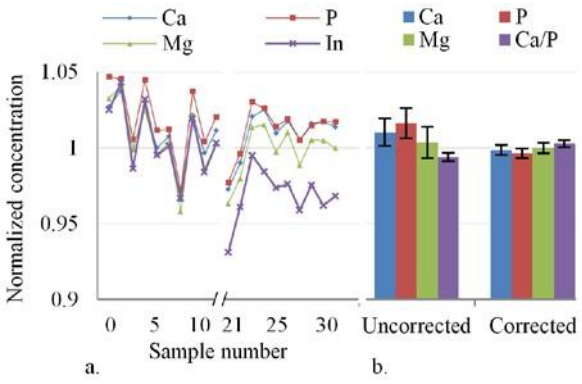

Fig. 1: (a) Variation of Ca, P, Mg and In successive measurements of a Ca-P-Mg calibration standard. (b) Ca, P, Mg concentrations and Ca/P ratios without and with correction (n=20, error bars: standard deviation).

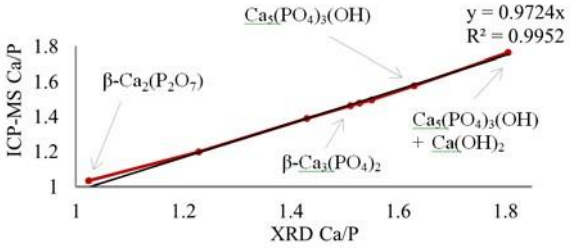

Fig. 2: Comparison between Ca/P ratios determined by ICP-MS and by XRD.

The Ca/P molar ratios of the eight CaP powders as determined by ICP-MS were very close to those determined by XRD (3% lower) (Fig 2). Both methods resulted in a low standard deviation (<0.8% in XRD and <1.3% in ICP-MS). The measured Mg/Ca ratio was always below 0.05%, which validated the accuracy of the XRD data.

DISCUSSION & CONCLUSIONS: The method developed here allowed to measure the concentrations of Ca-P-Mg standard solutions with a standard deviation of 1.6% and a mean recovery above 99.6%. Moreover stability was maintained over more than 3 hours. When considering CaP powders, a 97% agreement was found between Ca/P molar ratios determined by ICP-MS and XRD. In conclusion, ICP-MS is a very accurate tool for concentration measurements in future in vitro dissolution tests of CaP.

ACKNOWLEDGEMENTS:
B Andreatta, J Glatthard

Interaction of ultra-high purity magnesium with artificial body fluids for biodegradable implant applications

M. Pawelkiewicz[1], L. Leoty[1], A. Bruinink[2], P. Uggowitzer[3], P. Schmutz[1]

[1]Laboratory for Joining Technologies and Corrosion, [2]Laboratory for Biointerfaces Empa, Dübendorf, CH, [3]Laboratory for Metal Physics and Technology, ETH, Zürich, CH

INTRODUCTION: Today, there is a great interest in very reactive corroding Mg-based alloys for biodegradable implant applications. Use of those materials as implant devices is still limited since their mechanical integrity is often lost before the tissue/bone healing processes are finished. Fast degradation of the Mg based materials is potentially harmful for implant surrounding tissues due to accumulation of dissolving ions (even if non-toxic) and massive hydrogen evolution occurring during the metal fast corrosion process. Ultra high purity (uhp) Mg and its alloys are the most promising materials for implant applications taking under account the very detrimental role of impurities on Mg dissolution rate.

METHODS: In this study, the investigation of the corrosion mechanisms of uhp-Mg produced via vacuum distillation process is shown [1]. The corrosion behavior has been assessed in different artificial body fluids, from simple NaCl to highly complex cell culture media (RPMI-1640) via H_2 evolution measurement, Electrochemical Impedance Spectroscopy (EIS), Inductively Coupled Plasma Mass Spectrometry (ICPMS) and surface characterization techniques.

RESULTS: The influence of several parameters, such as the nature of buffer systems (Tris, CO_2) (Fig.1a-d and g), and presence of surface active species such as Zn^{2+} ions and proteins (Bovine Serum Albumin-BSA) on the in vitro degradation of uhp-Mg was investigated. Zn is a promising allowing element for Mg based implant alloys, enhancing their mechanical properties. The influence of Zn^{2+} (from the dissolution of the implant and naturally present in the tissues) on corrosion properties of Mg based material is however still not well understood. The interaction between Zn^{2+} from electrolyte and uhp Mg surface with its corrosion accelerating role is presented. The effect of BSA on the dissolution of uhp-Mg was investigated and the protein was found to either increase (in Ringer solution), decrease (in SBF) or not to impact (in NaCl) the corrosion resistance of uhp-Mg. Finally, the potential cytotoxicity of the released constituents over degradation of both anodized and bare uhp-Mg devices has been assessed via Live/Dead assays[2]

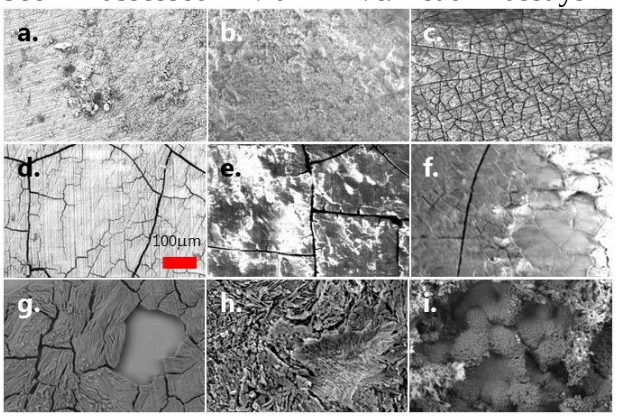

Fig.1: Corrosion products formed after 7 days immersion in a. u-SBF, b. RS, c. RPMI, d. b-SBF, e.b-SBF+3g/l BSA, f.b-SBF+10g/l BSA, g. b-NaCl, h. b-NaCl+1mMZn^{2+} and i. b-NaCl+5mMZn^{2+}

DISCUSSION & CONCLUSIONS: Immersion of uhp-Mg in 1mmol of Zn^{2+} containing media already resulted in incorporation of Zn to the corrosion product, improving corrosion protection in the early stage of immersion but leading to higher dissolution rates later on as observed by the rough corrosion products (Fig.1g-i). Interactions of proteins (BSA) with dissolving uhp-Mg surfaces have a complex nature. Presence of protein decreased corrosion resistance of uhp-Mg in SBF by hindering the formation of protective CaP layer (Fig.1d-f). Cytotoxicity test showed promising results for uhp-Mg. Fibroblast cells survived and spread out close to the uhp-Mg devices. Lack of living cells on the Mg device can be explained by fast degradation of the surface combined with high local pH.

.

Age-related biomechanical changes in articular cartilage and osteoarthritis

PR Moshtagh[1,2], AA Zadpoor[1], N Korthagen[3], H Weinans[1,2]

[1]*Faculty of Mechanical, Maritime, and Materials Engineering, Delft University, the Netherlands*

[2]*Department of Orthopedics, University Medical Center Utrecht, the Netherlands*

[3]*Faculty of Veterinary Medicine, Department of Equine Sciences, Utrecht University, the Netherlands*

INTRODUCTION: Aging is a major risk factor of osteoarthritis (OA). Synthesis and degradation of the collagen matrix are affected by age-related accumulation of advanced glycation end products (AGEs) that induce collagen crosslinking[1]. In this study, we used L-threose to artificially induce the aging effect in cartilage and studied the resulting changes in the mechanical behavior of cartilage at both nano- and micro-scales.

METHODS: Intact knee joints were obtained from 7 week old rats. Cartilage samples were taken from the left (as control) and right (as test / crosslink induced) femoral condyle joints of the same rat. In order to induce crosslinking, the cartilage was incubated (7 days at 37 ºC) with a solution of 100 mM L-threose (Sigma) in PBS, while the control sample was incubated with PBS only. Both solutions contained protease inhibitors (Roche, Germany).

Nano scale indentation: Atomic force microscopy (IT-AFM; Bruker, Dimension V, Japan) was used to obtain indentation-based force-displacement curves. A nano-scale pyramidal tip (radius: 15 nm, cantilever spring constant: 0.06 N/m) was used. 800 measurements were done at 3 Hz frequency and a depth of 500 nm. The Young's modulus was calculated using Nanoscope analysis software based on Sneddon's indentation theory and was quantified using the finite Gaussian mixture model[2].

Micro scale indentation: Micro-indentations were performed on the same samples using a Piuma indenter (Optics11, Amsterdam, Netherlands) with a spherical indenter (radius: 59 µm, cantilever stiffness: 12 N/m). Indentation measurements were done at a depth of 12µm and a 4×4 grid (165µm distance between each point, n=16). The Young's modulus was calculated based on the Oliver-Pharr theory.

RESULTS: More than 3-fold changes in the cartilage, caused by L-threose incubation, were detected by the Piuma indenter (Table 1). The nanoscale data detected remarkable changes in the modulus of each component of the cartilage tissue (Fig 2). The first and second regions are related to the nano-stiffness of the GAGs and collagen fibers respectively[3]. By comparing control sample at day 0 and 7, the modulus numbers decreased in all 3 regions due to normal degradation after 7 days incubation at 37 ºC; However after 7 days L-threose incubation (test at day 0 vs. day 7), all 3 regions illustrate an increasing trend. Moreover, the data shows that L-threose can prevent the normal degradation (control vs. test at day7). By comparing the GAG peak stiffness, it can be concluded that the sugar has an influence on the polysaccharide chains as well.

Table 1*. Micro-scale modulus measured by Piuma*

Sample name	Elastic Modulus (MPa)(mean±SD)
Control (PBS) at day 7	1.05±0.47
Test (L-Threose) at day7	3.52 ±1.54

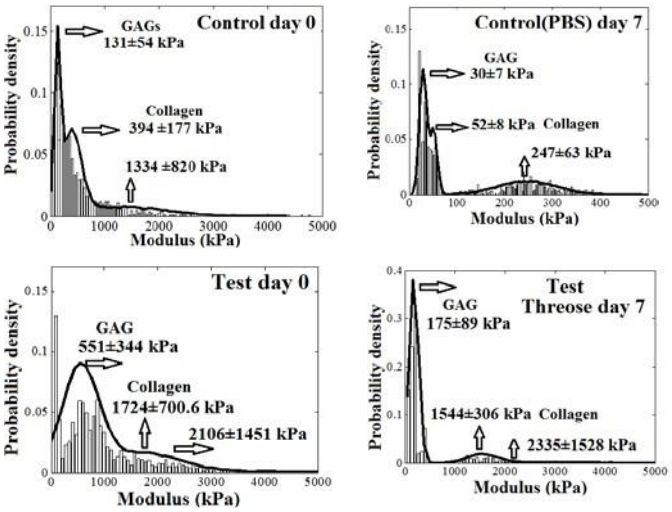

Fig 1. Elastic modulus distribution of AFM tests.

DISCUSSION & CONCLUSIONS: In this study, we examined the effects of L-threose crosslinking on the mechanical properties of the cartilage matrix in a rat at different scales. We found > 3-fold rise in overall tissue stiffness at micro-scale level. At the nano-scale, we detected an effect of crosslinking on both the collagen and GAGs components separately with more severe effects on collagen. AGEs also might prevent enzymatic degradation of the collagens, explaining the small difference between 0 and 7 days in the modulus distribution of the collagen in the AFM tests.

ACKNOWLEDGEMENTS: Dutch Arthr. Ass. and Kavli Institute of Nanoscience (TUDelft).

Hydrophobicity of PDMS affects collagen I assembly, stem cell early signalling events and osteogenic differentiation – an underappreciated confounding factor

T Razafiarison[1], JG Snedeker[1]

[1] *Department of Orthopedics, Balgrist University Hospital, University of Zurich, Zurich, Switzerland and Institute for Biomechanics, ETH Zurich, Zurich, Switzerland*

INTRODUCTION: Experiments focused on stem cell-substrate interactions using Polydimethyl-siloxane (PDMS) widely attribute cell response to factors such as substrate compliance or topology [1]. Such studies often directly compare highly hydrophobic PDMS substrate culture results to more hydrophilic substrates like polyacrylamide, although inherent differences in wettability are widely neglected. Because wettability can affect protein deposition, folding, and ligand activity, we sought to clarify the role of wettability itself as a potentially confounding factor in stem cell adhesion and osteogenic differentiation.

METHODS: We developed and characterized a hydrophilic PDMS-based platform polyethylene oxide-polydimethylsiloxane (PEO-PDMS) with the ability to tune wettability of the elastomeric substrate with otherwise equivalent topology, ligand loading, and mechanical properties. Human bone marrow stromal cells (hBMSCS) were cultured on hydrophobic and hydrophilic substrates of various stiffness covalently functionalized with different ligands (collagen I, GFOGER and RGD). Difference in ligand conformation was assessed by scanning electron microscopy (SEM). Quantitative differentiation assays and molecular investigations were performed to evaluate effects on stem cell early signalling events. To evaluate the difference in cell mechanical coupling to the different substrates, we are implementing a traction force microscopy with embedded fluorescent beads to quantify the substrate deformation.

RESULTS: Human bone marrow stromal cells (hBMSCs) seeded and cultured on stiff substrates (1.3-1.4MPa) functionalized at similar ligand density indicated similar attachment and morphology but higher levels of focal adhesion-related gene expression on hydrophilic substrates after 24h. Differentiation studies showed higher osteogenic differentiation on the hydrophilic substrates (Fig.1 and Fig.2). Molecular investigations revealed higher levels of gene expression for α1 and β1 integrin subunits and discoidin domain receptors (DDR1 and DDR2) on hydrophilic substrates after 24h, however α2 integrin subunit expression was similar after 24h on the different substrates but higher after 7 days on hydrophilic substrates.

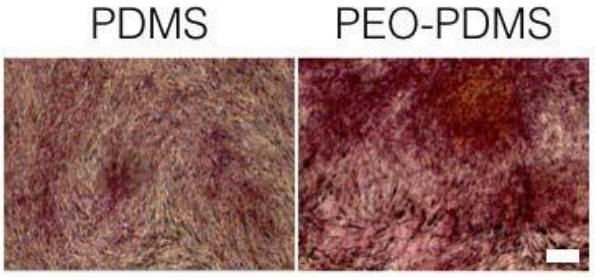

Fig. 1: Alizarin red staining of hBMSCs on stiff PDMS and PEO-PDMS substrates in culture for 7 days in induction medium. Scale bar = 200 μm.

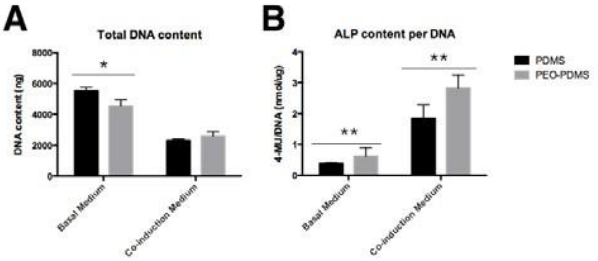

Fig. 2: Differentiation of hBMSCs after 7-day culture on stiff PDMS and PEO-PDMS substrates. (A) Total DNA content after 7-day culture in basal growth medium and in co-induction medium; mean± s.d(n=4-5); *p=0.0198; (B) Total alkaline phosphatase (ALP) content per DNA indicated a higher osteogenic differentiation on PEO-PDMS substrates when compared to PDMS substrates; mean± s.d (n=5); **p=0.0022 (basal); **p=0.0071 (co-induction).

DISCUSSION & CONCLUSIONS: The first results demonstrate that PDMS wettability modulates the nature of covalently bound collagen I assembly on the surface, and affect α1β1 integrin/DDR1 signaling, the ERK/MAPK pathway, and eventually stem cell differentiation. We conclude that substrate wettability is a non-neglectable factor that must be incorporated into experimental designs intended to elucidate substrate driven cell response.

Novel synthetic surfaces to study stem cell receptors & signaling

M. Rusch[1], L. C. Bouchez[1]

[1] *Novartis Institute for Biomedical Research, Basel, CH.*

INTRODUCTION: Stem cells have great potential for understanding early development, treating human diseases, tissue trauma and early phase drug discovery. The factors that control the regulation of stem cell survival, proliferation, migration and differentiation are still emerging. Some evidences now exist demonstrating the potent effects of various receptors and G-protein coupled receptor (GPCR)-ligands on the biology of stem cells.[1] In this context, we would like to develop novel synthetic surfaces to study stem cell receptors and their signaling, with a particular interest for biocompatible materials.

METHODS: These synthetic surfaces will present a series of small molecules that are anticipated to act both as agonists/ or antagonists and targeting agents of protein receptors and/or growth factor receptors located at the surface of our stem cells of choice. A special interest will be given to extracellular receptor-ligand interactions and how they enhance and/ or inhibit their cellular responses, as well as how they activate/silence their connected pathway(s). LGR4 (leucine-rich repeat containing G protein-coupled receptor 4), and its interaction with its natural ligand R-Spondin 1 will be first used as a proof of concept in mouse preosteoblasts (mMC3T3). Activation of R-Spondin 1-modified surfaces will be first evaluated and validated in various cellular assays (*e.g.* adhesion, differentiation, signaling assay & on receptor specificity) before being employed in competition experiments to screen compounds affecting the interaction of the immobilized ligand with its receptor. Finally, the immobilization of identified hit compounds on the surface will permit to conclude on their cell surface specificity when presenting similar cellular effects as free compounds. Ultimately, this screening tool is aimed to be developed in a high-throughput format and applied broadly to various GPCR-ligands couple of interest.

RESULTS: We were able to chemically functionnalize chitosan films with an ETAC ("Equilibrium Transfer Alkylating Cross-link")[2] which served well for the covalent immobilization of R-Spondin 1 proteins, through addition-elimination at their his-Tag. Subsequently, the biocompatibility of chitosan films, allowed us to demonstrate the capacity of our R-Spondin 1 modified surface to activate LGR4 receptors and downstream signaling.

CONCLUSION: Preliminary results look very promising, we are currently reproducing these results before applying the same methodology to various GPCRs of interest.

ACKNOWLEDGEMENTS: We are grateful to to Guillaume Ngo and Elodie Osmont for their technical support with FTIR spectroscopy.

The effects of age on bone implant integration: *in vivo* monitoring in a rat model

VA Stadelmann, C Guenther, U Eberli, K Camenisch and S Zeiter[1]

[1] *AO Research Institute, AO Foundation, Davos, CH*

INTRODUCTION: The impact of age on implant fixation is unclear. Some authors believe that implant fixation is problematic in humans over 60 years of age, but experimental and clinical data is still too sparse to support or reject the claim. Most likely, confounding factors such as osteoporosis or reduced physical activity interfere with the perceived effect of age.

Here, we investigated the time course of implant integration in healthy adult rats aged 45 or 63 weeks and compared these with ovariectomized (OVX) rats.

METHODS: Nineteen female Wistar rats were split into 3 groups: healthy adults (45w, n=11), healthy seniors (63w, n=3) and OVX (45w, n=5). All rats received a screw in the proximal tibia, as previously described[1]. They were scanned *in vivo* at 0, 3, 6, 9, 14, 20 and 28 days post surgery. Bone-implant-contact (BIC) was computed at the surface of the screws and bone fraction (BV/TV) in the periprosthetic trabecular region. Bone formation and resorption were computed from differences in consecutive scans. Overall implant stability was evaluated from image-based finite element modeling (microFE).

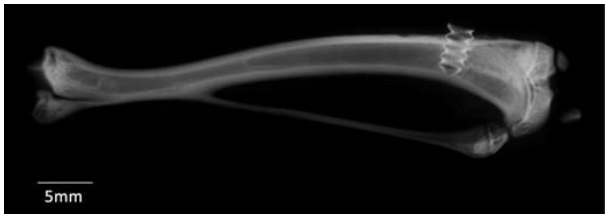

Figure 1 - Experimental model: a PEEK screw in the medio-proximal region of the rat tibia

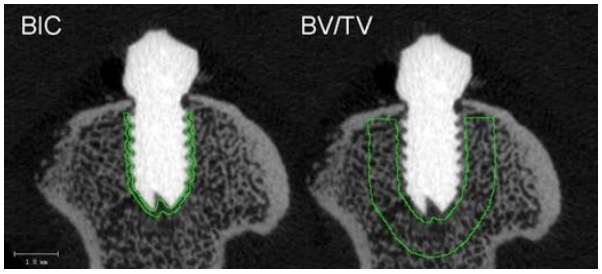

Figure 2 - Definition of the regions of interest where bone-implant contact (BIC) and bone fraction (BV/TV) were computed.

RESULTS: Healthy adults had significantly higher baseline BIC and BV/TV values (70±6% and 43±5% respectively) than healthy seniors and OVX rats, which presented with identical baseline values (BIC=50±10%, BV/TV=32±4%). Both adults and seniors showed rapid increases in BIC and BV/TV for 10 days following surgery, followed by slower increases or plateaus. By day 28, healthy seniors had reached adult BIC values (BIC=80±10%, BV/TV=45±11%).

OVX rats displayed increases in BIC and BV/TV until day 9 (BIC=70±8%, BV/TV=34±3%), but in contrast to healthy adults and seniors, the increases were immediately followed by decreases, with both BIC and BV/TV returning to baseline values by day 28.

The results were similar in terms of implant stability as assessed by microFE.

DISCUSSION & CONCLUSIONS: While senior baseline values were lower than adults, the profiles were similar, and final levels were equal. This supports the theory of an optimum integration state reached independently of initial bone stock in healthy animals, just slower in older individuals.

In our particular model, the optimum is around 80% BIC and 45% BV/TV, but these values are most likely dependent on the model choice (implant shape, animal strain …).

Our data suggests that the optimum state cannot be reached in osteoporotic specimens: although their immediate post-op reaction is similar to healthy specimens, up until day 9, newly formed bone is then resorbed within a month.

The effect of age in model is slightly slower implant integration. This preliminary data supports the idea that age in itself has a limited effect on implant integration and that osteoporotic condition is much more problematic.

Phosphate Test 2.0
A high throughput, hands-off approach using microwave chemical digestion

Etienne Stalder[1], Andreas Zumbuehl[1]
[1] Department of Chemistry, University of Fribourg, Fribourg, Switzerland.

INTRODUCTION: The determination of the phospholipid concentration in liposomal suspensions is a key step in phospholipid science. Standard phosphate tests date back several decades and require extended hands-on time. The procedures consist in a chemical digestion step where the phosphodiester moiety of the phospholipid is oxidized to an orthophosphate. This step is often carried out by heating the phospholipid suspension in the presence of a strong acid or oxidizing agent in an open reaction flask. The partial or total evaporation (or explosion) of solutes calls for an extra, time consuming volumetric standardization step. The orthophosphate is then detected colorimetrically as a metallo complex. Many coloring agents can be used, mainly molybdenum compounds such as vanadomolybdophosphoric acid, molybdenum blue or phophomolybdenum-malachite green complex[1]. There is a need for a high-throughput, hands-off method for the quantification of the phosphate content of a suspension. We have therefore presented such a test by combining microwave assisted chemical digestion and the microplate reading technology. The result is a widely applicable phosphate test.

METHODS: 200 µL of the analyte was mixed with 500 µL of $HNO3/H_2SO_4$ (3/1 v/v) in a microwave vial and then irradiated at 180 °C for 20 min (Biotage Initiator). To the oxidized sample was added, in sequence, water (2.7 mL), coloring agent (1 mL) (ammonium vanadomolybdate)[2] and NaOH (1 mL). The sample was then allowed to stand 10 min. followed by a pipetting step into a 96 microwell plate and the absorbance was analyzed at 405 nm.

RESULTS: The sensitivity of the detection allows analyses of phosphate in the broad concentration range of 2 µM to 200 µM. The accuracy for a liposome suspension with a 1 mg/mL phospholipid concentration is over 95%, in level with standard phosphate tests. Parallel testing would further increase the level of accuracy. Neither the nature of the buffer (as long as it is not a phosphate based buffer) nor the presence of an encapsulated dye (such as 5(6)-carboxyfluoresceine or rhodamine) were found to interfere with the accuracy of the measurement.

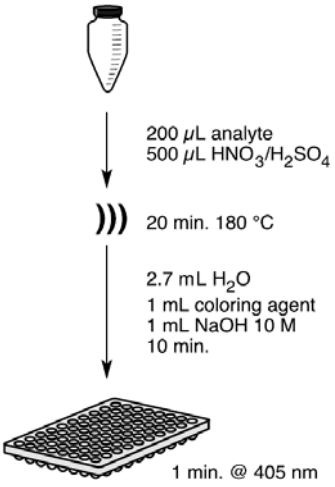

Fig. 1: Flow diagram of the microwave assisted chemical digestion of liposome suspension followed by colorimetric analysis.

DISCUSSION & CONCLUSIONS: We presented a hands-off, machine-based method allowing for a high throughput of experiments. As no solvent is evaporated, no volumetric measurements are needed, speeding up the experimental time. The samples can be tested in parallel in a multiwell plate at no additional time cost. This test is now used as a standard phosphate test in our research group.

ACKNOWLEDGEMENTS: The authors thank the Swiss National Science Foundation (PP00P2_138926/1) and the University of Fribourg for financial support.

Searching the counterpart of histology in micro tomography data to approach the regenerative capacity of bone grafting materials

Anja K. Stalder, Bernd Ilgenstein, Simone E. Hieber, and Bert Müller

Biomaterials Science Center, University of Basel, Basel, Switzerland

INTRODUCTION: Analysing biopsies after bone grafting, both the conventional histology and advanced micro computed tomography (µCT) exhibit the architecture of the trabecular bone and the shape of remaining biomaterial. Whereas µCT yields local X-ray absorption, the histology represents functional information on bone formation. Therefore, the two techniques can be regarded as complementary [1]. The size of a dataset from µCT is often orders of magnitudes larger than the size of a single histology slice. As a consequence it is a challenging task to identify the exact location of the two-dimensional (2D) histology counterpart within the huge three-dimensional (3D) data set.

METHODS: Synchrotron radiation-based µCT measurements of a biopsy containing the bone grafting material Bio-Oss® (Geistlich Pharma AG, Wolhusen, Switzerland) were performed at the beamline W2 (DORIS, Hamburg, Germany) that was operated by the Helmholtz Zentrum Geesthacht [2]. The following parameters were selected: photon energy 25 keV, pixel size 2.2 µm, and number of radiographs 721 aquiangular between 0 and 180°. The data were reconstructed using a filtered back-projection algorithm after fourfold binning to increase the density resolution. Subsequent to µCT 300 µm-thin histological sections were prepared using a saw (Leica 1SP 1600, Leica Instruments GmbH, Germany). Thinning was achieved through grinding (EXAKT 400 CS, EXAKT Apparatebau GmbH, Germany). The polished sections were etched by formic acid and stained with toluidine blue.

RESULTS: The protocol of the histological sectioning provides hints for the localization of the counterpart within the µCT data. The counterpart identification is a challenging task even for experienced personnel and was performed by a time-consuming visual inspection. For example, one can use the visualization software VG Studio Max 2.0 (Volume Graphics, Heidelberg, Germany) to inspect the µCT data slice by slice with the aim to find characteristic visual landmarks. In detail, Figure 1 displays the histology slice. It contains morphological features of bone and biomaterial, as the entire 3D µCT data.

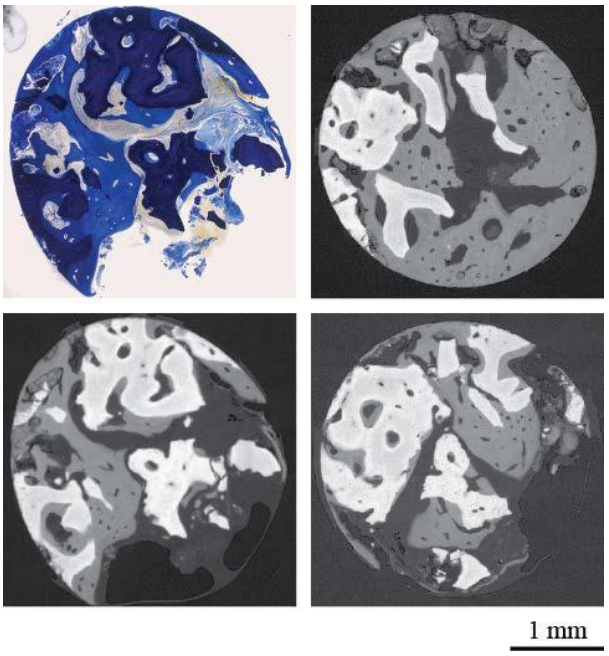

Fig. 1: Manual determination of the counterpart to the histology slice (top, left) within µCT data by landmark identification. The two images on the right are virtual cuts with characteristic features similar to the ones in the histology slice. Intentionally tilting and mirroring the µCT data one iteratively searches for the best suitable cut through the µCT data set. The X-ray absorption image below histology is a characteristic result of such a manual registration.

Evaluating the µCT-data perpendicular to the axis of the cylindrical biopsy, one finds the images given on the right of Figure 1. They contain a very few features (top-left and centre) similar to histology. Note the mirror symmetry. The elliptical shape of the histology slice further indicates the tilt. These observations result in the counterpart of histology given just below the histology slice.

DISCUSSION & CONCLUSIONS: The results of the manual search depend on the personal perspective, but they can be used as the starting point for automatic registration algorithms [1,3].

Nucleus pulposus contain progenitor-like cells able to differentiate into osteogenic and adipogenic lineages *in vitro*

A Tekari[1], SCW Chan[1,2], DA Frauchiger[1], K Wuertz[3,4], D Sakai[4,5], LM Benneker[4,6], S Grad[4,7], B Gantenbein[1,4]

[1]Tissue and Organ Mechanobiology Group, Institute for Surgical Technology & Biomechanics, University of Bern, CH, [2]Bioactive materials, EMPA, Swiss Federal Laboratories for Materials Science and Technology, St Gallen, CH, [3]Institute for Biomechanics, ETH Zurich, CH, [4], AOSpine Research Network, Duebendorf, CH, [5]Department of Orthopedic Surgery, Tokai University School of Medicine, Isehara, Kanagawa, Japan, [6]Department for Orthopaedic Surgery, Inselspital, University of Bern, Bern, Switzerland, [7]AO Research Institute, Davos, Switzerland

INTRODUCTION: The intervertebral disc (IVD) has a limited regenerative potential and low back pain represents a leading cause of disability [1]. IVD repair strategies require an appropriate cell source that is able to regenerate the damaged tissue such as progenitor stem cells. Recently, progenitor cells that are positive for the angiopoietin receptor (Tie2) in the nucleus pulposus were identified [2]. Here we isolated primary cells from bovine IVD and sorted bovine nucleus pulposus progenitor cells (NPPC) for the marker Tie2. Furthermore, we tested whether Tie2 expressing cells can differentiate into osteogenic and adipogenic lineages *in vitro*.

METHODS: NP cells were obtained from one year old bovine tails by sequential digestion with pronase for 1 hour and collagenase overnight. Sorted Tie2- and Tie2+ cells were cultured in osteogenic and adipogenic medium for 3 weeks. The formed cell layers from both subpopulations were stained for calcium deposition and fat droplets. Colony forming units were prepared for both cell suspensions in methylcellulose-based medium and formed colonies (> 10 cells) were analyzed macroscopically after 8 days.

RESULTS: After 3 weeks of culture, sorted Tie2+ cells were able to differentiate into osteocytes and adipocytes as characterized by calcium deposition and fat droplet formation. By contrast, Tie2- cells generated a weak staining for calcium and no fat droplets were obtained (Figure 1). Sorted Tie2- and Tie2+ subpopulations of cells both formed colonies, however with different morphologies. The colonies formed from Tie2+ cells were spheroid in shape whereas those from Tie2- cells were spread and fibroblastic.

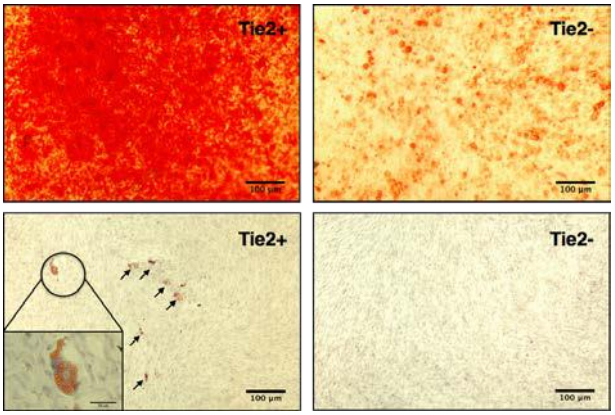

Fig. 1: Differentiation assays of Tie2+ and Tie2- bovine nucleus pulpous cells: Osteogenesis (top row) and adipogenesis (lower row).

DISCUSSION & CONCLUSIONS: Our data showed that Tie2+ cells of the nucleus pulposus cells are progenitor-like cells that are able to differentiate into osteogenic and adipogenic lineages. Sorting of NPPC for Tie2 may represent a promising strategy with the potential to be used in the clinics for treatment of intervertebral disc damage.

ACKNOWLEDGEMENTS: This project was funded by two projects of the Swiss National Science Foundation grant number #IZK0Z3_154384 and #310030_153411.

Combination of micro computed tomography and histology for the investigation of bone grafting

Peter Thalmann[1], Anja Katrin Stalder[1], Bernd Ilgenstein[1], Natalia Chicherova[1,2], Hans Deyhle[1], Felix Beckmann[3], Bert Müller[1], and Simone Elke Hieber[1]

[1] *Biomaterials Science Center, University of Basel, Basel, Switzerland.* [2] *Medical Image Analysis Center, University of Basel, Basel, Switzerland.* [3] *Helmholtz-Zentrum Geesthacht, Institute of Materials Research, Geesthacht, Germany*

INTRODUCTION: Bone grafting is often an inevitable procedure to ensure the required bone offer for the successful insertion of dental implants. In clinical studies, bone grafting is usually analysed by histology. In the present study we additionally investigated bone grafting by means of synchrotron radiation-based micro computed tomography (SRμCT) and multimodal imaging[1].

METHODS: The extraction defect was filled with a Bio-Oss® block (Geistlich Pharma AG, Wolhusen, Switzerland) and covered with a Bio-Gide® collagen membrane (Geistlich Pharma AG, Wolhusen, Switzerland). After eleven months the biopsy was harvested. The synchrotron radiation tomogram was acquired at the beamline W2 operated by HZG at DORIS III (DESY, Hamburg, Germany) in absorption-contrast mode with a photon energy of 25 keV and a pixel size of 2.2 μm. Subsequent to the SRμCT, histological slices were prepared and toluidine-blue stained. Finally, the corresponding tomographic slice was selected from the volumetric SRμCT data. Due to the limited information in the two-dimensional (2D) histology with respect to the three-dimensional (3D) SRμCT data, first a pre-selection of the corresponding μCT slice was performed - manually and automatically - followed by 2D-2D non-rigid registration.

RESULTS: After grafting material insertion and healing period, there was sufficient bone to place the implant. Figure 1 shows the joint histogram of the histology slice and the corresponding tomogram as well as the related slices. The distinct attenuation coefficients of bone, grafting material and soft tissue/embedding material give rise to three well-defined clusters. The histogram of the μCT data set allowed distinguishing the biopsy components by intensity-based segmentation (thresholding). The specimen included 14.2 vol% newly formed bone (gray), 57 vol% soft tissue/embedding material (black) and 25.7 vol% bone augmentation material (white).

DISCUSSION & CONCLUSIONS: The SRμCT directly allowed for the segmentation of bone augmentation material and newly formed bone. Previous studies[2,3] have shown that this is not always the case. Often, the grafting material cannot readily be distinguished from forming bone based on attenuation alone. In these cases, the combination of histology and CT allows to master this challenge.

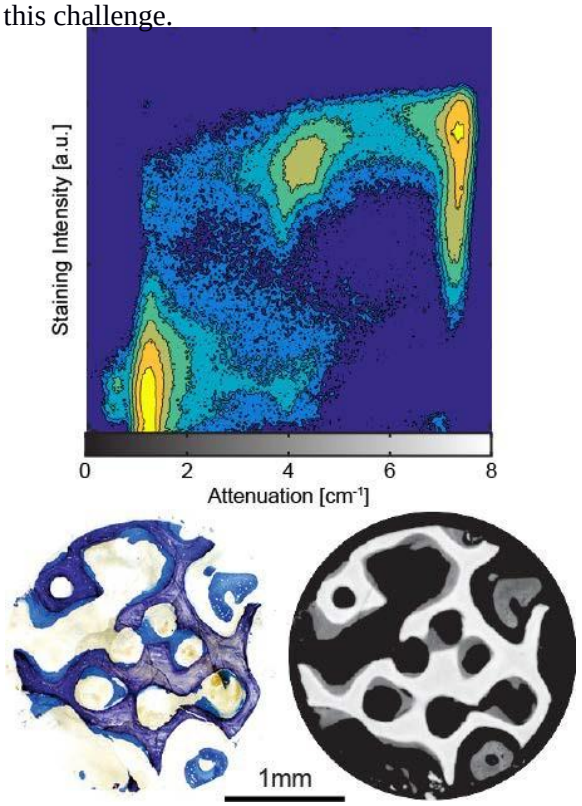

Fig. 1: Joint-histogram (top) of a histology slice (ordinate) and a SRμCT slice (abscissa). The related slices are displayed on the bottom.

In this study the discrimination between the less mineralized, newly formed bone and the fully mineralized bone is easier in the SRμCT data than in the histology data.

Viscoelastic properties of Polydimethylsiloxane studied by cantilever bending

Tino Töpper, Bekim Osmani, Florian Weiss, and Bert Müller

Biomaterials Science Center, University of Basel, c/o University Hospital, 4031 Basel, Switzerland

INTRODUCTION: The mechanical properties including viscoelasticity of micro- to nanometer-thin polymer films are crucial for efficient, electrically activated polymer (EAP) actuators [1]. Here, we demonstrate the actuation response with the cantilever bending bar method [2] as a quantitative measure of the degree of cross-linking of Polydimethylsiloxane (PDMS) films. Siloxane-based polymers are well known for their elasticity with strains levels of up to 117 % and dielectric behavior [1]. Especially, the millisecond response [1] and biocompatibility make it suitable for biomimetic applications in the human body such as artificial muscles [3].

METHODS: The 4 µm-thin polymer films were spin-coated on Polyetheretherketone (PEEK) substrates (APTIV 2000, Victrex, Lancashire, UK) with a thickness of 25 µm embedded between 15 nm-thin sputtered Au electrodes. This asymmetric EAP-microstructure was characterized by applying a voltage [2]. The actuation mode is based on the COULOMB attraction between the oppositely charged electrodes. The squeeze of the incompressible polymer results in an expansion in *x*- and *y*- direction causing a torque of the cantilever, detected by a displacement of a reflected laser beam on a position sensitive detector. Cross-linking was realized through heat curing at curing temperatures of 80 °C.

RESULTS: The actuation of 0.5 h heat-cured Elastosil A/B over a period of 15 s is presented in Figure 1 for actuation voltages between 150 and 400 V. The deflection at 150 V applied voltage increases within a time period of 2 s before it reaches equilibrium. For higher actuation voltages of 300 V the maximal deflection increases according to the MAXWELL pressure quadratic with the applied voltage but drops down within a few seconds to equilibrium. The relaxation process can be characterized using the difference between maximal and equilibrated deflection *d* and the time constant τ. The fitted exponential function $d(t) = C\,exp(-t/\tau)$ is included as a line into Figure 1. With a further increase to 400 V this effect becomes even more pronounced with a 43 % relaxation of the maximal deflection compared to a 23 % relaxation of deflection at 300 V. Furthermore this relaxation process slows down for higher applied strains to polymer network with an increased time constant of τ = (1.52 ± 0.01) s at 400 V compared to τ = (0.85 ± 0.02) s at 300 V. For 2 h heat-cured polymer films no relaxation of the actuation under applied strain was observed.

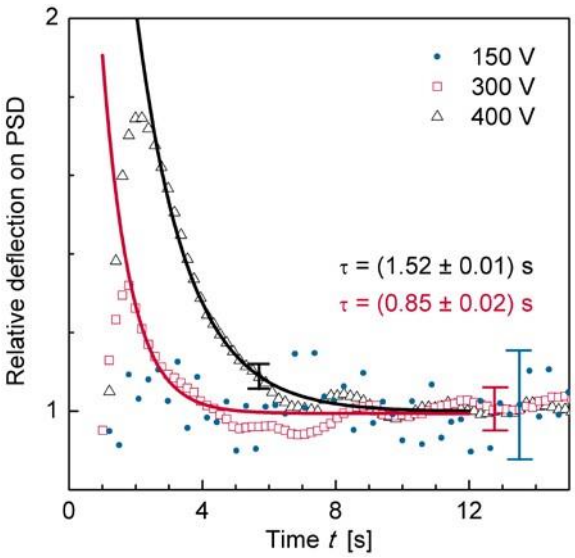

Fig. 1: Actuation of EAP-microstructures on PEEK cantilevers is presented for 0.5 h heat-cured polymer at actuation voltages of 150 to 400 V.

DISCUSSION & CONCLUSIONS: We found that polymeric thin films exhibit curing-time-dependent compliance under strain. As completely cross-linked PDMS is known to be incompressible we relate this phenomenon to the degree of network cross-linking, which is increased with curing time. Thus, the presented cantilever bending method can deliver quantities about the viscoelastic properties of a polymer film.

ACKNOWLEDGEMENTS: The financial support of the nano-tera.ch initiative *SmartSphincter* is gratefully acknowledged. Furthermore, the authors thank VICTREX for supporting us with PEEK films.

Surface treatment of polyetherketoneketone for load-bearing implants

Prabitha Urwyler[1,2], Alfons Pascual[3], Helmut Schift[4], and Bert Müller[1]

[1]Biomaterials Science Center, University of Basel, Basel, Switzerland, [2]Gerontechnology and Rehabilitation group, University of Bern, Bern, Switzerland, [3]Institute of Polymer Engineering, University of Applied Sciences and Arts Northwestern Switzerland, Windisch, Switzerland, [4]Laboratory for Micro- and Nanotechnology, Paul Scherrer Institut, Villigen PSI, Switzerland.

INTRODUCTION: Polyetherketoneketone (PEKK) is a promising biomaterial for load-bearing implants due to mechanical behaviour, radiolucency, MR-compatibility, and chemical inertness. For bone implants, however, PEKK surfaces have to be intentionally modified to allow for proper cell attachment. Plasma and ultra violet ozone (UVO) treatments are common processes to chemically activate polymer surfaces. The oxygen plasma treatment of PEKK films also results in well reproducible nanostructures, tailored adjusting plasma power and treatment time [1]. UVO surface treatments with 20 minutes duration are permissible for polymer micro-cantilevers [2, 3]. In this communication, we investigate the influence of the treatments on the chemical nature of PEKK.

METHODS: Commercially available 60 µm-thick PEKK films (OXPEKK PermettaTM, Oxford Performance Materials, South Windsor, USA) were activated using the oxygen plasma treatment with the RIE System Plasmalab 80 Plus, Oxford Instruments, Abingdon, UK at a power of 10 W for a period of 5 minutes. The UVO treatment with the UV Clean Model 13550, Boekel Scientific, Feasterville PA, USA took 20 minutes. Changes of the surface chemistry were studied using reflection Fourier transform infrared spectroscopy (FT-IR). The spectra were recorded using a Centaurus IR-microscope coupled to a Nexus IR spectrometer (Thermo Electron Corporation, Thermo Fisher Scientific, Dreieich, Germany) with a grid of 300 µm × 300 µm.

RESULTS: Figure 1 demonstrates that the FT-IR spectra of the basic and plasma-treated PEEK films do not show significant differences. The spectra of UVO-treated films, however, differ from the basic material. One finds additional carbonyl groups present at a wavenumber of about 1700 cm^{-1}. It should be noted that differential scanning calorimetry measurements showed no changes in thermal behaviour between the basic and the plasma-treated films. For the UVO-treated films, however, an increase of the glass transition temperature by 4 K was observed.

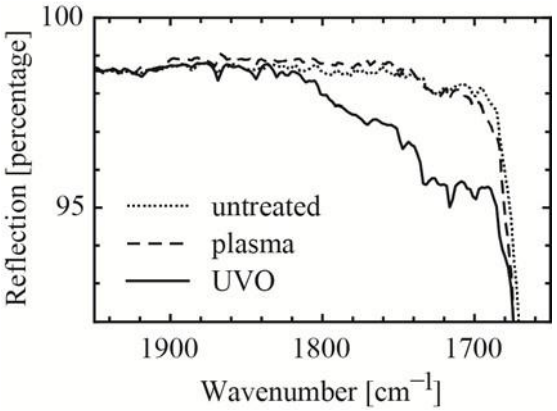

Fig. 1: Characteristic FT-IR spectra of the basic material (untreated), oxygen-plasma- and UVO-treated PEKK films.

DISCUSSION & CONCLUSIONS: The correlation between carbonyl signals and the increase in the glass transition temperature after UVO-treatment indicates a chemical ageing of the PEKK films. Therefore, we conclude that plasma treatment using a power of 10 W is favourable for the surface preparation of load-bearing implants made out of the high-performance polymer PEKK. At this moderate plasma power the nanostructuring effect is negligible. Owing to the similar chemical structure, PEKK exhibits a comparable behaviour to the well-established high-performance polymer polyetheretherketone (PEEK).

ACKNOWLEDGEMENTS: The authors thank the Swiss Nanoscience Institute and the Swiss Academy of Engineering Sciences for providing financial support. The technical assistance of the C. Spreu, X. Zhao, R. Schelldorfer, and K. Vogelsang is gratefully acknowledged.

Incompatibility of dental alloys: Evaluation by ec-pen corrosion measurements

Florian M. Weiss[1], Fredy Schmidli[2], Markus Jungo[1], and Bert Müller[1]

[1] *Biomaterials Science Center, University of Basel, Switzerland* [2] *School of Dental Medicine, University of Basel, Switzerland*

INTRODUCTION: Metallic reconstructions of crowns, bridges and/or prosthesis exposed to the conditions in the oral cavity have varying corrosion resistances. Metal ion diffusion due to redox reactions of the reconstructions can cause symptoms including pain and irritations of the mucous membrane, taste irritations, dry mouth or tongue burning. Patients suffering from these incompatibility reactions are examined using time-consuming evaluations. Energy-dispersive X-ray (EDX) spectroscopy of splints from the metallic dental reconstruction is applied to know their composition followed by an atomic absorption spectroscopy (AAS) of the surrounding soft tissue to evaluate if it contains some of the metals comprised in the dental construction. The results may allow concluding that the metals used for constructions corrode. A rather fast and supportive *in vivo* method for such an analysis is an electrochemistry technique termed ec-pen used for more than nine years. In this presentation, the challenges during the measurement and analysis are discussed.

METHODS: The ec-pen has a setup similar to a cyclic voltammetry experiment. The pen itself contains a working electrode (WE) and a reference electrode (RE) both immersed into the electrolyte (lactic acid 10.01g/L – sodium chloride 5.8g/L in distilled H_2O), which is enclosed in the reservoir within the pen. By pressing the pen tip against the material of interest, it emits some of the electrolyte causing a wetting of the construction surface and, therefore, allows for the electrochemical analysis as soon the counter electrode (CE) is in contact with the construct as well, see Fig. 1. More detailed description of the ec-pen setup and functionality has been discussed previously [1-4].

RESULTS: To obtain appropriate results it is of particular importance, where and how the measurements are carried out. Depending on the contact and wetting area of the pen tip, the results can deviate significantly. Therefore, it should be well documented, where and how the measurements are taken (tip angle relative to the construction, crown area/edge, soldering points, crevice etc.). These deviations are demonstrated on the construction displayed in Fig. 1 and summarised in Table 1.

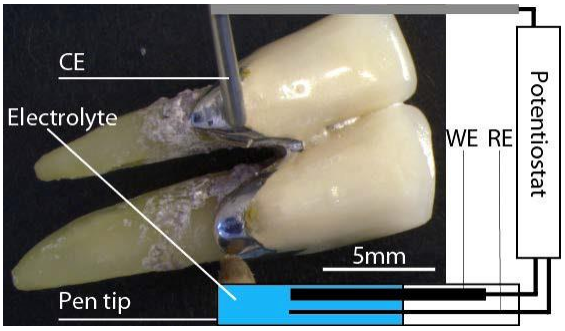

Fig. 1: The ex vivo measurement set up of a metallic dental construction using the ec-pen.

Table 1. The results depend on contact area and location.

	Impedance [Ω cm^2]	Phase [degree]
Tip 90° rel. to sample	354 ± 119	50 ± 6
Tip 45° rel. to sample	206 ± 65	48 ± 10
Crown area	262 ± 83	49 ± 14
Crown edge	307 ± 92	11 ± 16
Base	186 ± 48	37 ± 4
Soldering point	60 ± 4	27 ± 3

DISCUSSION & CONCLUSIONS: Albeit one can identify such deviations it was possible to seriously evaluate the dental constructions of more than 120 patients with material's incompatibility reactions. The results of the evaluation compared with EDX and AAS showed that the ec-pen method is a valuable alternative to get results concerning corrosion induced incompatibility reactions in patients within minutes. The authors recommend the growing number of people, who suffer from irritations in the oral cavity, to consult the specialized dentists at the University of Basel.

Novel model to study intervertebral disc degeneration under simulated microgravity condition

S. L. Wuest[1], M. Horn[1,2], R. Baumann[2], M. Egli[1]

[1] *CC Aerospace Biomedical Science and Technology, Lucerne University of Applied Sciences and Arts, Hergiswil, Switzerland.*

[2] *CC Mechanical Systems, Lucerne University of Applied Sciences and Arts, Horw, Switzerland.*

INTRODUCTION: Astronauts usually suffer from low back pain during space flight and are at elevated risk of herniated nucleus pulposus post flight. It is thought that the back pain is caused due to swelling of the intervertebral disc (IVD), since the spine of astronauts elongates in microgravity. Because IVDs are highly mechanosensitive, several experiments were performed under microgravity to explore the effect of mechanical unloading. Rats flown aboard a biosatellite for 14 days showed a significant reduction of wet and dry weights and the collagen-to-proteoglycan ratio was significantly greater [1]. This finding could be confirmed in a later space shuttle mission lasting five days [2].

METHODS: Random Positioning Machines (RPM) are used as a ground based model for simulating microgravity through the principle of gravity vector averaging (*Fig. 1*). Thereby the samples are continuously rotated about two perpendicular axis. The RPM showed good correlation to space experiments for several mammalian cells [3]. However, to date the RPM has not been compared to space experiments at the level of mammalian organs.

Our RPM, that is equipped additionally with an incubator (*Fig. 1*), will now be upgraded with a novel device, which will allow the cultivation of two IVDs for multiple days. The device (Fig. 2) will expose the IVDs to programmable static and dynamic compression cycles to mimic physiological use (*Fig. 2*). But because this is installed on a RPM, the IVD will simultaneously experience simulated microgravity.

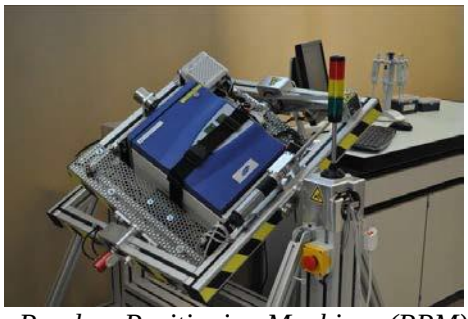

Fig. 1: Random Positioning Machines (RPM) are used as a ground based model for simulated microgravity.

RESULTS: The concept study has been finished for the realization of a novel device for studying IVD degeneration as observed during space flights. This relatively cheap and accessible ground based device allows conducting pre- and post-flight studies at affordable costs.

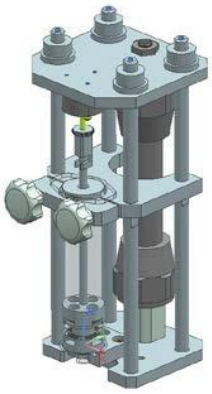

Fig. 2: Two such devices are inserted on the RPM, each encompassing one IVD. While the RPM creates a condition of simulated microgravity, the device allows the exposure of the IVDs to static and dynamic compressive loading.

DISCUSSION & CONCLUSIONS: The proposed IVD device allows studying IVDs under simulated microgravity conditions created by the RPM. Since there are results from space flights available, data generated by our novel device can be easily compared and thus the quality achieved assessed. The additional option of applying static and dynamic compression at various patterns to the discs, allows to study possible countermeasures during long space flights in addition.

ACKNOWLEDGEMENTS: We thank Daniela Frauchiger and Dr. Benjamin Gantenbein from the Tissue and Organ Mechanobiology Group, University of Bern, of the fruitful collaboration.

Long-term effects of knitted silk-collagen sponge scaffold on anteriorcruciate ligament reconstruction and osteoarthritis prevention

Weiliang Shen[1], Dominique Pioletti[2], Hong-wei Ouyang[1]

[1]Department of Orthopedic Surgery, 2nd Affiliated Hospital, School of Medicine, Zhejiang University, Zhejiang, China. 2Laboratory of Biomechanical Orthopedics, EPF Lausanne, Switzerland

INTRODUCTION: Anterior cruciate ligament (ACL) is difficult to heal after injury due to the dynamic fluid environment of joint. Previously, we have achieved satisfactory regeneration of subcutaneous tendon/ligament with knitted silk-collagen sponge scaffold due to its specific "internal-space-preservation" property. This study aims to investigate the short and long-term effects of knitted silk-collagen sponge scaffold on ACL regeneration and osteoarthritis (OA) prevention.

METHODS: The knitted silk-collagen sponge scaffold (S-C scaffold) was fabricated and implanted into a rabbit ACL injury model(Fig. 1).

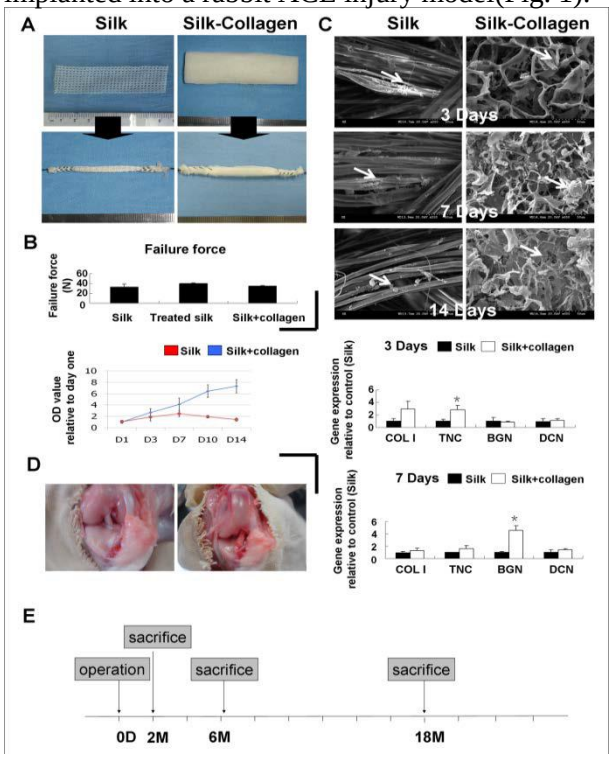

Fig. 1: Preparation and characterization of scaffolds.

RESULTS: The S-C scaffold was found to enhance migration and adhesion of spindle-shaped cells into the scaffold at 2 months post-surgery. After 6 months, ACL treated with the S-C scaffold exhibited increased expression of ligament genes and better microstructural morphology. After 18 months, S-C treated group had more mature ligament structure and direct ligament-to-bone healing (Fig. 2).

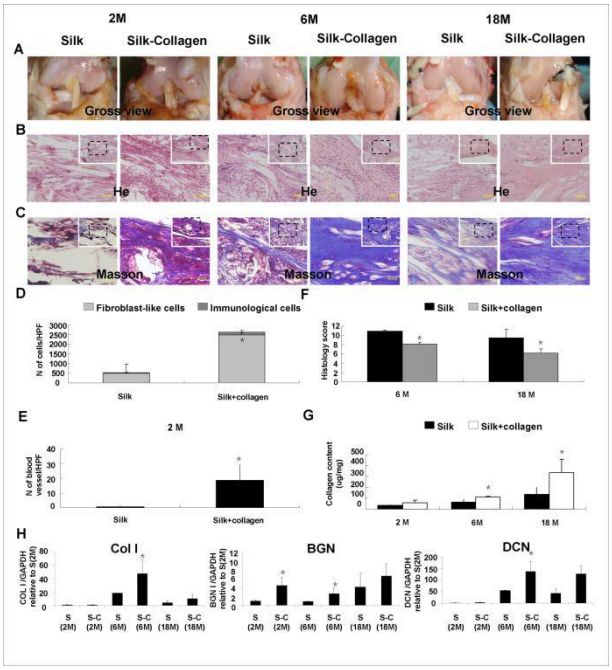

Fig. 2: ACL regeneration at 2, 6 and 18 months post-operation.

Furthermore, the S-C scaffold effectively protected joint surface cartilage and preserved joint space for up to 18 months post-surgery.(Fig. 3)

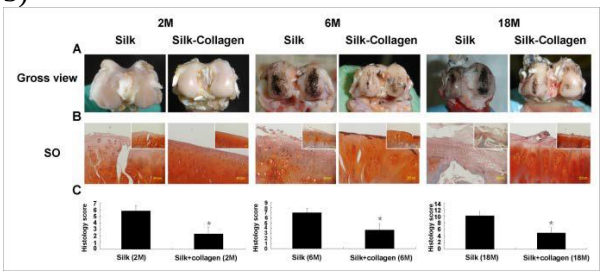

Fig. 3: Cartilage maintenance and OA progression at 2, 6 and 18 months post-operation

DISCUSSION & CONCLUSIONS: The S-C scaffold can regenerate functional ACL and prevent OA in the long-term, suggesting its clinical use as a functional bioscaffold for ACL.

ACKNOWLEDGEMENTS: This work was supported by NSFC grants (81330041, 81125014, 31271041, 81201396, 81271970, J1103603).

A novel method for *in vitro* evaluation of apatite forming ability of chemically treated titanium metals

W Zhao, J Lemaître, P Bowen

Powder Technology Laboratory (LTP), École Polytechnique Fédérale de Lausanne (EPFL), CH

INTRODUCTION: Artificial materials which have the ability to spontaneously bond to living bone, when implanted into bone defects, are of great interest as implant materials. It is commonly accepted that a spontaneous formation of a hydroxyapatite ($Ca_5(PO_4)_3(OH)$, HA) layer on the surface of the material under *in vivo* conditions is the key step for osseointegration, and this process can be simulated in an acellular environment using a simulated body fluid (SBF).[1,2] However, the current widely used SBF, proposed by Kokubo et al. lacks critical components of human blood plasma (HBP), such as proteins,[2] which play an important role when interacting with foreign surfaces. Besides, the buffering system employing TRIS used in the c-SBF does not match the actual buffering system in human blood, where the pH is buffered by a partial pressure of CO_2 at 5% atm. In addition, several examples have shown the predictions using SBF led to false positive and false negative results.[3]

In 2009, Bohner and Lemaître published a paper proposing a revised method for performing the Apatite Forming Ability (AFA) test, where the pH is buffered in the incubator with a partial pressure of CO_2 at 5% atm.[4] A simplified recipe for preparing SBF was also proposed (JL2). After this starting point of the research, we have further tuned the SBF composition by thermodynamic calculations. The revised recipe JL2-r is given in Table 1, along with conventional c-SBF.

	Concentration/ mM			
Ion	HBP	c-SBF	JL2	JL2-r
Na^+	142.0	142.0	142.0	142.0
Mg^{2+}	1.5	1.5	--	--
Ca^{2+}	2.5	2.5	2.31	2.31
Cl^-	103.0	147.8	108.96	121.64
HCO_3^-	27.0	4.2	34.88	22.20
HPO_4^{2-}	1.0	1.0	1.39	1.39
SO_4^{2-}	0.5	0.5	--	--
TRIS	--	50.0	--	--
HCl	--	~ 40 mL	0.94 mL	1.36 mL
CO_2	~5% atm.	--	5% atm.	5% atm.

Table 1. SBF compositions and HBP composition.

METHODS: Commercial Medical grade titanium bars were cut into discs of ~2 cm in diameter and 1 mm in thickness, which were finely polished (R_a ~ 0.2 - 0.4μm). The titanium discs were treated with 65% HNO_3 solution for 30 minutes followed by 24h at 60°C in 5M NaOH aqueous solution. Some of the samples were also annealed under air for 2h at 550°C. The AFA test was conducted by immersing the sample in ~ 5mL of JL2-r solution with the active surface facing down. A CO_2 partial pressure of 5% atm. and a temperature of 37°C were maintained. The samples were taken out for observation after 1 week (SEM, XRD).

RESULTS: The results obtained using JL2-r solution for alkaline etched Ti metal are similar to the results produced with conventional SBF. The surface before and after the AFA test are shown in Fig. 1. HA was observed on the surface.

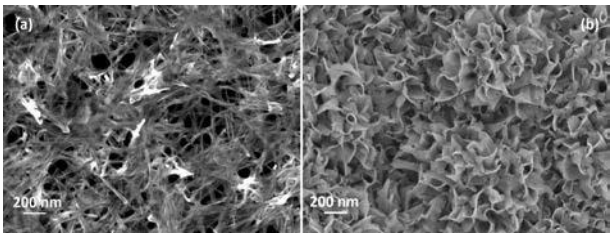

Fig. 1: SEM images of alkaline etched Ti surfaces before (a) and after AFA test (b).

DISCUSSION & CONCLUSIONS:

Alkaline etched Ti metals are well-known to be bioactive materials and the results demonstrate that JL2-r solution is capable for accurate prediction of the bioactivity of alkaline etched Ti metals, a first step in validating the new method. Follow up research are currently being conducted.

ACKNOWLEDGEMENTS: The authors would like to thank Swiss National Science Foundation (Project No: 205321_150193) for providing financial support for this work.

Synthesis and characterization of hyaluronan amphiphilic derivatives for biomedical applications

D Petta[1,2], D Eglin[1], DW Grijpma[2], M D'Este[1]

[1]*AO Research Institute Davos, Davos, CH,* [2]*Department of Biomaterials Science and Technology, University of Twente, Enschede, NL*

INTRODUCTION: Amphiphilic bio-co-polymers display singular physico-chemical properties making them attractive biomaterials for regenerative medicine and drug delivery [1]. In this study, we prepared and characterized a series of short hyaluronan (HA) alkyl derivatives. A novel derivatization method based on amidation promoted by 4-(4,6-dimethoxy-1,3,5-triazin-2-yl)-4-methylmorpholinium (DMTMM) was used [2]. Products were characterized by ^{1}H nuclear magnetic resonance (NMR) and rheology.

METHODS: HA-butylamine (HA-B) and HA-propylamine (HA-P) were synthesized by reacting HA (molecular weight = 280 KDa) with each amine in presence of DMTMM in water and 2-(N-morpholino)ethanesulfonic acid (MES) buffer, pH = 5.5. ^{1}H NMR (Bruker Avance AV-500 18 MHz spectrometer) was applied for the determination of the molar degree of substitution (DS%). Flow and oscillatory rheological measurements were performed for 5% v/w solutions of HA-P and HA-B after a thermal treatment (92°C for 1h 30') with an Anton Paar MCR-302 rheometer. Absence of free amine in the final product was assessed via Ninhydrin assay.

RESULTS: Generally, derivatives are turbid, but become transparent and with gel-like texture after thermal treatment. Figure 1 shows the kinetics of formation at room temperature in MES buffer and in water for HA:amine:DMTMM = 1:1:1.

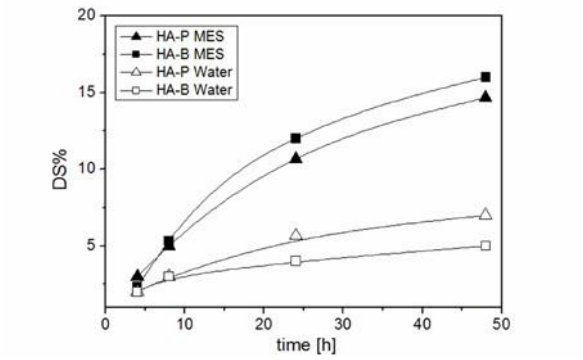

Fig. 1: DS% versus reaction time for HA-B and HA-P (ratio 1:1:1, RT) performed in water (empty shapes) or in MES Buffer (full shapes).

With increasing temperature and feed ratio, DS% up to 51% could be achieved. Compared to pristine HA the derivatives show significantly higher storage modulus G'. G' and DS% are inversely correlated, except for values of DS% below 3, where they are directly correlated (fig. 2).

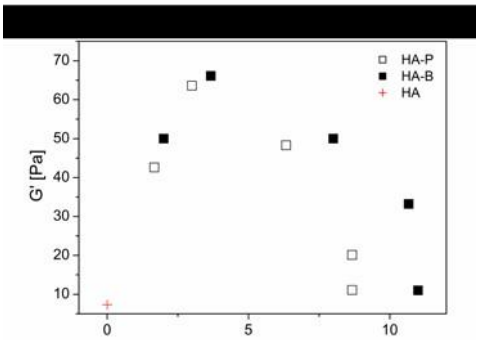

Fig. 2: G' versus DS% in MES (ratio 1:1:0.5, RT). Full shapes indicate HA-B, empty shapes HA-P and the red cross represents the pristine HA.

DISCUSSION & CONCLUSIONS: The aspect change after thermal treatment let presume a rearrangement of the hydrophilic and hydrophobic domains within the co-polymers. G' vs DS% plot displays a complex correlation, with maximum G' achieved around DS%= 4 for both derivatives. For DS% higher or lower, G' goes back to values in the range of pristine HA. Owing to this singular rheological behavior HA-P and HA-B could be used as biomaterials and hydrogels for drug delivery and regenerative medicine. Further investigations are needed to understand the nature of the molecular network within these gels.

ACKNOWLEDGEMENTS: Ms. Doris Sutter from ETH-Zurich, for performing NMR measurement.

Improvement of mechanical properties of 3D printed hydroxyapatite scaffolds by culture of osteoblast-like cells under perfusion flow

N Rimmer[1], F Burgio[1], A Rohner[1], P. Chavanne[1], S Zimmermann[1], P Gruner[2], R Schumacher[1], M de Wild[1], A Papadimitropoulos[3,4], I Martin[3], M Beaufils-Hugot[1], U Pieles[1]

[1]*FHNW, University of Applied Sciences and Arts of Northwestern Switzerland, Muttenz CH,* [2]*Medicoat AG, Mägenwil CH,* [3]*DBM, Department of Biomedicine, University Hospital Basel CH,* [4]*Cellec Biotek AG, Basel CH*

INTRODUCTION: 3D-printed hydroxyapatite (HA) scaffolds with defined macro porosity have emerged as attractive biomaterials in tissue engineering. However their brittleness restricts their practical applications. In this study, we aimed at improving their mechanical properties by (i) surface treatment (oxygen-plasma) during the production, and (ii) deposition of extracellular matrix (ECM) by human osteoblastic cells (MG-63) during culture under perfusion flow. Mechanical compression tests were performed to measure the stiffness of the resulting materials.

METHODS: Untreated and plasma-treated 3D printed HA scaffolds (diameter 10mm, thickness 4mm, Z-510 3D-Systems, HA powder Medicoat AG) were seeded with 1Mio MG-63 with the use of a perfusion bioreactor device (U-CUP; Cellec Biotek AG) in complete medium. Following 3 days of culture, the medium was supplemented with osteoblast stimulators to induce differentiation for up to 28 days. Samples were analysed at different time points by scanning electron microscopy, MTT and DNA content assays to evaluate cell attachment, distribution and proliferation. Quantitative real-time PCR and alkaline phosphatase (ALP) activity assay were performed to assess osteoblast differentiation. Mechanical tests were done on scaffolds in wet state after 28 days of culture. Constructs in static conditions and empty scaffolds were used as controls.

RESULTS: Under dynamic conditions, cells were found to be uniformly distributed within the pores of the scaffolds (MTT; Fig.1A) following an 18 hours seeding process, while cell numbers were found to be significantly higher at each time point (DNA content; Fig.1B), as compared to the static conditions. Hydrophilic surface modification by oxygen-plasma treatment contributed also to accelerate the on-set of ECM deposition, as indicated by the earlier (i) saturation of proliferation (Fig.1B, red), and (ii) up-regulation of osteoblastic-related genes, as compared to un-treated scaffolds (ALP mRNA up-regulation at Day7 (4.5-fold)). Importantly, the elastic gradient of this cell-enhanced biomaterial generated in perfusion bioreactors (n=3) increased from 14.3 ± 0.08 to 19.3 ± 0.03 MPa from empty to matrix deposition scaffolds.

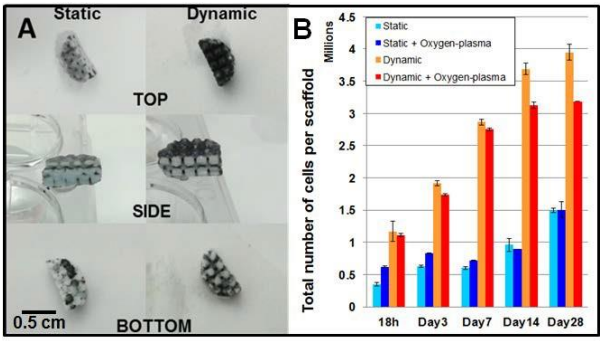

Fig. 1: MG-63 proliferation on 3D-printed HA scaffold. (A) MTT staining after 18 hours seeding in static (left) and dynamic (right) conditions. (B) DNA content assay of cells seeded on untreated (light blue and orange) or plasma-treated (dark blue and red) scaffolds for up to 28 days of culture under static (blue) and dynamic (red) conditions.

DISCUSSION & CONCLUSIONS: Plasma-treated 3D-printed porous HA scaffolds (cell-enhanced biomaterials) seeded with human osteoblast-like cells cultured dynamically in perfusion bioreactor showed clearly a mechanical improvement in terms of stiffness. This experimental setup shall be assessed by using stem cells, which typically have a higher potential of ECM deposition than MG-63 cells.

ACKNOWLEDGEMENTS: This work is supported by a grant from the Schweizerischer Nationalfonds (SNF) (Grant number: 51NF40-144618).